Fermilab

FERMILAB-THESIS-2000-01

OBSERVATION OF NEUTRINO INDUCED NEUTRAL CURRENT CHARM EVENTS.

by

ANDREW K. ALTON

B.S., University of Iowa, 1992

M.S., Ball State University, 1996

A DISSERTATION

submitted in partial fulfillment of the

requirements for the degree

DOCTOR OF PHILOSOPHY

Department of Physics

College of Arts and Sciences

KANSAS STATE UNIVERSITY

Manhattan, Kansas

2000

Approved By:

Major Professor

Tim A. Bolton

ABSTRACT

We report results from the analysis of wrong sign muon(WSM) events in deep inelastic $\nu_\mu N$ and $\bar{\nu}_\mu N$ scattering with the NuTeV experiment at the Fermi National Accelerator Laboratory. These measurements are made possible by the high-purity NuTeV sign-selected beams. Using the anti-neutrino mode (WSM) sample we extract the normalizations for all known sources of beam impurities. The corrected charm production at the target measures the cross section, $\sigma_{p+p\to c\bar{c}} = 49.3 \pm 11 \pm 5.6\ \mu b$, using linear atomic mass dependence. Using a boson-gluon fusion model and the neutrino mode WSM sample open neutral current charm production in neutrino scattering has been observed, and the charm mass is determined to be $m_c = 1.40^{+0.83}_{-0.36} \pm 0.26$ GeV/c^2. The average energy of neutrinos which produce a pair of charm quarks is 154 GeV, and at this energy the cross section is $\sigma_{\nu+N\to c\bar{c}} = (2.14^{+1.76}_{-1.54}) \times 10^{-1} fb$. A search for Flavor-Changing Neutral-Current (FCNC) production of bottom and charm has demonstrated a new method of placing limits on FCNC. These limits are of comparable sensitivity to the current best limits, and effectivly limit other decay modes.

Acknowledgements

I here have the pleasure of thanking the people who made this thesis possible. It is impossible for me to remember everyone, and I apologize to anyone I've forgetten. First of all I would like to thank Don Lincoln and Donna Naples who helped me get to KSU. They are the people who taught me to love HEP. They have inspired me, encouraged me and taught me, what physics is really about.

I would like to thank Tim Bolton for helping me get started, advising me even when I wasn't his student, and for picking me up as an advisee when Donna left KSU. He provided support when the quals were hard, and I know I wouldn't have made it without his help. He has taught me how to polish an analysis, and how to present my works (*ie* "Sex Sells"). It is due to many hours of reading and re-reading on his part that this thesis is a thorough and well written work.

I would be remiss if I didn't mention Larry Weaver, who took months of his time to teach me all of the HEP theory I know. He has taught me something about almost every subject in physics and has advised me through many hard times. Specifically he stood by and helped me learn everything I needed to know to pass the qualifying exams.

I am pleased to thank Noel Stanton for all he taught me about designing and constructing drift chambers. He taught me to start low-tech and only complicate things when it was necessary. I'd like to thank Panagiotis Spentzouris for teaching me all about the muon reconstruction code and the cruncher in general. I'd like to thank Kevin McFarland for all his help in netherworlds of the flux, and for paying close (sometimes too close) attention to this analysis. I'd like to take this opportunity to thank Todd Adams for his help when stupid McNuTeV bugs killed me, for writing the FCNC bottom code and for all his help.

Two people who have been most influential in my graduate school experience are Jesse Goldman and Max Goncharov. They have been my friends, teachers and students. They have often been the first to view and criticize my work. This wouldn't have been as easy without them. I would like to thank Jesse for all the time and energy he put into supporting our computers and answering all my stupid computer questions and showing me how to solve any number of qualifying exam problems, not to mention helping me understand QCD. I am also glad to have had Sam Zeller as my "Bobsie Twin" for all my work on drift chambers. She taught me a lot about fixing chambers and the flux. She helped me in more ways then I can count. I would also like to thank Kathleen Pierce who managed to solve uncountable unsolvable problems, and who has added a bit of sanity and balance to the KSU-HEP group.

There are many people who have contributed to my grad school experinece, many of them professors: Bill Reay, Ron Sidwell, Mike Shaevitz, Randy Johnson, and Bob Bernstein. I'd like to mention a number of the graduate students at KSU: Patrick Berghaus, Daniel Mihalcea, Shih-Wen Yang, Arun Tripathi, Chris Verzani, James Norris, Alice Churukian, Alicia Allbaugh, and Ridvan Unal. I'd also like to mention the NuTeV graduate

students who've learned with me: Dave Mason, Sergie Avvakumov, Artur Vaitaitis, Bonnie Fleming, and Joe Formaggio.

I would like to thank three undergraduates who hopefully didn't suffer too badly by having me advise them, and who certainly taught me a lot about how to teach. They are Mark Herynk, Jenna Burroughs, and Jasmine Foster.

Finally I would like to thank my family. My parents have supported my decision to go to grad school while making it clear that it wasn't necessary in their eyes. I thank My siblings for their support. Most importantly I thank my wife Julie Alton. She encouraged me to start graduate school and follow my intellectual desires. She then promptly started encouraging me to finish graduate school. I'm sure it would have taken many more years without her. She endured many long conversations about quarks, leptons, colors and flavors, none of which entertained her nearly as much as they entertained me. She has read most of this thesis multiple times in order to make it more readable. I love her and thank her for all she's done to make this happen.

TABLE OF CONTENTS

LIST OF FIGURES

LIST OF TABLES

Chapter 1

Introduction

NuTeV is a third generation deep-inelastic scattering(DIS) neutrino experiment. One of NuTeV's major improvements over previous experiments is the use of a high purity *sign selected* beam. The selected sign of the hadrons determine if they will produce a ν or an $\overline{\nu}$; positive for ν, and negative for $\overline{\nu}$. The sign-selected quadrapole-train(SSQT) has a rate of about 10^{-3} $\overline{\nu}(\nu)$ events in ν-mode($\overline{\nu}$-mode)

The purity of the beam allows us to look for *wrong sign muons*(WSMs). In ν-mode, we expect events with a μ^- so a single muon event with a μ^+ is a WSM. Similarly, a single μ^- appearing while running in $\bar{\nu}$-mode is a WSM. Wrong sign muons come from a variety of sources. The most interesting conventional source is neutral current charm production. An unconventional source would be production of charm or bottom from the flavor-changing neutral-current(FCNC) process $\nu + u \to \nu + c$ or $\nu + d \to \nu + b$.

The first case we examine is production of a charm anti-charm($c\bar{c}$) pair through gluon-boson fusion, which will be described in Sec. 2.5. This analysis starts with the ansatz that there is no *intrinsic* charm in the nucleon,

and that all charm is due to gluon-boson fusion. The case of single charm production via a neutral current exchange is not allowed in the Standard Model(SM) of electroweak physics and will be discussed further in Sec. 2.5.

No one has ever observed neutral current open charm production in neutrino interactions. In gluon-boson fusion the charm mass suppresses the production of neutral current charm by a factor of $\sim 1 - 4m_c^2/\hat{s}$, where $\sqrt{\hat{s}}$ is the effective neutrino-gluon center-of-mass energy. For this reason, it should be possible to measure the charm mass in neutral current interactions. One can test whether the charm mass will be the same as the value measured in charged current charm production, 1.31 $\pm$ .24 GeV/c^2 at leading order(LO)[29] and 1.70$\pm$.19 GeV/c^2 at Next-to-Leading order(NLO)[32]). One can also determine whether the NC charm mass is the same as the value extracted from charmonium spectroscopy(values in the range of 1.33 GeV/c^2 to 1.54 GeV/c^2)[33, 34, 35] and photon-gluon fusion. Differences in the charm mass might point to new physics; such as flavor-changing neutral currents, intrinsic charm, or an additional mechanism for charm production not covered by our model. Since the only external input to the gluon-boson fusion model is the gluon distribution, the WSM event rate may also constrain this distribution.

The remainder of this thesis is organized as follows: Chapter two gives an introduction to the physics. Chapter three describes the experimental apparatus. Chapter four discusses data reconstruction and event selection. Chapter five describes simulations used for backgrounds and signal sources. Chapter six discusses the fit to $\bar{\nu}$-mode beam impurities. Chapter seven gives the results of the m_c measurement and the cross section $\sigma_{\nu+N\to c\bar{c}X}$. Chapter eight gives the results of the FCNC analysis. Chapter nine gives some concluding remarks. Details of the neutral current charm cross section and the beam simulation are included in Appendices A and B, respectively.

Chapter 2

Theoretical Motivation

2.1 The Standard Model

The Standard Model(SM) is a description of the fundamental particles and fields in nature. The model includes four forces: strong, electromagnetic, weak, and gravitational. The electromagnetic and weak forces have been combined into a common electroweak force [2, 4]. The dynamics of each force are determined by an underlying gauge symmetry[1]: $SU(3)$-color for the strong interaction, $SU(2)$ weak isospin for the weak force, and $U(1)$ charge symmetry for the electromagnetic force. Collectively the theory obeys an $SU(3) \otimes SU(2) \otimes U(1)$ symmetry. Forces are propagated through fields of bosons. The strong force is propagated by eight types of gluons(g), and the electroweak force is propagated by the photon (γ), Z^0, and $W^{\pm}$.

The fundamental fermions of the SM are given in Table 2.1. Fermions are divided into two types, leptons and quarks. Quarks combine to form all the hadrons one finds in the world. Quarks are held together by the strong nuclear force, which is explained by the theory of quantum chromodynamics(QCD)[5, 6]. QCD is a three charge force. The three charges are usually given the

Table 2.1: The particles of the standard model

Type	First Generation	Second Generation	Third Generation	Strong	EM Charge	Weak
Quarks	up(u)	charm(c)	top(t)	Y	Y	Y
	down(d)	strange(s)	bottom(b)	Y	Y	Y
Leptons	electron(e)	muon(μ)	tau(τ)	N	Y	Y
	e-neutrino(ν_e)	μ-neutrino(ν_μ)	τ-neutrino(ν_τ)	N	N	Y

names red, green and blue. According to QCD, in order for a particle to exist it must be color neutral, or, more formally, it must belong to a singlet of $SU(3)$. The simplest two types of color neutral particles are mesons and baryons. A meson, composed of a quark and an anti-quark, is the singlet of $3 \otimes \bar{3}$. It can be thought of as color neutral because the anti-quark has the anti-color of the quark. A baryon, composed of three quarks or three anti-quarks, is the singlet of $3 \otimes 3 \otimes 3$. It can be thought of as color neutral because red + blue + green =white.

2.2 Neutrino Interactions

This experiment uses neutrino and anti-neutrino beams to study the forces of nature and the structure of matter. Neutrinos are utilized because, as point-like particles, they interact in a way that is well understood. Neutrinos interact through exchange of a $W^{\pm}$ or a Z^o. When the interaction is through the $W^{\pm}$ the neutrino transforms into a charged lepton of the same generation, and this is referred to as a charged current(CC) event. When the interaction is through the Z^0 the neutrino stays a neutrino; this is a neutral current(NC) event. This section will introduce the kinematics of a charged current event, and of charged current charm production. As will be

apparent, an immediate drawback of neutrinos is that for neutral current interactions it is impossible to reconstruct the kinematics of each event.

2.2.1 Charged Current Kinematics

The Feynman diagram for a charged current(CC) event is shown in Fig. 2.1. The four-momenta for the incoming $\nu(k)$ and quark(xP), and the outgoing $\mu(k')$ are labeled. For CC events, four variables are measured: the hadron energy (E_{had}), the muon energy (E_μ), and the angles of the muon (θ_μ,ϕ_μ). From these parameters, one can determine the neutrino's energy (E_ν) and the kinematics of the interaction.

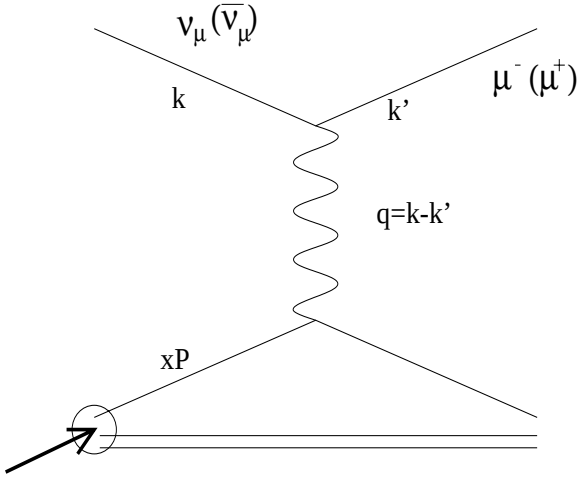

Figure 2.1: Kinematics of Neutrino Nucleon Scattering.

The four-momenta of the lepton and hadron in the lab frame are, explicitly:

$$k = (E_\nu, 0, 0, E_\nu) \tag{2.1}$$

$$k' = (E_\mu, p_\mu \sin\theta_\mu \cos\phi_\mu, p_\mu \sin\theta_\mu \sin\phi_\mu, p_\mu \cos\theta_\mu)$$

$$P = (M, 0, 0, 0)$$

$$P' = P + q = P + (k - k')$$

These equations enable one to determine the squared momentum transfer to the hadronic system (Q^2), the fraction of momentum carried by the struck parton (x), and the inelasticity (y).

$$Q^2 = -q^2 = (k - k')^2 = m^2 + 2E_\nu(E_\mu - p_\mu cos\theta_\mu) \tag{2.2}$$

$$x = \frac{-q^2}{2P \cdot q} = \frac{Q^2}{2ME_{had}} \tag{2.3}$$

$$y = \frac{P \cdot q}{P \cdot k} = \frac{E_{had}}{E_\nu} \tag{2.4}$$

2.2.2 Charged Current Charm Production

The charged current data sample contains a small number of events with two oppositely charged muons. Almost all of these *dimuons* arise from the charged current charm production process shown in Fig. 2.2. There is a small additional contribution to the dimuon sample due to a π or K in the hadronic shower of a CC event decaying before it interacts hadronically (π/K decay).

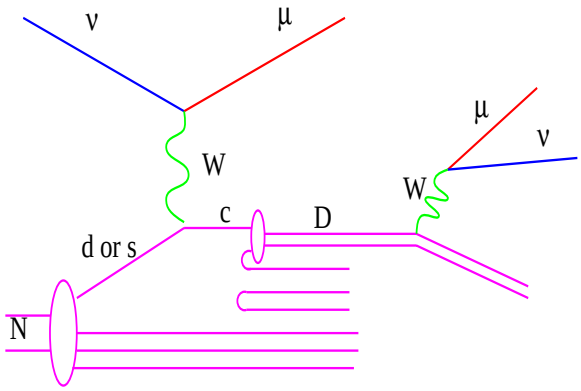

Figure 2.2: Kinematics of charged current charm production.

Charged current charm production takes place when a W boson interacts with a strange quark. It also happens when the W interacts with a down

quark, however this is suppressed by the V_{cd} matrix element(see Sec. 2.5.1).

2.3 The Parton Model and QCD

One calculates the cross section using Fermi's Golden Rule:

$$d\sigma = \frac{2\pi}{\hbar} d\Gamma \frac{|M|^2}{\Phi}, \tag{2.5}$$

where $d\Gamma$ is the phase space factor, Φ is the flux, and $|M|^2$ is the squared matrix element. The matrix element squared is the probability of transition from the initial state to the final state. Feynman rules describe in detail how to find the matrix element[6] in terms of a leptonic current coupled to a hadronic current through a propagator. For neutrino nucleon scattering, the propagator and lepton current are well understood; however, the hadronic current must be empirically determined. When the matrix is squared the hadronic term can be represented by a tensor $W^{\alpha\beta}$, constructed from p^μ and q^μ. The most general tensor that satisfies Lorentz invariance is of the form:

$$W^{\alpha\beta} = W_1 g^{\mu\nu} + \frac{W_2}{M^2} p^\mu q^\nu - \frac{W_3}{2M^2} \epsilon^{\mu\nu\alpha\beta} p_\alpha p_\beta + \frac{W_4}{M^2} q^\mu q^\nu + W_5 \frac{p^\mu p^\nu + q^\mu p^\nu}{M^2} + W_6 i \frac{p^\mu p^\nu - q^\mu p^\nu}{M^2}, \tag{2.6}$$

where the W's are functions of q^2,$q \cdot P$, and M_p^2, $\epsilon^{\mu\nu\alpha\beta}$ is the totally anti-symmetric Tensor, and $g^{\mu\nu}$ is the relativistic metric. W_4,W_5, and W_6 only contribute to the cross section at the order of the lepton mass, so one neglects them at high energies. Contracting $L_{\mu\nu} W^{\mu\nu}$ in the high energy limit yields:

$$L_{\mu\nu} W^{\mu\nu} = 2 E_\nu E_\mu \left\{ 2 \sin^2 \frac{\theta_\mu}{2} W_1 + cos^2 \frac{\theta_\mu}{2} W_2 \mp W_3 \frac{(E_\nu + E_\mu)}{M} \sin^2 \frac{\theta_\mu}{2} \right\}. \tag{2.7}$$

2.3.1 The Parton Model

The parton model begins by imagining a frame of reference in which the proton is moving ultra-relativistically; this is known as the infinite momentum frame. In this frame, the mass of the proton is negligible. Now, assume that the proton is built of a number of parts(partons). In this frame, the partons are all traveling at the speed of light, and collinear with the proton. The struck parton's final momentum obeys:

$$(xP + q)^2 = m^2 = 0, \tag{2.8}$$

$$x^2P^2 + 2xP \cdot q + q^2 = 0. \tag{2.9}$$

Because $x^2P^2 \ll -q^2$, Eq. 2.9 simplifies to:

$$x = \frac{-q^2}{2P \cdot q} = \frac{Q^2}{2M\nu}. \tag{2.10}$$

The relationship between q^2 and $P \cdot q$ was predicted by Bjorken [7]. This hypothesis presents the idea that as $q^2 \to \infty$ and $\nu \to \infty$ the structure functions remain finite; so they must depend only on the ratio of these two quantities. With this observation the cross section is usually rewritten as:

$$\frac{d^2\sigma^{\nu(\bar{\nu})}}{dxdy} = \frac{G_F^2 ME}{\pi}\left[(1-y)F_2^{\nu(\bar{\nu})}(x) + \frac{y^2}{2}2xF_1^{\nu(\bar{\nu})}(x) \pm y\left(1-\frac{y}{2}\right)xF_3^{\nu(\bar{\nu})}(x)\right]. \tag{2.11}$$

In the parton model, one considers scattering of neutrinos by free quarks, anti-quarks and gluons. Neutrinos always have left-handed helicity, and they only interact with left-handed particles or right handed anti-particles. In the center of mass frame, the neutrino collides head on with the parton. The neutrino-quark system forms a spin 0 state, and is thus spherically symmetric. The neutrino-anti-quark system forms a spin 1 state, and thus has a $(\frac{1+\cos\theta^*}{2})$ cross section dependence. In the case of a neutrino interacting

with a spin 0 particle (should such a particle exist in the nucleon), one acquires an additional $2\cos\frac{\theta^*}{2}$ term in the cross section. Since θ^* is related to y by the relation:

$$1 - y = \frac{1 + \cos\theta^*}{2}$$

one finds:

$$\frac{d\sigma^{\nu q}}{dy} = \frac{d\sigma^{\bar{\nu} q}}{dy} = \frac{G_F^2 s}{\pi}, \tag{2.12}$$

$$\frac{d\sigma^{\nu \bar{q}}}{dy} = \frac{d\sigma^{\bar{\nu} q}}{dy} = \frac{G_F^2 s}{\pi}(1-y)^2, \tag{2.13}$$

$$\frac{d\sigma^{\nu k}}{dy} = \frac{d\sigma^{\bar{\nu} k}}{dy} = \frac{G_F^2 s}{\pi} 2(1-y). \tag{2.14}$$

One define $q(x, Q^2)$,$\bar{q}(x, Q^2)$, $k(x, Q^2)$ to be the probability of finding a particle of the appropriate type with fractional momentum x inside the nucleon. This leads to the neutrino nucleon cross-section:

$$\frac{d^2\sigma^{\nu N}}{dxdy} = \frac{G^2 xs}{\pi}[q(x) + \bar{q}(x)(1-y)^2 + k(x)2(1-y)], \tag{2.15}$$

$$\frac{d^2\sigma^{\bar{\nu} N}}{dxdy} = \frac{G^2 xs}{\pi}[q(x)(1-y)^2 + \bar{q}(x) + k(x)2(1-y)]. \tag{2.16}$$

Comparing to Eq. 2.11, one can make the identifications:

$$2xF_1 = xq(x) + x\bar{q}(x), \tag{2.17}$$

$$F_2 = xq(x) + x\bar{q}(x) + 2k(x),$$

$$xF_3 = xq(x) - x\bar{q}(x).$$

2.3.2 Asymptotic Freedom

Asymptotic freedom is the idea that when a high energy projectile scatters off a parton, the parton recoils as if it were a free particle. In high energy

scattering, the scatter takes place on a much shorter time scale than interactions among the nucleon's constituents. Theoretical support for asymptotic freedom can be found in the "running" of the strong coupling constant α_s. The strong coupling constant runs due to diagrams like Fig. 2.3; an analogous effect occurs in QED.

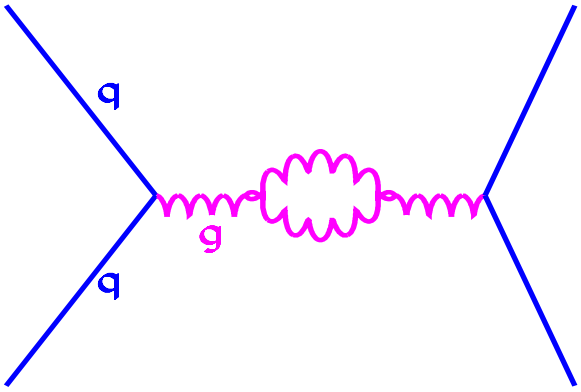

Figure 2.3: Gluon screening.

In electrodynamics, photon fluctuations into polarized e^+e^- pairs screen the real particle's electric charge. This effectively reduces the charge of those particles. In QCD a similar screening effect occurs for gluon fluctuations into $q\bar{q}$ pairs, but gluons also fluctuate into gluon pairs producing an anti-screening effect. Gluon pairs effectively increase the real quarks charge so that as $q^2 \to 0$, $\alpha_s \to \infty$. In leading order

$$\alpha_s(|q^2|) = \frac{\alpha_s(\mu^2)}{1 + (\alpha_s(\mu^2)/12\pi)(11n - 2f)\log(|q^2|/\mu^2)} \tag{2.18}$$

where n is the number of colors, f is the number of flavors and μ is determined by experiment such that $\alpha_s(\mu^2) \ll 1$ to justify using perturbation theory. Often times α_s is presented in terms of Λ_{QCD} where

$$\log \Lambda^2_{QCD} = \log \mu^2 - \frac{12\pi}{[(11n - 2f)\alpha_s(\mu^2)]} \tag{2.19}$$

and

$$\alpha_s(|q^2|) = \frac{12\pi}{(11n - 2f)\log(|q^2|/\Lambda^2_{QCD})} \tag{2.20}$$

From these equations one sees that the strong force is weaker at large $|q^2|$ or, equivalently, short distances.

If $\Lambda_{QCD} \ll -q^2$ the perturbative description of QCD is valid. When $\Lambda_{QCD} \simeq q^2$, asymptotic freedom breaks down, and the parton model is not valid. The value of Λ_{QCD} is around 200 MeV[77].

2.4 The Charm Mass

Since, similar to lunch, there is no such thing as a free quark, what does one mean when one refers to the mass of the charm quark? A naive method to determine m_c would be to take half the pion mass as the mass of both the up and down, then from the D meson($c\bar{u}$) mass one would find m_c to be $\sim$ 1.8 GeV/c^2. However the Λ_c baryon (udc) would indicate m_c should be more like 2.1 GeV/c^2, and the J/ψ meson ($c\bar{c}$) indicates 1.55 GeV/c^2. This simple model is too naive as binding energy is often more important than the quark's actual mass. The charm mass parameter differs depending on what process one is studying or what model one is using. In perturbative QCD(pQCD), however, m_c can be defined consistently.

2.4.1 Charged Current Production

The mass of the charm quark in charged current charm production is known to be in the range from 1.1 to 1.7 GeV/c^2. If m_c is not negligible compared to Q^2, Eq. 2.9 is not true. Instead the fraction of the momentum ξ is obtained by solving

$$\xi^2 P^2 + 2\xi P \cdot q + q^2 = m_c^2, \tag{2.21}$$

which yields

$$\xi \simeq x\left(1+\frac{m_c^2}{Q^2}\right)\left(1-\frac{x^2M^2}{q^2}\right). \tag{2.22}$$

The substitution of x for ξ in parton cross section models is, for historical reasons, called "slow rescaling"[31]. The slow rescaling procedure has been used to perform a number of analyses of CC charm production[32]. In a leading order (LO) analysis of charged current charm, it is assumed that all of the charm is produced from d and s quarks. In a next-to-leading order(NLO) analysis charm is assumed to also come from gluon-boson fusion process that involve $c\bar{s}$ or $s\bar{c}$ production. The LO analyses result in charm mass measurements of 1.31 $\pm$ 0.24 GeV/c^2[29] or 1.79 $\pm$ 0.38 GeV/c^2[30], while a NLO analysis gives 1.70 $\pm$ 0.19 GeV/c^2 [32].

2.4.2 Charmonium

Bound states of $c\bar{c}$ are referred to as charmonium. The charmonium spectrum can be seen in Fig. 2.4 and is labeled in the standard spectroscopic manner $^{2S+1}L_J$ where S, L and J are the intrinsic spin, orbital angular momentum, and total angular momentum, respectively, of the $c\bar{c}$ system.

Charmonium is in first approximation a nice two body problem that can be solved by analogy to the positronium system. For charmonium the binding energy is an order of magnitude smaller than the charm mass, justifying the use of non-relativistic formalism. The energy level spacing between states allows one to determine m_c. A thorough discussion can be found in the analyses of charmonium spectrum, which give values of the charm mass from 1.33 to 1.54 GeV/c^2 [33, 34, 35].

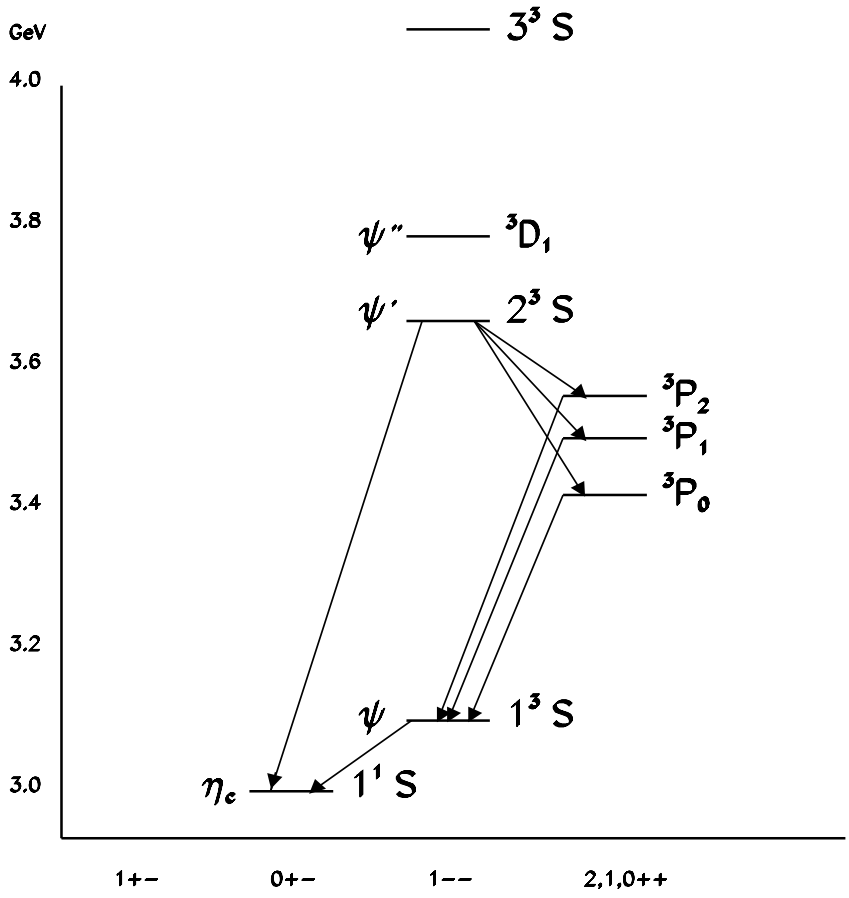

Figure 2.4: Observed charmonium spectrum.

2.4.3 Photoproduction

Collisions between a photon and nucleon can produce charm through a process known as photon-gluon fusion as shown in Fig. 2.5. This process can be thought of as a gluon temporarily splitting into a quark anti-quark pair and the photon striking one of the quarks.

Photon-gluon fusion has been tested over a large range of kinematics, from the high energies of HERA[12, 13] down to the fixed target experi-

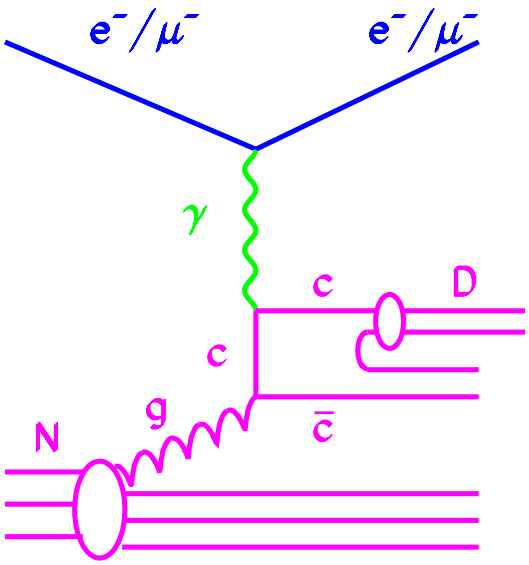

Figure 2.5: Photoproduction with a virtual photon.

ments like EMC[15], FOCUS [18] and FNAL-E687[18]. HERA and EMC use charged leptons to scatter off hadronic targets. A virtual photon, emitted from the lepton, interacts with a gluon, emitted from the hadron, and produces charm quarks. FOCUS and E687 scatter a beam of photons off hadrons and photoproduce as shown in Fig. 2.6.

The photon-gluon cross section depends directly on the charm mass and the gluon distribution of the nucleon. A NLO QCD analysis yields $m_c = 1.74^{+0.13}_{-0.18} GeV/c^2$[36].

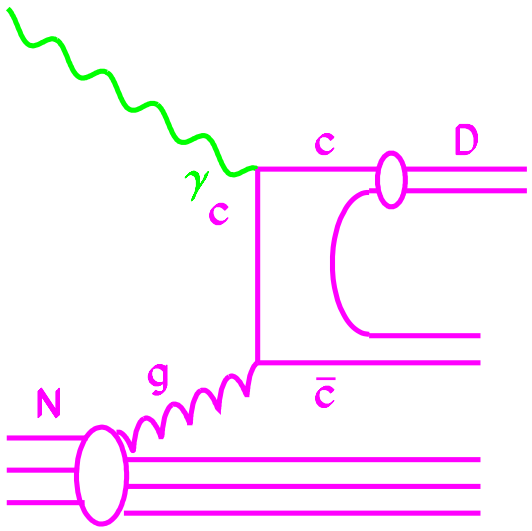

Figure 2.6: Photoproduction with a real photon.

2.5 Neutral Current Charm Production

Charm can be produced in a neutral current neutrino scattering interaction as indicated in Fig. 2.7. In this case a gluon in the nucleon temporarily splits into a $c\bar{c}$ pair, and the Z boson interacts with one of these quarks. This is simply the weak analog to photon-gluon fusion, with a couple of subtle differences. The mass of the propagator(Z^0) will give preference to higher Q^2 interactions relative to electromagnetic probes. The other difference is that photoproduction is purely vector, while the weak force has both a vector and an axial vector component.

Neutral-current open charm production has been studied in both a collider environment[12, 13] and in a fixed target experiment [15]. However, all

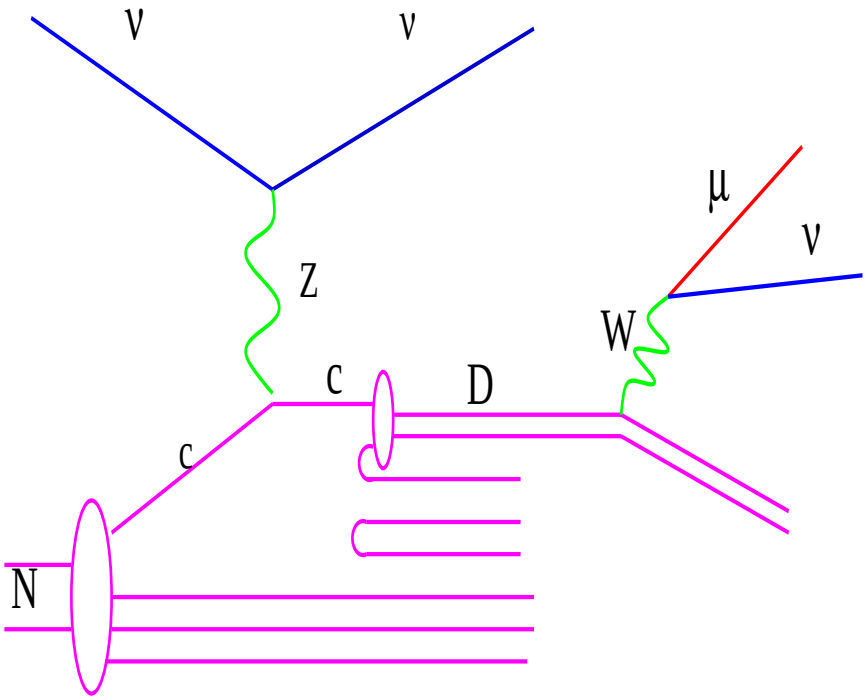

Figure 2.7: Kinematics of neutral current charm production.

of these experiments used a charged lepton, and therefore they were dominated by photon-gluon fusion. Our experiment uses a neutrino beam, and thus looks exclusively at the Z boson-gluon fusion. One assumes that boson-gluon fusion occurs in a similar fashion to photon-gluon fusion, however Z boson-gluon fusion has not yet been observed.

In addition to demonstrating the existence of Z boson-gluon fusion, neutral current charm production provides a good probe of the charm mass (m_c) and the gluon distribution(g(x)). The cross section is very sensitive to these parameters because it is basically integration of a function of m_c times the gluon distribution with integration limits of ξ and a, where:

$$a = \frac{1}{1 + 4m_c^2/Q^2} \tag{2.23}$$

Details of the cross section calculations may be found in Ref. 11 and Appendix A.

2.5.1 Alternative Neutral Current Charm Production

While photon-gluon fusion is the SM form of neutral-current charm production, there are a couple of alternative forms of neutral-current charm production. The first form allows for a intrinsic charm content of the nucleon, and is a SM process. The second is FCNC production of charm, and goes beyond the SM.

Some phenomenologists [8, 9] claim that there may be a charm sea, in analogy to the strange sea. The strange quark is a unique situation[11]. The mass of the strange quark is much smaller than the q^2's we are dealing with. However, the charm mass is about the same as the q^2. This analysis assumes $c(x, Q^2) \simeq 0$ in our Q^2 regime. This hypothesis can be checked with our data, because an unexpectedly low m_c from gluon-boson fusion model might imply the presence of a charm sea.

One could ask why one does not consider production of charm off the $u(x)$ distribution in the same way that one can produce charm off the $d(x)$ distribution. This type of reaction is called a flavor-changing neutral-current and is forbidden by the Standard Model[3]. The weak eigenstates of the down-like quarks are admixtures of the mass eigenstates of the down-like quarks:

$$V = \begin{pmatrix} d' \\ s' \\ b' \end{pmatrix} = \begin{pmatrix} V_{ud} & V_{us} & V_{ub} \\ V_{cd} & V_{cs} & V_{cb} \\ V_{td} & V_{ts} & V_{tb} \end{pmatrix} \begin{pmatrix} d \\ s \\ b \end{pmatrix} \tag{2.24}$$

This is the CKM matrix which is assumed to be unitary. Because $V^\dagger V = 1$ there are no cross terms in the NC processes and hence no flavor-changing neutral-currents.

2.6 Neutral Current Charm Production of Wrong Sign Muons

It is possible to isolate the fraction of neutral-current charm events in which a ν strikes the charm quark and the charmed meson decays to a muon because this gives a final state wrong signed muon:

$$\begin{aligned} \nu_\mu + c &\rightarrow \nu_\mu + c \\ &\hookrightarrow D^+/D^0 \\ &\hookrightarrow \mu^+. \end{aligned} \tag{2.25}$$

Similarly one can isolate the cases of $\bar{\nu}$ striking charm anti-quarks and the anti-charmed meson decaying to a muon.

$$\begin{aligned} \bar{\nu}_\mu + \bar{c} &\rightarrow \bar{\nu}_\mu + \bar{c} \\ &\hookrightarrow D^-/\bar{D^0} \\ &\hookrightarrow \mu^-. \end{aligned} \tag{2.26}$$

2.7 Other Sources of Wrong Sign Muons

Wrong sign muons(WSM's) come from a variety of sources, one being the neutral current charm described above. Other sources will be referred to as backgrounds.

The dominate background source of WSM's is beam impurities. Approximately 0.1% of the interactions in ν-mode are from $\bar{\nu}_\mu$s, with a similar rate for $\bar{\nu}$-mode. Beam impurities come mainly from secondary interactions

in the beamline("scraping"), μ decay and charmed hadrons produced in the target and dump. Charmed hadrons ($D^{\pm}$,D^0,$\bar{D}^0$, and Λ_c) decay promptly, and produce a wide spectrum of both varieties of neutrinos. Beam impurities from charm are especially important because they reach higher energies than ν from scraping. Beam impurities also come from K_L decays, wrong charged hadrons which decay before sign selection, and $K \rightarrow 3\pi$ cascade decays ; however, these are smaller sources.

Another important background source of WSM's is charged current charm production. When a dimuon is produced from CC charm production the second muon is of the wrong charge. If the primary muon is of a low enough energy or at a wide angle the primary muon might not be identified. In $\nu(\bar{\nu})$-mode 1.9(1.3)% of the beam is ν_e and when these generate CC charm the primary lepton will be an electron which will always get lost in the hadron shower. In these cases, the event is identified as a WSM. Notice that π/K decay mentioned in Sec. 2.2.2 can lead to WSM's if it creates a dimuon where the primary muon is undetected. Pion or kaon decay can also lead to a WSM if it occurs in a neutral-current event.

The final source of WSM's is charge mis-measurement in the toroid. A muon's energy and charge can be incorrectly measured in a couple of ways: First, if the muon suffers a hard scatter with the iron the muon may reconstruct with a different energy or even the wrong charge. Second, the muon can interact and produce a shower of secondary tracks which might get used in the track reconstruction instead of the real muon track.

Chapter 3

The Experimental Apparatus

This chapter gives a brief description of the experimental apparatus used in conducting NuTeV(FNAL-E815). It consists of sections which describe the beam-line, the main detector, and the calibration beam. An instrumented "decay channel" upstream of the calorimeter also existed[14], but it is not relevant for this analysis.

3.1 The Sign Selected Neutrino Beam

NuTeV's beam-line is call the Sign-Selected Quadrupole Train(SSQT) [10]. Figure 3.1 shows the path which turns the Tevatron's protons into NuTeV's neutrinos.

The Tevatron collides 800 GeV protons with a beryllium oxide(BeO) target. Beryllium oxide was chosen because low-Z materials are more efficient for producing neutrinos, and BeO has good thermal and structural properties. Interaction between protons and the target produces many hadrons, mainly pions and kaons. If operating in neutrino mode, a dipole magnet di-

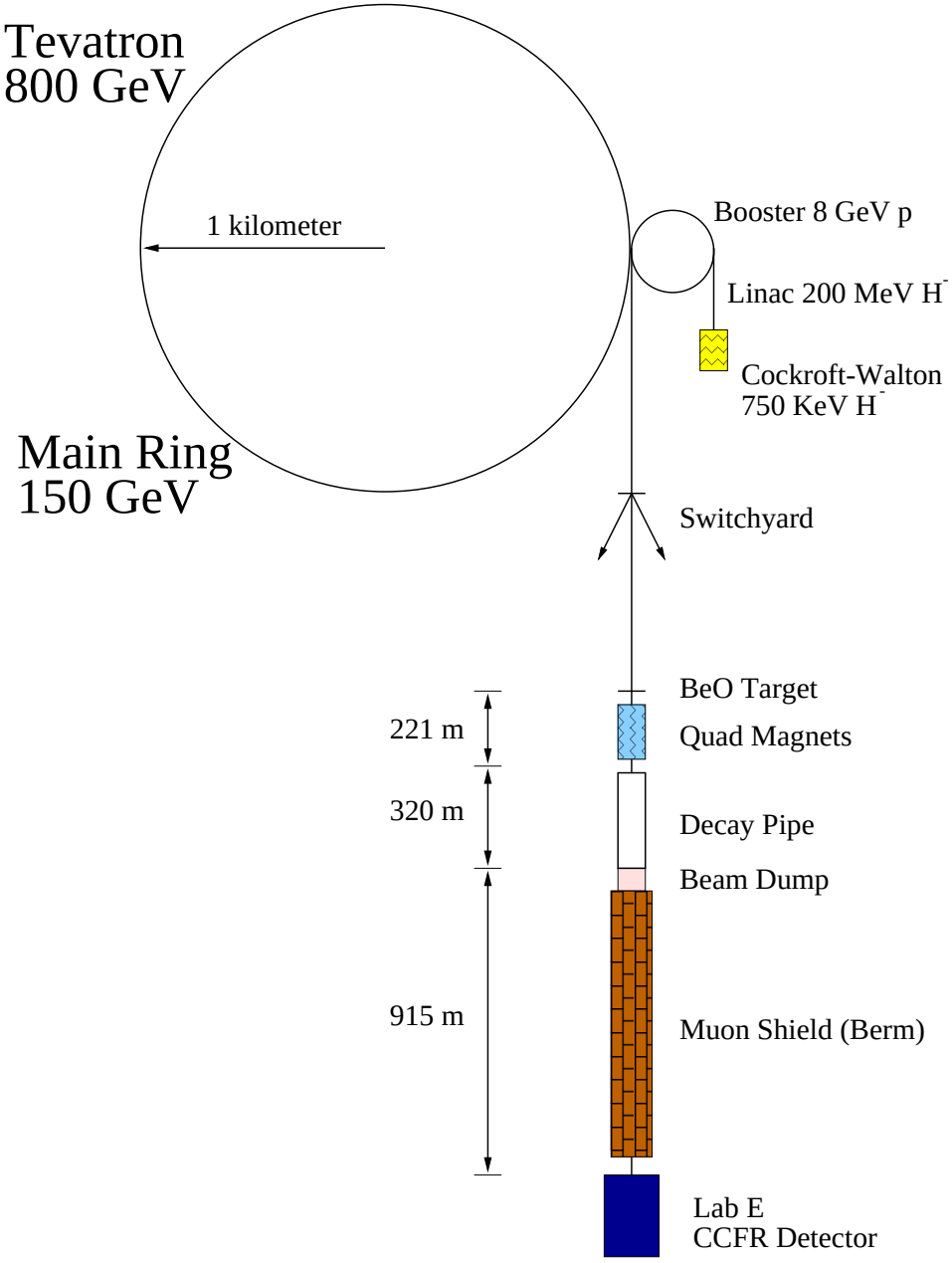

Figure 3.1: The Fermilab Tevatron and neutrino-beamline.

rects positively charged particles down the beam line, and forces negatively charged particles into a dump. In anti-neutrino mode positively charged particles are directed into a dump by magnets, and negatively charged particles are directed down the beam line.

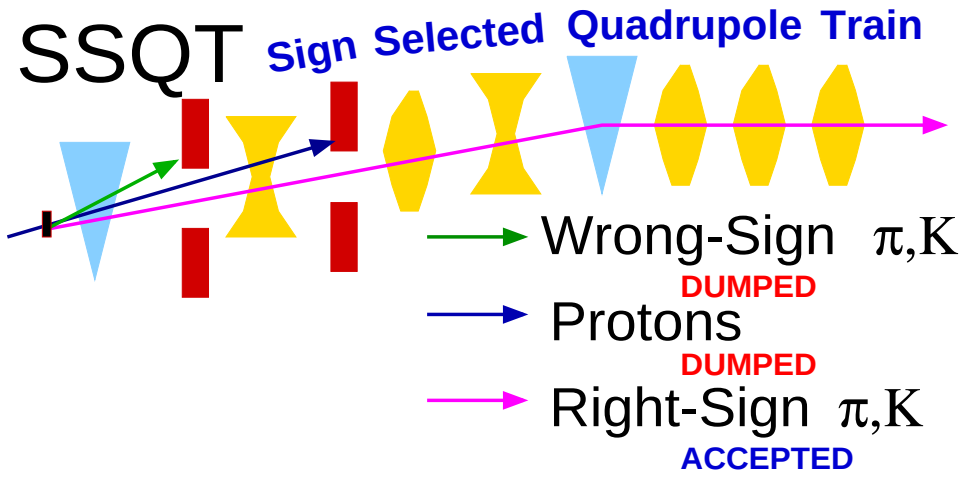

Figure 3.2: The SSQT beamline.

After traveling through the magnets shown in Fig. 3.2 the beam consists of π's, K's and p's of the correct sign with momenta distributed about 250 GeV/c. This beam of secondaries travels down a 320m decay pipe in which about 5% of them decay into a muon and a neutrino of the appropriate type. After this comes a muon shield, known as the berm, consisting of 915m of iron, earth and other absorbers. All muons produced in the decay pipe stop in the berm, leaving neutrinos to arrive at the main detector. Some fraction of the neutrinos interact in the downstream portion of the berm and the muons from these interactions can make it to the main detector. These muons are called straight through muons and are used for alignment and calibration.

Neutrino interactions look similar to cosmic rays, and neutrinos interact

very rarely. Thus, it is better to have a short-burst, high intensity beam, rather than a less intense "slow spill". To satisfy these requirements the proton beam to the neutrino area has a ping structure. Over a 60 second interval there are up to five 4 ms long pings of 10^{12} protons which strike the target. The period of time during which neutrinos arrive at the main detector is referred to as the neutrino gate, or fast gate. The rest of the cycle is the slow gate. The slow gate is used to take calibration events and cosmic ray events for background studies.

3.2 The Lab E Detector

The detector, shown in Fig. 3.3, weighs over 1000 tons and is approximately 3 meters tall, 3 meters across, and 28 meters long. The upstream 18 m comprises the calorimeter target; the last 10 meters is the toroid spectrometer. The calorimeter has a basic structure of one drift chamber, one sheet of iron, a scintillation counter, two sheets of iron, a scintillation counter, and one sheet of iron that repeats 42 times. This detector has been used for many years, and the details of its construction can be found in several places[39][57].

Scintillation counters are used in a calorimeter to measure the hadronic energy(for a full discussion of calorimetry see Ref. 19). The basic principle of a calorimeter is that primary particles interact, creating secondary particles which will also interact, forming a shower of hadrons. The detector then "samples" (counts the number of particles in) the shower at a number of different places throughout the shower. The basic unit for counting is the energy given off by one minimum ionizing particle (MIP) as it passes through the counter. The number of particles is proportional to the energy of the

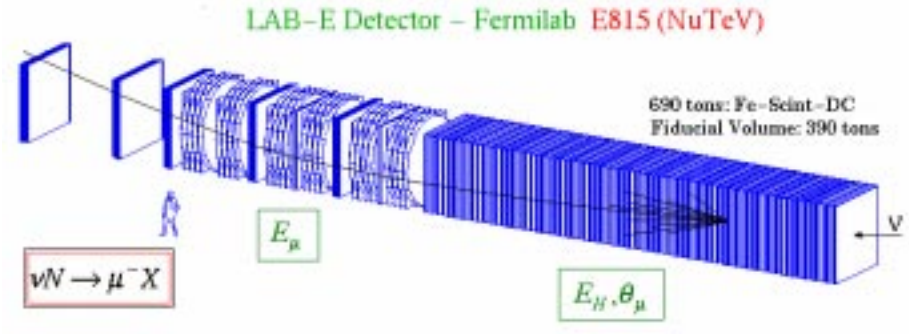

Figure 3.3: NuTeV's main detector.

primary particle and from this we determine the energy of the hadronic component of the interactions energy. NuTeV's calorimeter samples about 5% of the hadronic energy and has a hadron resolution of

$$\frac{\sigma_E}{E} = 0.024 \oplus \frac{87.4\%}{\sqrt{E}} \oplus \frac{4.38 \times 10^{-6}}{E} \tag{3.1}$$

The energy that the muon has when it enters the toroid is known as EMUFF, which stands for E_μ at the front face of the toroid. This energy is measured by the toroid spectrometer. The muon also loses energy as it travels from the vertex to the spectrometer. The portion due to dE/dx is reconstructed using the pulse heights measured by the counters after the shower. The toroid has a resolution of $\frac{\Delta E_{\mu ff}}{E_{\mu ff}} = 11\%$, which is dominated by multiple Coulomb scattering. The dE/dx is usually a small fraction of the muons energy, and is known to much better then 11%. The results is that $\frac{\Delta E_\mu}{E_\mu} = 11\%$.

The toroid spectrometer measures the muon momentum and the charge of the muon. A charged particle in a magnetic field bends with a radius of curvature which is proportional to its momentum. A measure of the radius of curvature hence determines the momentum. The polarity of the magnets is changed to focus the type of muons that are produced by the beam. It focuses positive muons in anti-neutrino mode and negative muons

in neutrino mode. Note that WSM's are always de-focused. The toroid consists of 3 sets of toroidal magnets separated from each other by a set of drift chambers. The chamber regions are called gaps. Of importance to this analysis is the second gap, where, in addition to chambers, there is a large very efficient counter called T2. T2 is part of the charged current trigger, which will be described bellow.

The data acquisition system only reads out information from these detectors when an event trips one of the triggers. NuTeV has 12 triggers to gather neutrino data, cosmic ray data, calibration events, pedestals and other types of events. The triggers are listed in Table 3.1; for this analysis the trigger of importance is trigger one. Trigger one looks for charged current events with toroid analyzed muons by searching for consecutive counters on in the main detector and a signal in T2.

3.3 The Calibration Beam

In order to convert light from scintillators into a measure of the energy one must know the constant of proportionality between the two. To determine these constants (one for hadrons and another for electrons) and calibrate the magnetic spectrometer, NuTeV constructed a calibration beam. The calibration beam delivered beams of hadrons, electrons and muons at known momenta over the energy range 5-200 GeV[22].

The calibration beam layout is shown in Fig. 3.4. It consists of a number of DC's and dipole magnets with variable power supplies, scintillator paddles, Cerenkov counter and a transition radiation detector(TRD). The DC's are used to track the particle. The magnets are adjusted so that particles

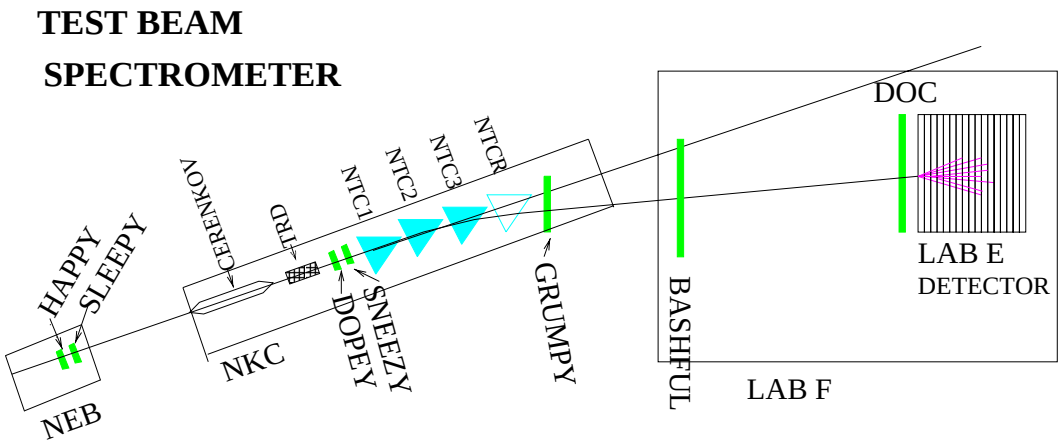

Figure 3.4: The NuTeV Testbeam spectrometer.

of the correct momentum are directed to the main detector. The tracking is used to measure the particles exact momentum in the same way that the toroid spectrometer measured E_μ. Scintillator paddles shaped to detect only particles which travel through the well understood portion of the magnet, generate a trigger. The Cerenkov and TRD allow one to differentiate between electrons and pions.

Trigger	*Name*	*Requirements*
1	Charged Current Trigger	• counters on upstream of toroid washer 1 • counters on in both toroid gaps • no upstream veto
2	Neutral Current Trigger	• energy deposition in calorimeter • no upstream veto
3	Range-Out/Exit Trigger	• 1/4 MIP in each of 16 non-consecutive counters • 4 GeV energy in any 8 adjacent counters • no upstream veto
4	Charged Current Trigger 2	• shower energy • hits in first cart upstream of toroid • muon track through one toroid quadrant
5	Test Beam Trigger	• slow spill
6	Straight through μ Trigger	• hits in each cart and one toroid quadrant
8	Cosmic Ray Trigger	• 40 counter muon requirement
10,11,12	Ped Triggers	• No other triggers

Table 3.1: Partial NuTeV trigger list with descriptions

Chapter 4

Data Analysis

This chapter will describe the data that is used in this analysis. It will focus on the selection criteria.

4.1 Event Reconstruction

A typical wrong-sign muon(WSM) event is shown in Fig. 4.1; note that the muon is bending out. A number of quantities are calculated for each event with a muon. Quantities of primary importance are hadronic energy, muon energy, and the angle at which the muon is emitted. Other quantities measured, such as the position of the interaction(the vertex) are mainly important in selecting events, and they will be discussed as they are encountered in the next section.

A software package called the "cruncher" takes raw information(DC times, counter pulse heights, etc) and calculates quantities of interest. The cruncher also "strips" out certain types of events. One of these "strips," called the "wrong charge out" strip, requires a trigger 1 in fast gate that

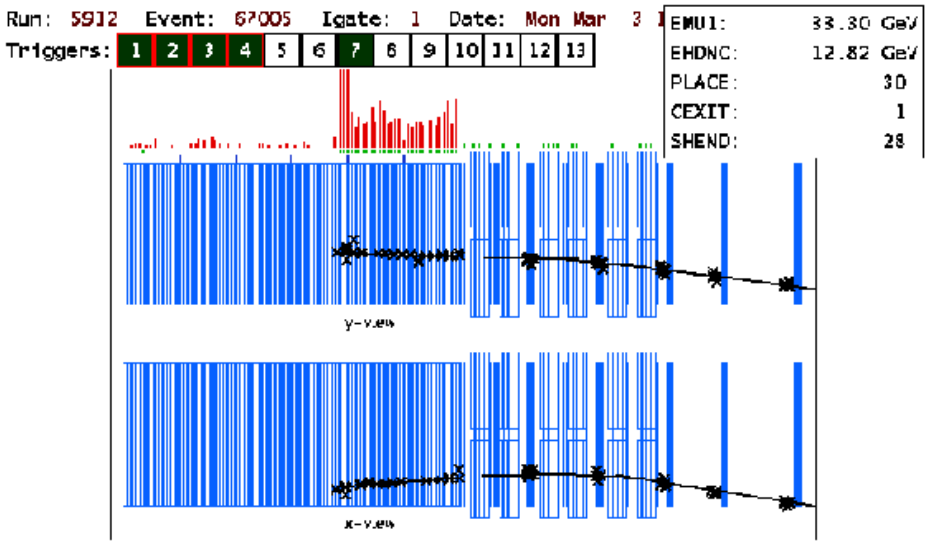

Figure 4.1: A typical wrong sign muon event.

passes loose fiducial volume cuts and has a toroid analyzed muon with a charge not equal to the toroid polarity. Further selection criteria, described below, are more restrictive than all of the requirements for the strip.

4.2 Selection Criteria

Selection criteria are chosen to reduce backgrounds in the WSM sample and to select a region in both real space and momentum space where one understands the response of the detector. Following are descriptions of the selection criteria("cuts"). Tables 4.1 and 4.2 summarize the percentage of events which pass each cut individually and cumulatively.

4.2.1 Fiducial Volume Definition

- $20 < Place < 80$: *Place* is a variable which defines the z location of the interaction. *Place* is the first of two consecutive counters with signals consistent with 4 or more MIPs. The counters are numbered starting with one at the front face of the toroid, and increasing to end at the most upstream counter, 84. This cut requires that the event started more then 4 counters downstream of the front of our detector, but at least 19 counters upstream of the end of the detector. This insures that interactions took place inside our detector and that the hadron shower is contained.

- "*Vertex Box*": The *vertex* of the event is its transverse interaction position. In a charged current event, it is measured by reconstructing the muon track and following it upstream to place. The interaction must take place more then 25 cm from the outer edges of the detector in the transverse directions. This insures containment of the hadron shower.

- "In Time": The muon track must have coincidence with the hadronic shower to within 36 ns. This suppresses cosmic ray events.

- Fitted Muon Track: The event is required to have a reconstructed track in both the calorimeter and the toroid. The toroid track must have a 'good fit', and must make it through the second gap. A 'good fit' means that the code which links together track segments in the calorimeter and each of the gaps manages to converge.

- Front Face Cut: It is required that the muon enter the front face of the toroid within a 163 cm radius. This insures that the muon travels through the region of well-understood magnetic field.

- T2 Cut: T2 is a counter in the second gap of toroid. The T2 cut requires that the muon passed through T2 less than 140 cm from the center, in both x and y. This insures that the muon passes through the active area of toroid DCs.

- 80% Time in Steel: The toroid consists of three sets of iron rings(washers). The washers have been cut in half and have a horizontal gap of about 5 cm. It is required that while the muon passed through the toroid it spent most(80%) of its time in the steel, and not in the gap or the hole of the toroid.

- "Hole Cut": This cut removes events in which the muon entered the field-free central hole of the toroid. The hole has a radius of about 13 cm so events which are reconstructed with a front face radius of less than 15 cm are removed.

Of the 22339 events in the WSM strip, 3497 events survive fiducial cuts. Of these, 2364 are in ν-mode and 1132 are in $\overline{\nu}$-mode. The conditions described in the following section are then imposed

4.2.2 Kinematic Cuts

- Angle: The muon's angle must be less then 0.15 radians ($\theta_\mu < 0.15$). This insures that the muon travels through the toroid no matter what PLACE value the event had.

- Hadron Energy: A minimum hadron energy of 10 GeV is required. This suppresses cosmic rays and limits the number of beam impurity events.

- Muon Energy: The muon energy is required to lie in the range 10 to 150 GeV. In addition $E_{\mu ff}$ must be larger then 5 GeV. This limits the

number of charge misidentification events.

4.2.3 Purity Cuts

- Charge: The charge of the muon must reconstruct to be the opposite sign as expected by the beam setting.

- Single Track: Dimuon events (see Sec. 2.2.2), where only the charm-generated muon is toroid reconstructed, form a large background. To limit this source only events where only one track is reconstructed in each view of the calorimeter are included.

- Misidentification: The muon's momentum is reconstructed three times. The first time uses only the target track and the track segment found after the first set of washers. It is then recalculated using these segments and the track segment found in the next gap. Both of these measurements are required to be within 25% of the measurement calculated using the entire track. This procedure suppresses charge mismeasurement.

Cut	*Cumulative Percentage*	*Individual Percentage*
Place	48.6	48.6
Vertex box	39.6	89.0
In Time	38.7	57.8
Calorimeter Track	34.0	57.7
Front Face	28.7	86.3
T2 Cut	23.7	45.8
Time in Steel	23.3	93.7
Toroid Track	18.6	53.2
Good Track	18.0	71.9
Two Gaps	17.9	51.0
Hole cut	17.2	94.0

Table 4.1: "Individual percentage" denotes data events passing each listed fiducial cut separately. "Cumulative percentage" refers to the percentage of events which pass all previous cuts.

mode	ν-mode		$\bar{\nu}$-mode	
Cut	*Cumulative*	*Individual*	*Cumulative*	*Individual*
Theta	99.7	99.7	99.4	99.4
Hadron Energy	72.3	72.6	56.4	56.6
Muon Energy	64.4	89.2	51.3	92.6
Charge	64.0	99.4	50.9	99.3
Dimuon	30.9	63.1	37.5	81.5
Misidentification	22.0	52.3	33.1	45.2

Table 4.2: "Individual percentage" denotes data events passing each listed fiducial cut separately. "Cumulative percentage" refers to the percentage of events which pass all previous cuts.

Chapter 5

Signal and Background Simulation

As mentioned earlier, there are four significant background sources of WSM's. The two dominant ones are beam impurities and incompletely reconstructed charged current charm production. Two lesser backgrounds are charge misidentification and π/K decay events. The fractions of WSM's due to individual sources are shown in Table 5.1. This chapter explains how these backgrounds and the neutral current charm signal are simulated.

NuTeV uses a fast, parametric monte carlo(MC) simulation called Numonte for most neutrino event generation. Numonte contains a consistent leading order(LO) and next-to-leading order (NLO) cross section model. Numonte does not reconstruct simulated events, but instead "smears" the distributions of observables using parameterizations. The "smearing" algorithms are based on calibration and straight-through muon data. This allows Numonte to run quickly; and, for this reason, it is often called the fast monte carlo.

NuTeV also has a "hit level" monte carlo called McNuTeV, which is based on the GEANT simulation package[26]. For this analysis, Numonte was used to generate the kinematics of events. These generated quantities were then written to a file that McNuTeV read in and processed. McNuTeV's output is in the same format as the raw data produced by the detector. This output is then "crunched" like the real data.

The fraction of WSM's due to each source is given in Table 5.1.

Source	ν-mode	$\bar{\nu}$-mode
Beam Impurity	68%	83%
Charged Current Charm	19%	8%
Charge Misidentification	4%	5%
Neutral Current Charm	6%	2%
Neutral Current π/K decay	1%	1%
Charged Current π/K decay	1%	1%

Table 5.1: Percentage of sources of WSM's in each mode.

5.1 Neutral Current Charm

Neutral current charm is simulated using the cross section for boson-gluon fusion from Ref. 11 implemented in Numonte. Details are found in both Ref. 11 and Appendix A. The gluon distribution, the only external information needed by this cross section, is obtained from the GRV94 parton distribution set.

It is also necessary to implement a fragmentation model of the $c\bar{c}$ system into mesons or baryons, and a decay model of the charmed hadrons into muons. These models consist of the following steps:

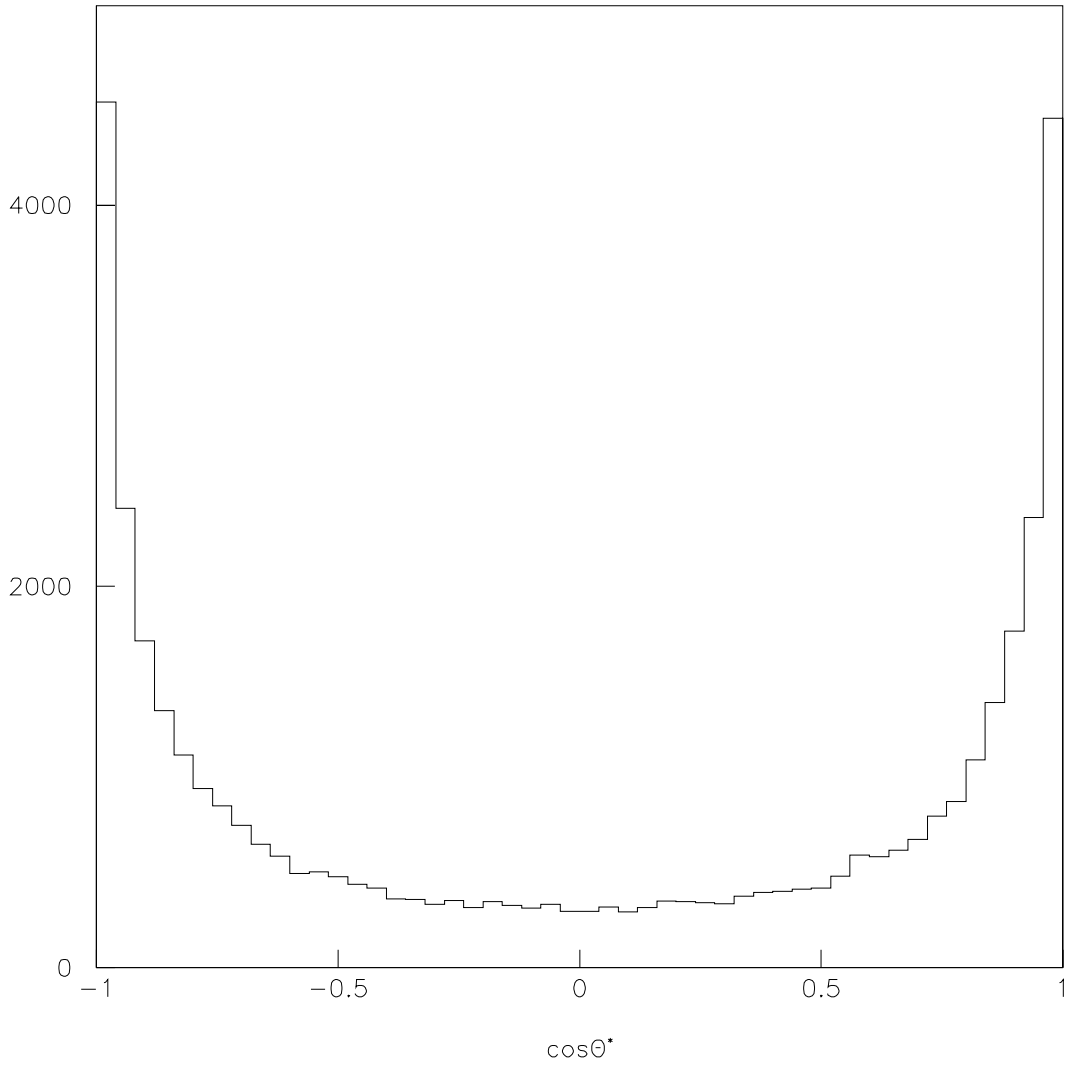

Figure 5.1: The simulated $\cos\theta^*$ distribution for the c quark.

- Determine the angle of the $c\bar{c}$ with respect to the neutrino direction.
- Determine which meson or baryon will form from each quark.
- Determine the momentum of each charm meson/baryon.
- Decay both hadrons.

The polar angle of the c quark with respect to the Z^0 direction in the center of mass, of the $g - Z^0$ frame is called θ^*. The distribution of $\cos\theta^*$ used for charm fragmentation is shown in Fig. 5.1. This distribution was calculated from gluon-boson fusion production of charm[40]. It is assumed that the azimuthal angular distribution is flat about the Z^0 direction. The meson or baryon type is determined based on a reanalysis of a neutrino emulsion experiment[41].

The maximum momentum available to the forward-going charm hadron in the $g - Z^0$ frame is

$$\|P^*_{fmax}\| = \frac{W^2}{4} - M^2_{hadron}, \tag{5.1}$$

where W^2 is the invariant mass of the hadronic system:

$$W^2 = M^2 + 2ME_{had} - Q^2.$$

The situation which gives the backward going hadron the most momentum is the one where the nucleon doesn't break up. In this case one finds

$$\|P^*_{bmax}\| = (\sqrt{P_{fmax}} - \gamma\beta * M_{nucleon})^2. \tag{5.2}$$

The distribution of the fraction of available momentum carried by a charmed hadron, Z, has been measured and fitted to several parameterizations[37, 38]. The functional form of this distributions is called a fragmentation function. The Collins-Spiller fragmentation function[37] is used in this analysis

and input of ϵ=0.81, and returns Z. The functions form is:

$$D(z) = \left[\frac{1-Z}{Z} + \epsilon\left(\frac{2-Z}{1-Z}\right)\right] \times (1+Z^2) \times \frac{1}{(1-\frac{1}{Z}-\frac{\epsilon}{1-Z})^2}. \qquad (5.3)$$

The absolute value of momentum is then $P = P_{fmax}Z$. The angles above then determine all the momentum components in the $g - Z^0$ center-of-mass frame.

The charmed hadrons are boosted back to the lab frame and allowed to decay. The decay routine formalism is based on Ref. 42 and 43. The form factors used are from measurements by FNAL-E791[44, 45, 46] for both pseudoscalar and vector meson decays. The decays modelled include $D^+ \to \bar{K}^0\mu^+\nu_\mu$, $D^+ \to \bar{K}^-\pi^+\mu^+\nu_\mu$ (both resonant $\bar{K}^{*0}$ and nonresonant), $D^+ \to \bar{\pi}^0\mu^+\nu_\mu$, $D^+ \to \rho^0\mu^+\nu_\mu$, $D^0 \to K^-\mu^+\nu_\mu$, $D^0 \to \bar{K}^0\pi^-\mu^+\nu_\mu$ (both resonant $\bar{K}^{*-}$ and nonresonant), $D^+ \to \pi^-\mu^+\nu_\mu$, $D_s^+ \to \eta\mu^+\nu_\mu$, $D_s^+ \to \eta'\mu^+\nu_\mu$, $D_s^+ \to \phi\mu^+\nu_\mu$, and $D_s^+ \to \phi\mu^+\nu_\mu$. One of the two charmed hadrons is forced to decay into a muon, and the probability for decay into a muon is included in the event weight.

5.2 Beam Impurities

Beam impurities are the largest source of WSM's, thus a flux model that properly included beam impurities is essential. To implement this it is necessary to have a good simulation of the beam line. All previous flux models used by NuTeV had been determined by the simulation package TURTLE[27]. TURTLE uses geometric magnetic optics to trace trajectories of particles to their decay point. This procedure works well for determining neutrinos of the right type; however, wrong type neutrinos due to scraping, muon decay, and $K \to 3\pi$ cascade decays cannot be generated in TURTLE.

To handle the wrong-sign flux, a GEANT-based simulation of the beam-

line is used. The production of secondaries at the target uses a model developed by Malensek[20] using Atherton's data[21]. This model is also used for secondary production in the TURTLE flux. GEANT then transports secondaries through the beam line, allowing the particles to decay or interact with material in the beamline. Hadronic interactions are handled by the GHEISA[24] package.

The flux produced with this simulation is used to generate the backgrounds for this analysis, except for the dimuons, where it is desirable to use the dimuon sample used in the dimuon analysis. However, since the right sign flux from TURTLE and GEANT agree to the percent level this should be sufficient. This flux is fed to Numonte, and a sample of beam impurity events is generated. These events are run through McNuTeV and crunched. In order to actually be a background the event must pass the same cuts as the data.

	ν-mode		$\bar{\nu}$-mode	
	Eν >20 GeV	40 GeV	Eν >20 GeV	40 GeV
scrape	53%	46%	24%	17%
charm	10%	15%	25%	33%
K^0	12%	10%	16%	13%
other prompt	9%	8%	22%	19%
muon decay	11%	19%	11%	17%
$K \rightarrow$pi	5%	2%	2%	1%

Table 5.2: The percentage for each beam impurity source.

In $\nu(\overline{\nu})$-mode approximately 68%(83%) of WSM's are from beam impurities. Beam impurities are further divided into specific sources in Table 5.2.

5.3 Charged Current Charm

Charged current charm (dimuons) forms the next largest background. The dimuon sample was generated using a LO cross section model with parameters extracted from CCFR[29] which have been corroborated by a preliminary NuTeV analysis [28]. Charm quarks were fragmented into charmed mesons using the Collins-Spiller fragmentation function[37] with hardness parameter ϵ=0.81. The assumed charm semi-muonic branching ratio was 10.9%. The charm quark mass for dimuons was taken to be 1.32 GeV/c^2.

Figure 5.2 shows $Y_{vis} = \frac{E_{had}}{E_{had}+E_{\mu 2}}$ for dimuons in ν-mode, where both muons are toroid analyzed. $E_{\mu 2}$ is the muon with the wrong sign for the beam. The distribution of Y_{vis} for dimuons which reconstruct as WSM's would be similar. The χ^2 of 19 for 17 degrees of freedom between data and MC for this distribution lends confidence to simulation of the dimuon background. This agreement also gives us confidence in the fragmentation model which is also used for the neutral current charm simulation.

One source of charged current charm events that does not have any acceptance issues is CC charm from ν_es. About 1% of the beam is ν_es. This source results in 26 WSM events.

5.4 Pion and Kaon Decay

Pion and kaon decay events form a background for the dimuon analysis as well as this analysis. The rate of π/K decay events was determined in an analysis of same-sign dimuons by the CCFR experiment[39]. That analysis made it clear that the dominant source of same-sign dimuons is π/K decay, hence NuTeV's same-sign dimuons can be used to check the simulation of this source.

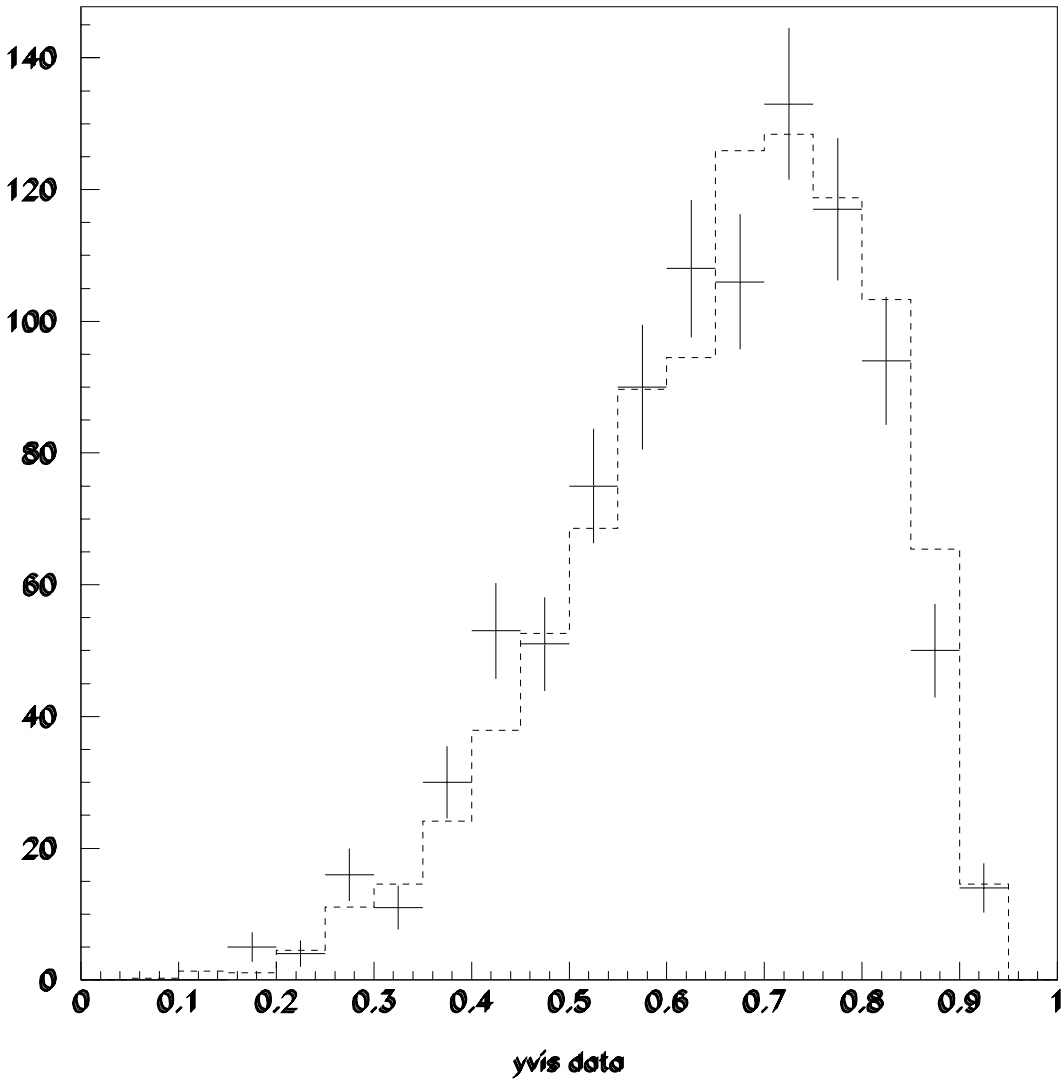

Figure 5.2: Comparison of Y_{vis} distribution for data(crosses) to MC(histogram) of $E_{had}/(E_{had} + E_{\mu 2})$ for toroid-toroid dimuon events.

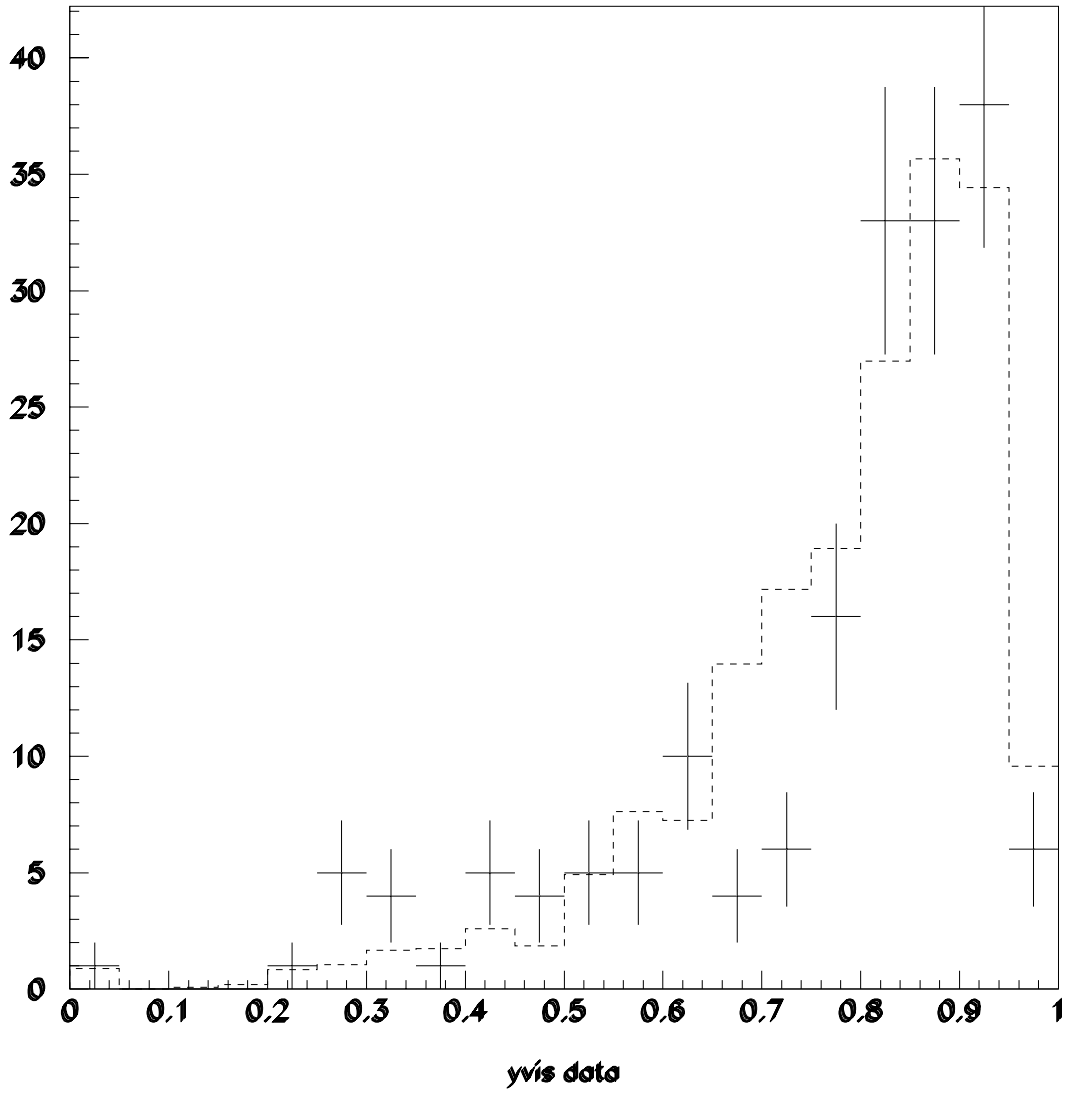

Figure 5.3: Comparison of Y_{vis} distribution for data(crosses) to MC(histogram) for same-sign dimuons.

Figure 5.3 is a plot of $\frac{E_{had}}{E_{had}+E_{\mu 2}}$ for NuTeV same-sign dimuon data, where $E_{\mu 2}$ is the muon with the smaller energy. In addition to standard cuts it was necessary to require that both muons originated within 50cm of each other and of the measured vertex. This was done to remove events which were actually overlays of two charged current events.

Figure 5.3 demonstrates that agreement between the π/K model and same-sign data is satisfactory, especially given that π/K decay background is the smallest background. It is predicted that NC π/K decay contributes 8.1 events to the WSM sample and CC π/K decay contributes 5.0. The uncertainty in the π/K model is estimated as 15% [39].

5.5 Charge Misidentification Events

The final type of background events are events where the charge of the muon is reconstructed incorrectly. Mis-identification(MID) events can form a large fraction of WSM events with a rate of 1.5 events per 10000 CC events if no cuts are applied; however, one can easily drop this rate to 2.6 per million CC events using the misidentification cut described in Sec. 4.2. Two alternative variables were analyzed to remove these events, but the previously selected one is better modeled. Other checks were performed in order to demonstrate this cut's effectiveness.

One obvious check is the χ^2 of the track, better viewed, so that the tails are evident, as a likelihood:

$$\mathcal{L} = 2 \ln \chi^2.$$

The other variable is based on the difference in radius at T2 between a straight line extrapolation from the front face of the toroid and what is measured at T2. This is called the Δr cut.

In order to simulate MID events, 5 million charged current events are generated and propagated through McNuTeV. Events where the generated charge is different from reconstructed charge are then collected and used for this background. When processing these events the hadronic interactions are turned off. This is done because the hadronic interactions take a long time to simulate. For this reason the hadronic energy of the MID events is simulated by the functional formula of Eq. 3.1.

To demonstrate that the cut does in fact remove the MID events, Figs. 5.4 and 5.5 are included. In the insert of Fig. 5.4, one notices the second bump, due to MID, between a likelihood of 10 and 25. These events are reduced by a factor of ten by application of the MID cut. Similarly, in the insert of Fig. 5.5, one notices the spike between 0 and positive one half, which is removed by the cut. The MC indicates that both of these structures are due to MID.

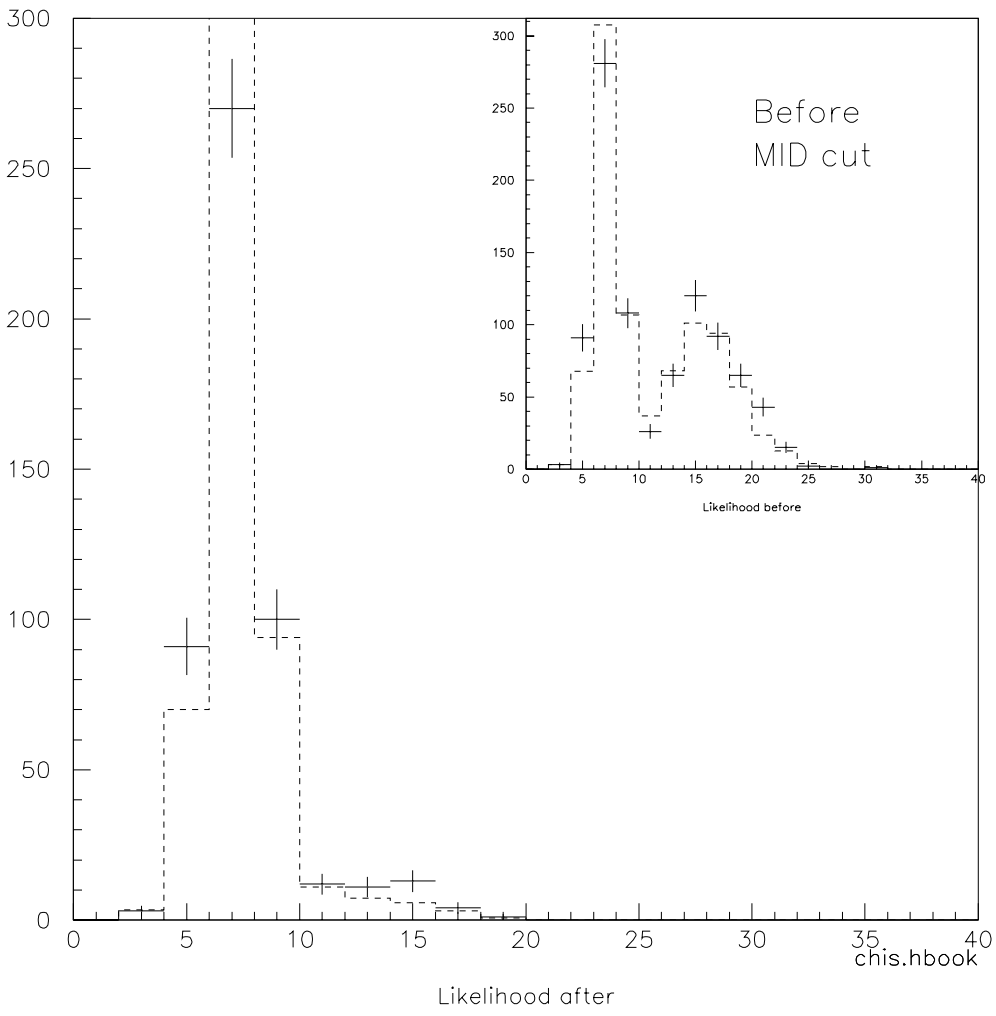

Figure 5.4: A plot of the track likelihood for data(crosses) and simulated backgrounds(histogram) before(inset) and after the charge mid-id cut.

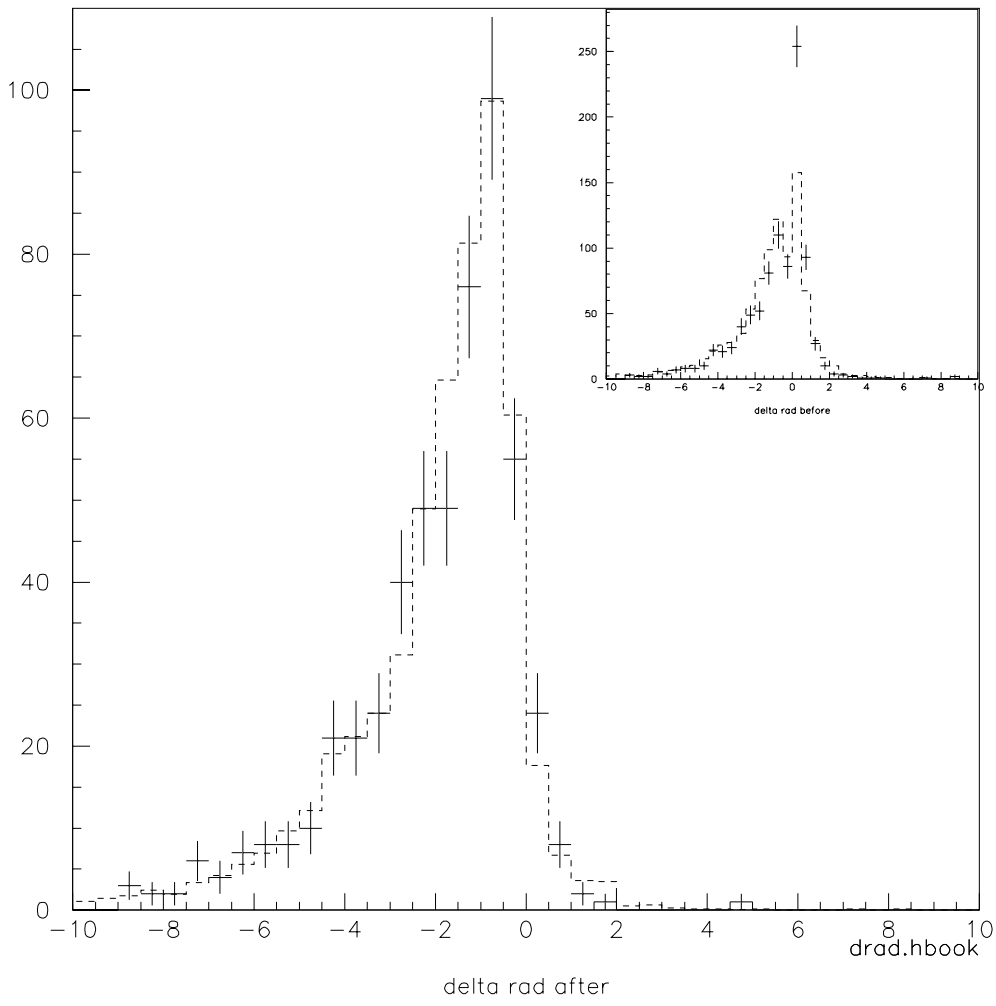

Figure 5.5: Distribution of Δr for data(crosses) and simulated backgrounds(histogram) before(inset) and after the charge mid-id cut.

Chapter 6

Anti-neutrino-mode Fit of Beam Impurities

In ν-mode the beam impurities are the largest source of WSM's; however, nearly half of the WSM's are from other sources. In $\overline{\nu}$-mode the beam impurities are nearly 90% of the WSM's. Many beam impurities have large errors associated with them, so large that the $\overline{\nu}$-mode WSM data can be used to measure their contributions.

There are 461 WSM events in $\bar{\nu}$-mode. Simulations using the central values of previous measurements indicate that 374±82 events are due to beam impurities and 39±4 events are due to other sources.

Beam impurities are due to scraping, muon decay, $K \rightarrow 3\pi$ cascade decays, charm production, K_L decays, and wrong-charged hadrons decaying before the dipoles. Charm production refers to the case when the proton strikes the BeO target and produces a $c\bar{c}$ pair. The $c(\bar{c})$ quarks have a 10% chance of decaying semi-muonically and producing a $\nu_\mu(\bar{\nu}_\mu)$.

There are relatively more beam impurities in $\overline{\nu}$-mode for two reasons: 1)

The fact that the ν cross-section is twice the $\overline{\nu}$ cross-section means that the beam impurities which are present interact twice as often in $\overline{\nu}$-mode as they do in ν-mode. 2) The fractional size of beam impurities is larger in $\overline{\nu}$-mode. The fractional increase of beam impurities for $\bar{\nu}$-mode is mainly due to the fact that the number of right sign particles, and thus neutrinos, goes down while charm and K_L's are produced in equal abundance.

In addition to discussing the beam impurities, this chapter will describe the fit performed to the $\overline{\nu}$-mode WSM data, and discuss what the results of that fit mean for $\sigma_{p+p\to c\bar{c}}$.

6.1 Beam Impurities

Each of type of beam impurity will be described in this section. Specific attention is given to the sources of uncertainty. Hadronic decays, $K \to 3\pi$ cascades, and wrong-charged hadrons which decay before the dipoles will be discussed first, followed by muon decay, K_L decays, scraping, and charm contributions.

6.1.1 Hadronic Decays

Hadronic decays that lead to beam impurities can be broken into two types, $K \to 3\pi$ cascades and wrong-charged hadrons which decay before the dipoles. The $K \to 3\pi$ cascade decays are fairly well constrained. These dominantly occur in the decay pipe region of the beamline, and thus originate from the same K's which make up the right-sign beam. The right-sign charged current events in our data and MC based on the GEANT flux agree at the 2% level. The $K \to 3\pi$ cascade branching ratio is also known to a bit better than 1%. This means that $K \to 3\pi$ cascade events are well understood.

Hadron decays before the dipole are somewhat less well understood. The number, momentum and angular spectrum of secondary K's and π's which come off the target in the simulation come from Malensek's parameterization[20] of Atherton's data[21]. Atherton's data has statistical errors between 2% and 6%. Malensek's fit gives the results of $\chi^2/dof \simeq 1$ if the data's errors are inflated to 10%. The more conservative estimate of 10% is used.

6.1.2 Muon Decays

Muon decay is a well understood process. The one concern in how muon decay is modeled is that the helicity of the muon affects how the energy is split between the ν_μ, ν_e and the e. The rate of ν_μ's at a given energy in a specific angular bin is given by[56]:

$$\frac{d^2 N_{\nu\mu}}{dx d\Omega} \propto \frac{2x^2}{4\pi}[(3-2x)+(1-2x)P_\mu \cos\theta] \tag{6.1}$$

Where $x \equiv 2E_\nu/m_\mu$, θ is the angle between the neutrino momentum vector and the muon spin direction, and P_μ is the average muon polarization along the beam direction.

One can calculate the average polarization of muons in the SSQT. In the decaying hadron rest frame, the muon comes off with a known helicity and momentum $\vec{p}$. In the lab frame the muon has a momentum $\vec{q}$. One finds that the probability for the muons helicity to flip in going from the rest frame of the hadron to the lab frame is the rotation matrix element for the angle between $\vec{p}$ and $\vec{q}$. Therefore the polarization is $P = \hat{p} \cdot \hat{q} = \cos\phi$ using the simplification that each π or K has no angle with respect to the z-axis. One find that:

$$\phi = \theta^* - \theta_{Lab}$$

Where θ^* is the angle with respect to z in the rest frame of the π/K and

$$\tan\theta_{Lab} \sim \theta_{Lab} = \frac{\sin\theta^*}{\gamma(\cos\theta^* - \beta)}$$

$\cos\theta^*$ is flat from 1 to -1. For the case of 200GeV K's the average polarization is 0.17, for 200 GeV π's it is 0.03. An average polarization of 0.1 has been used in generating the muon decay sample. The importance of the helicity in muon decay events was tested by generating muon decay samples assuming average polarizations of 0.0, -0.1, and -0.30 in ν-mode and 0.0, 0.1, and 0.3 in $\overline{\nu}$-mode.

Table 6.1: Results of some muon decay studies.

pol	ν_μ $< E >$(GeV)	Number of events	$\bar{\nu}_\mu$ $< E >$(GeV)	Number of events
0.0	105.1	17.3	97.56	11.2
0.1	107.1	17.8	98.97	11.6
0.3	109.7	18.4	101.7	12.1

The polarization changes the number of ν_μ events from μ decay by about 3%. This is an estimate of the uncertainty in the muon decay.

6.1.3 K_L Decays

The presence of neutral K's in neutrino beams has caused problems for neutrino analyses in the past[57]. The location of bending magnets in the SSQT was chosen to minimize the contribution from neutral particles. This results in the neutral K's only being responsible for 12% of the $\bar{\nu}$-mode beam impurities. Even though the SSQT minimizes the number of neutral K's, the uncertainties surrounding them remain the same. The K_L contribution to the beam impurities was assigned a 20% fractional uncertainty. This is predominantly due to the uncertainty in the cross section for production of

neutral K's relative to charged K's. Details of this may be found in Ref. 57.

6.1.4 Scraping

Scraping is the process where a beam particle interacts with a beam element and creates a hadron shower. Hadrons in this shower of both charges can decay and give ν of the wrong type. Scraping contributions depend on the production model, which was given an error of 10% in Sec. 6.1.1. When scraping occurs in the GEANT simulation of the beam, the model used for hadronization is GHEISHA[24]. There is reason to believe this model is only valid at the 35-40% level[23] [25]. A combined uncertainty of 40% is reasonable.

6.1.5 Charm Contribution

When the primary proton strikes the BeO target, there is a finite cross section to produce a $c\bar{c}$ pair, which will then fragment into charm mesons or baryons that quickly decay. There is a 10% chance of this decay including a ν_μ or $\overline{\nu}_\mu$. Because charm mesons decay so quickly there is no chance that the wrong charged meson will be bent out. The BeO target is only one interaction length long so about one third of the protons don't interact in the target; instead they strike the dump. The protons striking the dump can also produce a $c\bar{c}$ pair, and the acceptance for ν from charm in the dump is approximately the same as the target. The cross section for production in the dump is accounted for; as is the difference in acceptance.

Two experiments measure the inclusive cross section for production of $D^{\pm}$ and $D^0/\overline{D^0}$ with an 800 GeV proton beam(Ammar, *et al.*[58] and Kodama, *et al.*[59]). The two sets of measurements, given in Table 6.1.5, are

consistent within their large errors(30%).

Exp	$\sigma_{p+p\to D^{\pm}+X}[\mu b]$	$\sigma_{p+p\to D^{o}+X}[\mu b]$
Kodama(1991)	38±9±14	38±3±13
Ammar(1988)	26±4±6.5	22^{+9}_{-7}±5.5

The sum of $\sigma(D_i) \times BR(D_i \to \nu_\mu)$ is 6.0 ± 1.6 μb for Ammar, and 9.1 ± 3.1 μb for Kodama. The weighted average of these two is 6.6 ± 1.3 μb, which yields a 23% uncertainty. The weighted average is used as an initial estimate and indicates that one should expect 88±20. $\overline{\nu}$-mode WSM events due to charm production.

Given their large uncertainties, these measurements merit further discussion. Both experiments use an 800 GeV proton beam. The Ammar experiment collides this with liquid hydrogen in a bubble chamber, while the Kodama experiment uses emulsion, with A≃26.6 and assumes an A^1 cross section dependence. Both experiments searched for charm topologies. The Kodama experiment triggered on a muon as a decay product. Each experiment recorded roughly 100 charm events, of order the number of WSM's from $c\bar{c}$ in NuTeV. While NuTeV has a very different design, it should be possible to a measure the $c\bar{c}$ cross section with similar precision.

6.2 Fit Procedure

This fit compares simulations of all sources described in this chapter to the data in $\overline{\nu}$-mode. In addition to the cuts described in Chap. 4.2, the events in this sample are required to have $Y_{vis} < 0.5$. This is done to preserve the region $Y_{vis} > 0.5$ for FCNC studies. The energy and position of a WSM event are sensitive to which type of beam impurity creates the ν that interacts. The position in the bend direction is divided into 12 equally

spaced bins in the fiducial volume from -127 cm to +127 cm. The visible energy is divided into 15 equally spaced bins from 0 to 300 GeV.

A model is constructed from the six sources discussed previously added together with adjustable weights. A maximum likelihood fit is then performed to determine these weights from a best fit to the data. The likelihood is defined as:

$$\mathcal{L} = -\left(\sum_{i=1}^{nbins} N_d(i)\log(N_t(i)) - N_t(i)\right) + \mathcal{L}_{added} \tag{6.2}$$

where $N_d(i)$ the number of data events in bin i, and $N_t(i)$ is:

$$N_t(i) = \sum_{j=1}^{6} W_j \times S_j(i) \tag{6.3}$$

with W_j, the weight of source j, and $S_j(i)$, the predicted number of events in bin i due to source j. The weight values are defined to agree with previous measurements when they are equal to 1. The weights are also constrained to be consistent with their estimated error, in all cases except $c\bar{c}$ production, by adding a likelihood contribution:

$$\mathcal{L}_{added} = \sum_{j=1}^{6} \frac{(W_j - 1)^2}{\sigma_j^2}. \tag{6.4}$$

The fitter uses MINUIT[60] subroutines to find the minimum and report back the error bars.

6.3 Results

Table 6.3 gives the fit results and errors along with the *a priori* error estimates given previously. Most results are consistent with unity; only the charm rate is more then 1σ away from one.

Table 6.2: Results of $\bar{\nu}$-mode beam fits.

Source	Value	Error	Error Estimate
charm	1.47	0.33	0.30
K^0	1.01	0.29	0.20
scrape	1.22	0.34	0.40
other	1.00	fixed	0.03
muon	0.95	0.11	0.07
prompt	1.02	0.21	0.10

The charm result corresponds to $\sum_i \sigma(D_i) \times BR(D_i \rightarrow \nu_\mu) = (9.8 \pm 2.2)\mu b$. Recalling that there are two mesons for each $c\overline{c}$ pair, and given the BR(c$\rightarrow \mu$) of 9.9$\pm$1.2%[32]

$$\sigma_{p+p\rightarrow c\overline{c}} = (49 \pm 11)\mu b. \tag{6.5}$$

Figure 6.1 is a plot of the likelihood as a function of the charm normalization. Figure 6.2 shows the distribution of E_{vis} and the horizontal position. These are the distributions which are fitted to; however the events with $Y_{vis} > 0.5$ which were not included in the fit are included in these plots. Figure 6.2 a) shows E_{vis} before and after the fit, b) shows E_{vis} after the fit and breaks the model down into its larger components, c) shows the horizontal position before and after the fit, and d) shows the horizontal position and breaks the model down into the larger sources. Figure 6.3 has the same structure as Fig. 6.2 but shows E_μ and E_{had}.

6.3.1 Systematic Errors

Estimates of the systematic uncertainty can be obtained by varying model parameters within their uncertainties and changing cuts in a reasonable

way. Note that by including the uncertainty on other beam sources one effectively incorporates those systematic errors into the error on the fit. An explanation of each error follows. One obvious systematic is the uncertainty on BR(c$\rightarrow \mu$) which contributes an error of 5.0 μb.

The level of non-beam processes, approximately 17 events, is known to better then 10%. Changing the level by 10% amounts to a change of 0.2 μb. The non-beam sources are almost all charged-current charm. Most of the charged current charm events are removed with the dimuon cut described in Sec. 4.2. This cut removes events with two muons by forming a track from the DC hits, however another way one might remove dimuons is using the calorimeter information. The *stop* cut counts the number of of counters that are consistent with two or more MIP. The *stop* parameter is the first of three counter, downstream of the interaction, in a row with less than 1.5 MIPs. The cut requires that the length between the interaction and the *stop* counter be less then 15 counters. The difference between the *stop* cut and the tracking cut are used as a systematic error on the charged current charm contribution. This systematic gives 2.3 μb.

The energy measured by our detector is taken to be uncertain to 1% for muons and hadrons. One tests how sensitive this measurement is to this possible miscalibration, by changing the measured data's E_μ and E_{had} by 1% each direction. Shifting E_μ up changes the $\sigma_{p+p\rightarrow c\overline{c}}$ measurement by 0.3 μb, and shifting E_μ down changes $\sigma_{p+p\rightarrow c\overline{c}}$ by 0.5 μb. Shifting E_{had} up changes $\sigma_{p+p\rightarrow c\overline{c}}$ by 0.4 μb, and shifting it down changes it by 0.3 μb. The total error assigned to calibration is thus 0.7 μb.

It was checked if the values of P_t and X_f affect the fit. The weighted average of the values measured by Kodama and Ammar are used by default and sensitivity to these was tested by performing the fit using the values measured by Ammar. A systematic of 0.7 μb can be attributed to this

procedure.

It was checked if the $Y_{vis} < 0.5$ cut affected the results, by performing the fit without this cut. A systematic of 0.2 μb can be attributed to this procedure.

Systematic errors are assumed to be independent and thus can be added in quadrature, the total is 5.6 μb, yielding the final result

$$\sigma_{p+p\to c\overline{c}} = (49 \pm 11 \pm 5.6)\mu b. \tag{6.6}$$

Using PYTHIA's[61] fragmentation of c quarks into mesons one can transform Kodama's and Ammar's measurements into the measurements of $\sigma_{p+p\to c\overline{c}}$ found in Tab. 6.3.1.

Table 6.3: Previous charm meson production cross-sections transformed into charm quark production cross-sections.

Exp	$\sigma(p+p\to c\overline{c})$ from $D^{\pm}$ measurement	$\sigma(p+p\to c\overline{c})$ from D^0 measurement
Kodama(1991)	75±18±28	47±4±16
Ammar(1988)	51±8±13	27^{+11}_{-9}±7

Note that NuTeV's measurement has smaller errors than all of these, and this measurement is consistent within overlapping error bars of all previous measurements.

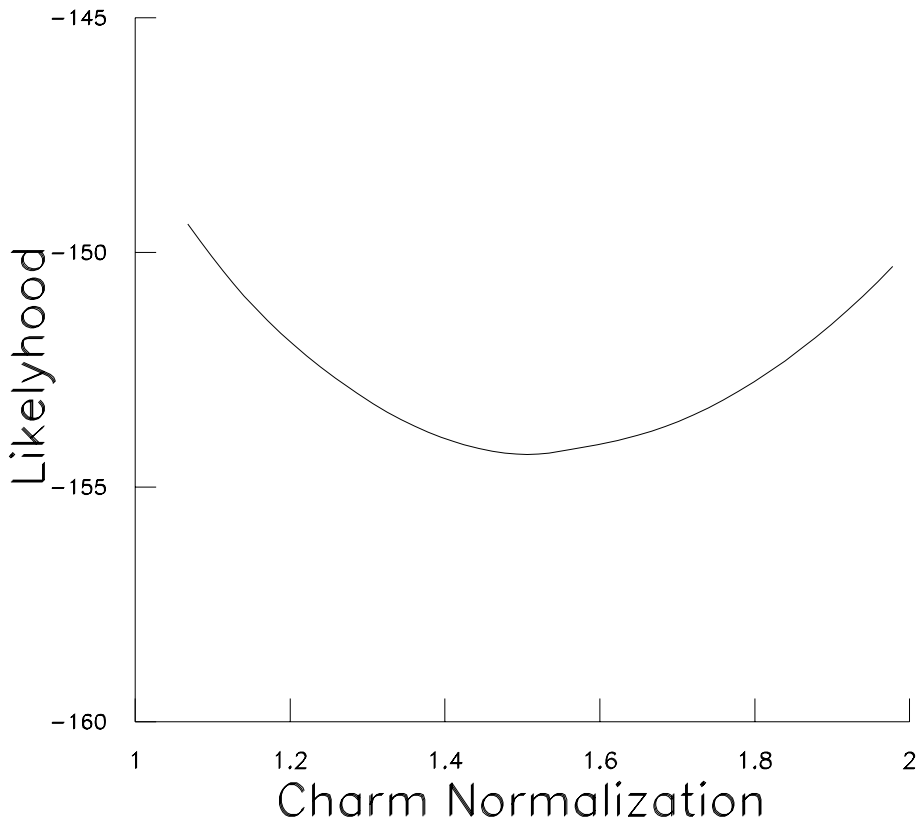

Figure 6.1: The likelihood function for the $\bar{\nu}$ WSM fit as a function of the charm normalization parameter.

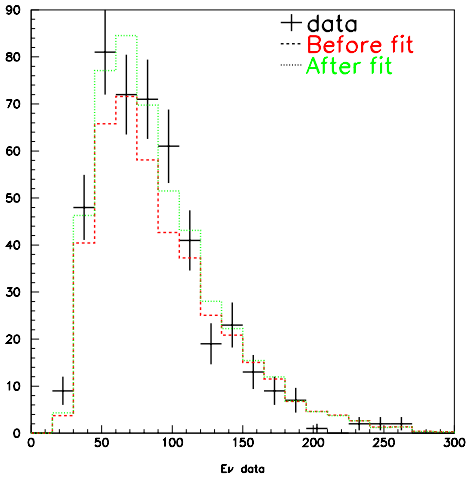
data
Before fit
After fit
Ev data

a)

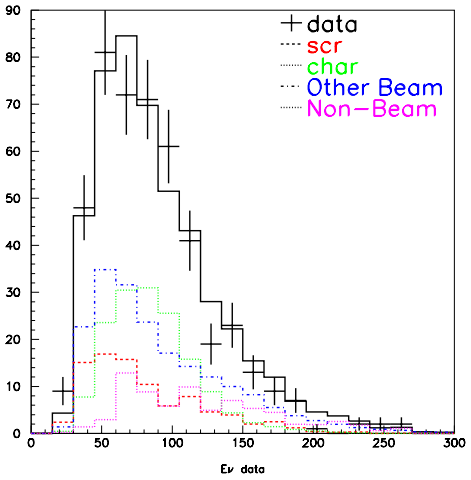
data
scr
char
Other Beam
Non−Beam
Ev data

b)

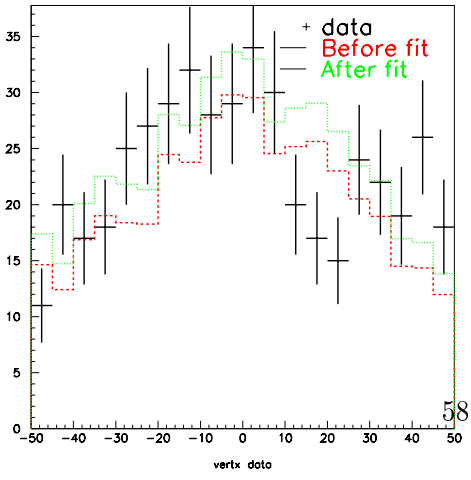
data
Before fit
After fit
vertx data

c)

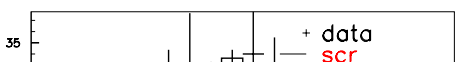
data
scr

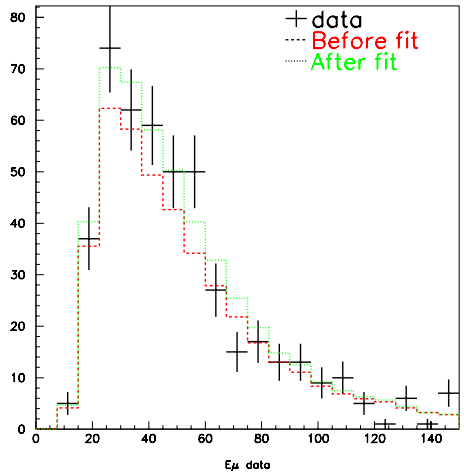
data
Before fit
After fit
Eμ data

a)

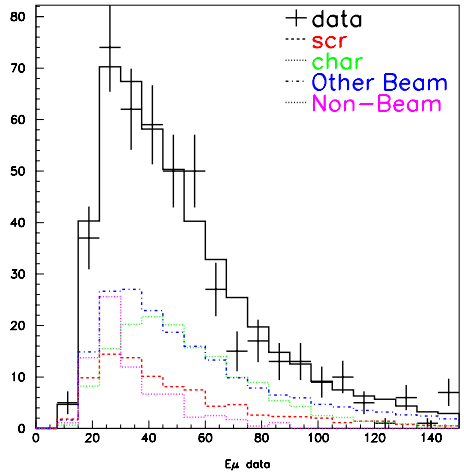
data
scr
char
Other Beam
Non−Beam
Eμ data

b)

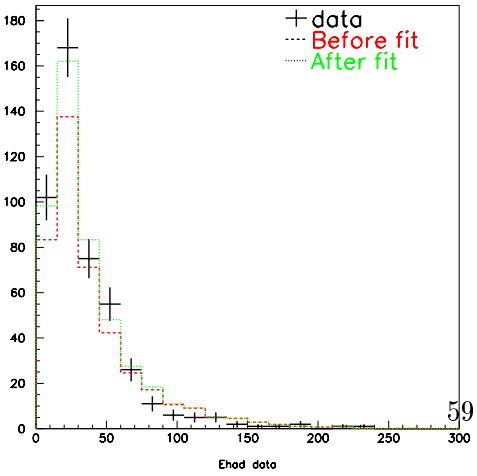
data
Before fit
After fit
Ehad data

c)


data
scr

Chapter 7

Gluon-boson Fusion Results

Neutrino mode WSM's provide a good test of the gluon-boson fusion model of NC charm production model. Two important inputs to the gluon-boson fusion model are the gluon distribution and the charm mass. Information about these factors is extracted with a fitter that compares the Y_{vis} distribution of data to a model distribution consisting of NC charm and all background sources.

The remainder of this chapter details the analysis procedure and gives the results. There is a description of the fitter, how it works, and some tests that it returns an unbiased result. The measurement of the charm mass, and cross section for gluon-boson fusion are given. Kinematic distributions of WSM's are examined and compared to simulations. Finally there is a thorough discussion of studies that are used to determine systematic errors.

7.1 Fit Procedure

In this analysis the WSM data is compared to MC samples of all known backgrounds and the NC charm signal. The normalization factors from the $\bar{\nu}$-mode beam fit have been applied to the ν-mode beam impurities. The Y_{vis} distribution is the most sensitive distribution that was found. This distribution was divided into 20 bins equally spaced from zero to one. The choice of 20 bins results in most bins having tens of events, and does not affect appreciably the sensitivity to the shape of the underlying distribution.

The fitter calculates the negative log likelihood($\mathcal{L}$) between data and model.

$$\mathcal{L} = -\left(\sum_{i=1}^{nbins} N_d(i)\log(N_t(i)) - N_t(i)\right), \tag{7.1}$$

where $N_d(i)$ the number of data events in bin i, and $N_t(i)$ is the sum of all the model. When the whole E_{had} spectrum is used, the program varies the charm mass parameter and the normalization of the beam impurities until it finds the minimum of $\mathcal{L}$. For the final result only events with $E_{had} > 50$ GeV are used, and in this case the normalization of beam impurities is fixed. The values of the parameters at this minimum are the results of the fit. The fitter also varies the parameters to determine error bars, which correspond to an increase of one unit of χ^2. A negative log likelihood fit was chosen because a χ^2 fit assumes Gaussian distributions, and in this case one is dealing with relatively small statistics.

Each of the backgrounds and the NC charm signal must be normalized to the data. The obvious way to do this is to normalize each source to the right sign single muons. In addition to this method, referred to as an "absolutely normalization", the dimuon and beam backgrounds can be normalized in other ways. The beam can be normalized to low E_{had} events, and the dimuons can be normalized to WSM's where two tracks are found in each

view. These different normalizations agree to better then 3%. As discussed previously, individual sources of beam impurities have large uncertainties. The fit results from Chap 6 are applied to those sources in ν-mode.

A number of studies were done to check that the fitter returned an unbiased result. These are called "fake data studies", because a sample of the various MC's is put together and used as the 'data' sample. Table 7.1 shows the results of ten m_c=1.3 GeV/c^2 fake data samples. Any pull the fitter could have is observed to be less then 4%, which is an order of magnitude less then the statistical error.

Data sample	m_c	Error	Norm	Error
90	1.133	0.163	0.913	0.0648
91	1.296	0.254	0.996	0.0622
92	1.171	0.172	0.906	0.0622
93	1.317	0.268	0.997	0.0623
94	1.333	0.266	1.01	0.0652
95	1.201	0.200	1.00	0.0638
96	1.426	0.296	1.09	0.0658
97	1.254	0.202	0.923	0.0628
98	1.658	0.476	1.00	0.0638
99	1.212	0.226	0.970	0.0637
all	Mean	rms/$\sqrt{N}$	Mean	rms/$\sqrt{N}$
all	1.300	0.048	0.980	0.018

Table 7.1: Results of fake data studies with input values of m_c=1.3 GeV/c^2 and a normalization of 1.0.

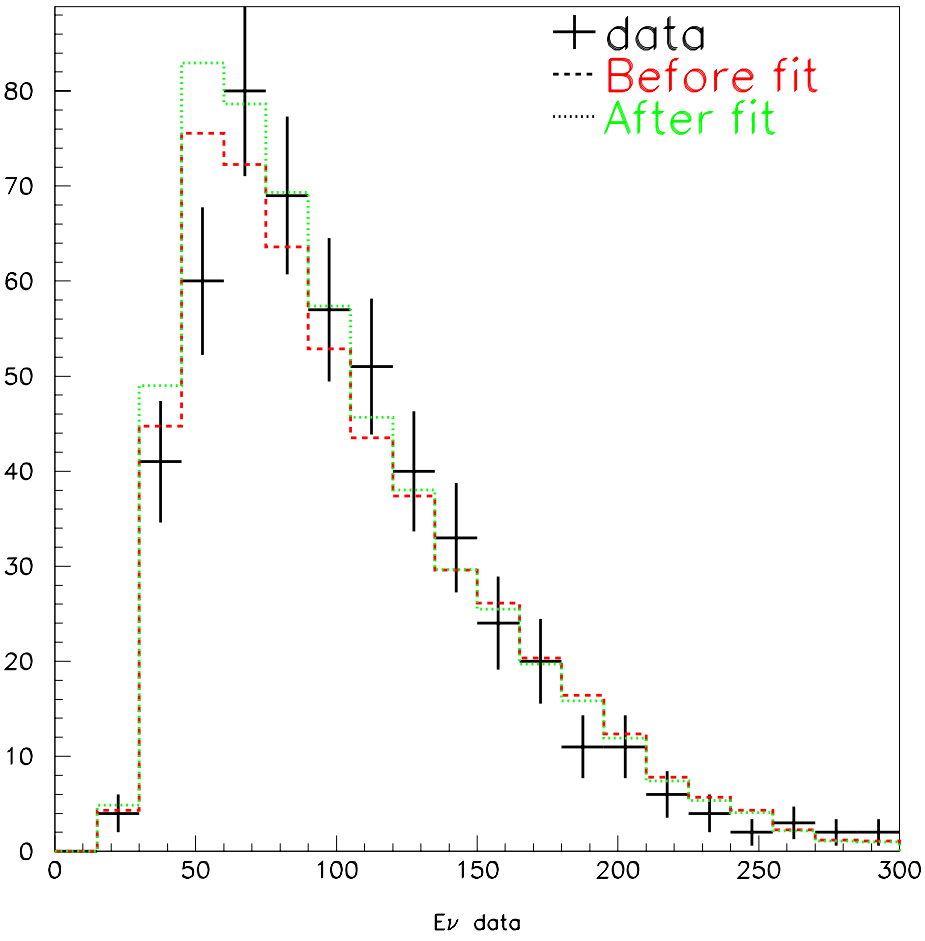

Figure 7.1: The E_ν spectrum before and after the beam fit.

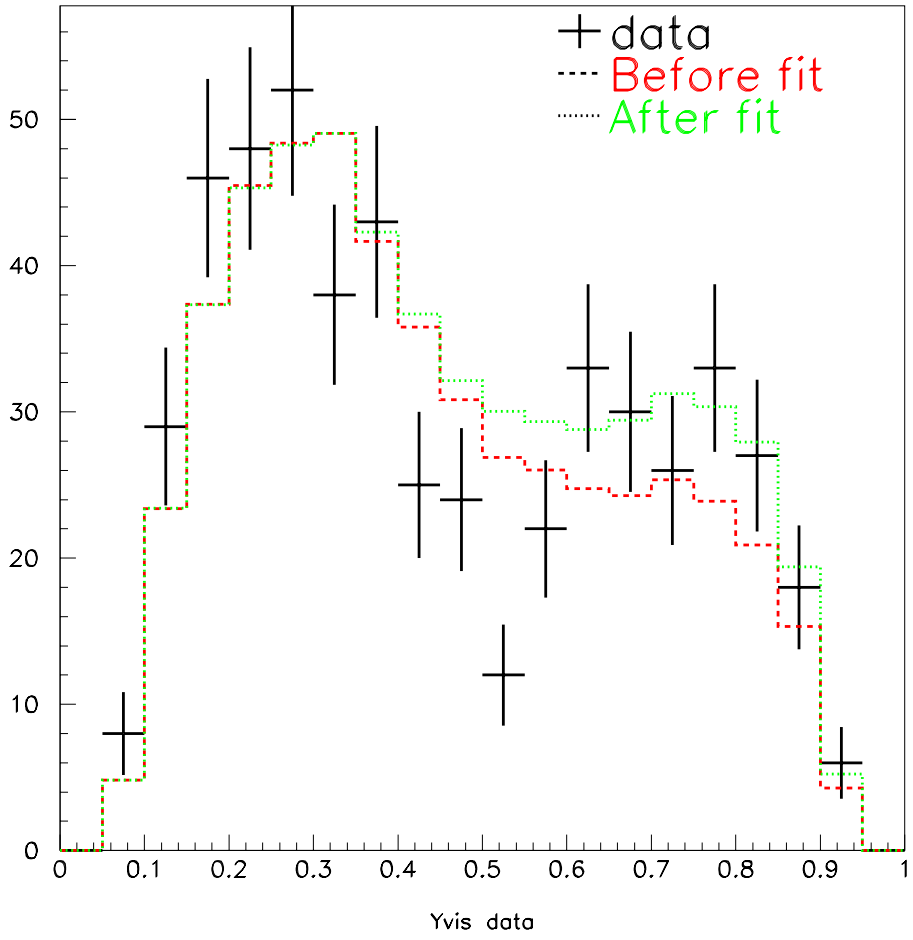

Figure 7.2: Y_{vis} distribution of ν-mode WSM's for Data(solid), background (dashed), and background plus signal(dotted).

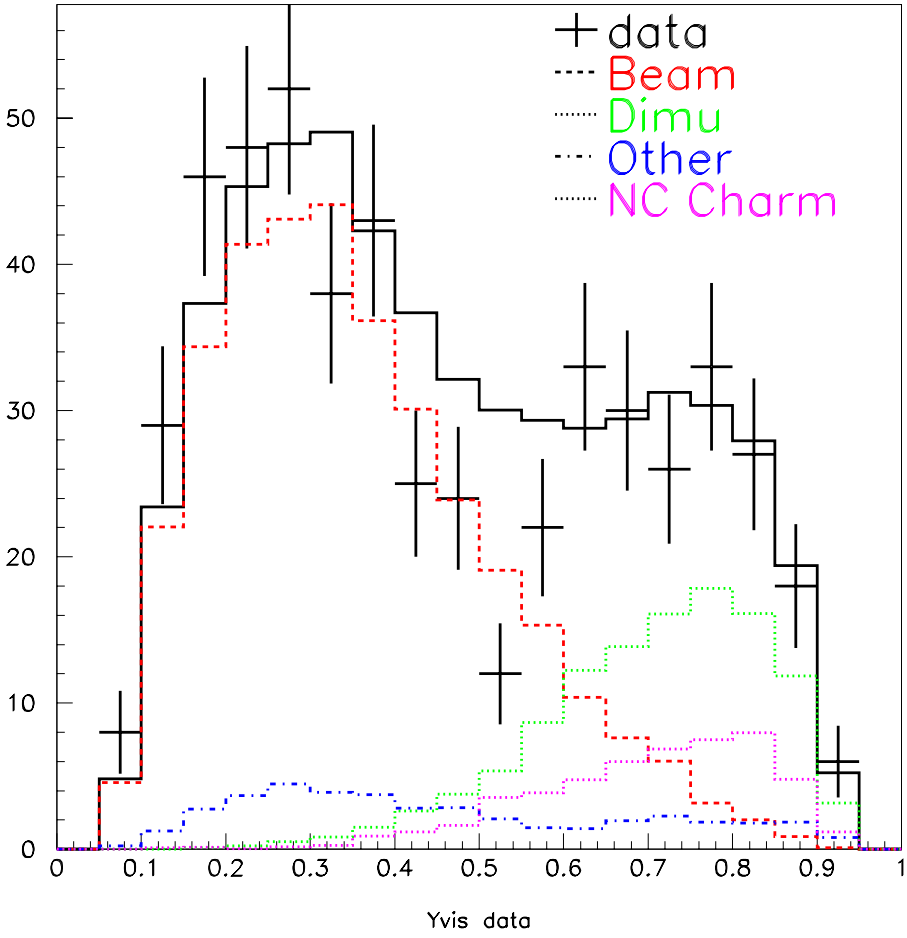

Figure 7.3: Y_{vis} distribution broken down into its various sources. The low Y_{vis} distribution is dominated by beam impurities. The larger high Y_{vis} sample is CC charm, and the smaller high Y_{vis} sample is NC charm. The roughly flat distribution is both the charge misidentification and and NC π/K decay events.

7.2 Extraction of M_C and $\sigma_{gZ\to c\overline{c}}$

The Y_{vis} distribution is shown in Fig. 7.2. The data are shown with error bars, the dashed histogram is all the backgrounds, and the dotted distribution is the backgrounds plus the best-fit NC charm signal. The shape clearly indicates a preference towards including the NC charm signal. The excess of events over backgrounds, for events passing the cuts described in Sec. 4.2, is 47 events out of 520. Requiring E_{had} be greater than 50 GeV removes most of the scraping, and one finds an excess of 29 out of 182 events, which corresponds to a statistical significance of 2.1 σ. The NC charm signal fits the shape of the excess, providing further evidence for the existence of NC charm. The likelihood of the fit result is -2538, and the likelihood not including the NC charm signal is -2488.

From Fig. 7.2 it is obvious that the data in the bin $0.50 < Y_{vis} < 0.55$ disagrees with the simulations. This disagreement cannot be accounted for. Removing this bin from the fit increases the charm mass by 0.13 GeV/c^2.

The WSM's are broken down into their sources in Fig. 7.3. Clearly the beam impurities are the largest contribution, and that the dimuons are a significant contribution. The MID and π/K decay are only small contributions.

In Fig. 7.4 the Y_{vis} distribution of WSM's is shown, however this time the events were required to have an E_{had} larger than 50 GeV. This cut removes 85% of the beam impurities while keeping 75% of the NC charm events. A side effect is that this removes about 75% of the CC charm and about 50% of the MID.

Fitting to the distribution in Fig. 7.2 results in an m_c of $1.42^{+0.77}_{-0.34} GeV/c^2$ and shift in the beam normalization of 1.002 $\pm$ 0.060. This supports the

claim that measurements made in $\bar{\nu}$-mode can be applied ν-mode. The fit is performed on the distribution in Fig. 7.4 and results in m_c of $1.40^{+0.83}_{-0.36} GeV/c^2$. The likelihood distribution for this fit is shown in Fig. 7.6. The likelihood shows a clear asymmetry. Increasing m_c can only remove the relatively small number of NC charm events; however decreasing m_c can add many more events. For this case the beam contributions are fixed at their nominal value, because there is not a clear enough beam sample.

7.3 Systematic Studies

Estimates of the systematic uncertainty are obtained by varying parameters and cuts by reasonable amounts. An explanation of each error follows. These systematic errors are assumed to be independent and thus can be added in quadrature.

Charged current charm events are removed with the dimuon cut described in Sec. 4.2. This cut removes events with two muons by forming a track from the DC hits, however another way one might remove dimuons is using the calorimeter information. The *stop* cut counts the number of counters that are consistent with two or more MIPs. The stop parameter is the first of three counter, downstream of the interaction, in a row with less than 1.5 MIPs. The cut requires that the length between the interaction and the stop counter be less then 15 counters. The difference between the stop cut and the tracking cut is used as a systematic error on the charged current charm contribution. This systematic shifts m_c by 0.04 GeV/c^2.

The dimuon WSM events are normalized using their normalization to right sign single muons, however one can also normalize the dimuons which appear to be WSM's to dimuons which appear to be dimuons. These two normalizations disagree by 3%. Using the other normalization shifts m_c by

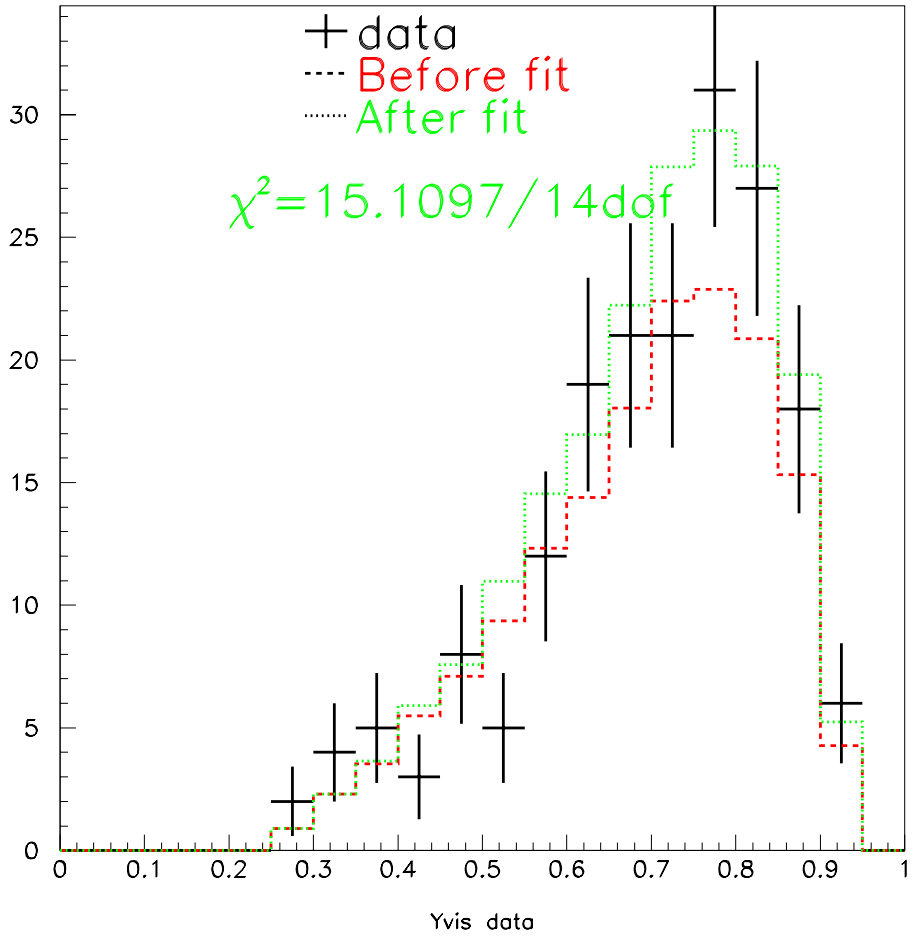

Figure 7.4: Y_{vis} distribution of WSM's for Data(solid), background (dashed), and background plus signal(dotted). An E_{had} larger than 50 GeV is required

0.10 GeV/c^2.

The energy measured by our detector could be incorrect at about the 1% level. One tests how sensitive this measurement is to that, by changing the measured data's E_μ and E_{had} by 1% each direction. Shifting E_μ up(down) changes m_c by 0.05(0.02) GeV/c^2. Shifting E_{had} up(down) changes m_c by 0.02(0.02) GeV/c^2. This gives a total of 0.05 GeV/c^2 systematic error attributable to calibration.

The fragmentation model has been described in Sec. 5.1. To check this model events with the same kinematics were used to create a $c\bar{c}$ pair using Lund's string fragmentation model[61]. The events generated using Lund increases m_c by 0.14 GeV/c^2.

The only input to this model besides the charm mass is the gluon PDF. This work has used the GRV 94 gluon distribution. Changing to CTEQ4M raises the m_c by 0.04 GeV/c^2. The CTEQ collaboration has studied the appropriate way to change the gluon PDF[16], and each of their six variations on the gluon distribution were used. The most extreme of those lowers m_c by 0.04 GeV/c^2. This shall be used as the systematic error on the gluon PDF.

The *EMC correction*[17] accounts for the fact that the neutrino scatters off a nucleon bound into a nucleus. It is not known if this correction should be applied to boson-gluon fusion so the result is measured without it. If the EMC correction is applied it increases the measured m_c by 0.12 GeV/c^2. This is included in the total systematic error.

The final systematic error is due to the size of the beam impurities. The beam fit described in Sec. 6 returns a normalization value and an error on that value for the 5 beam sources. To examine the sensitivity to these sources, each source is set one sigma high and the other sources'

normalizations are extracted. Then the source is set one sigma low and the other sources normalizations are extracted. These alternative settings are then applied to ν-mode beam impurities and the m_c is re-extracted. The largest change occurs in scraping and the second largest is for beam-produced charm. The sum, in quadrature, of all the changes is a shift in m_c of 0.13 GeV/c^2.

The sum of all systematic errors in quadrature is 0.26 GeV/c^2.

7.4 Conclusions

The result of $m_c = 1.40^{+0.83}_{-0.36} \pm 0.26 GeV/c^2$ corresponds to $\sigma_{\nu+N\to c\bar{c}} = (2.03\ ^{+1.77}_{-1.51}\ ^{+1.15}_{-0.70}) \times 10^{-1} fb$ at $< E >= 154 GeV/C^2$ using the GRV94 gluon PDF. The cross section, using this charm mass, is compared to photo-production data in Fig. 7.7. Our data is sensitive in a region that overlaps EMC but extends to slightly higher Q^2 and slightly lower x.

7.5 $b\bar{b}$ production

This chapter predominately deals with gluon-boson fusion of production of charm, however gluon-boson fusion production of bottom is also considered. The cross-section for this uses the same formalism, and only the NC couplings and quark mass need to change. The fragmentation is more complicated, and, for this reason LUND[61] fragmentation is used. Using a bottom mass of $m_b = 4.25$, which is a low estimate, we expect roughly 0.3 events in ν-mode 0.1 events in $\bar{\nu}$ mode. Clearly one will only see evidence for NC bottom production if it is orders of magnitude larger than expected.

A fit is then performed allowing the size of the $b\bar{b}$ source to be scaled by a

parameter. Since the $b\bar{b}$ signal has a similar distribution to the $c\bar{c}$ signal, the m_c is constrained to match the previous measurement of m_c from NLO CC charm production. The value of m_c=1.70 $\pm$ 0.19 GeV/c^2 is also conservative in that a higher m_c leaves an excess of events, and thus a less restrictive limit will be determined.

The fit results in a normalization of 7.3 $\pm$ 8.7. This in turn implies an upper limit on the cross section $\sigma_{\nu+N\to b\bar{b}}$ of $0.015 fb$ at 90% confidence level for $< E >= 154 GeV/C^2$.

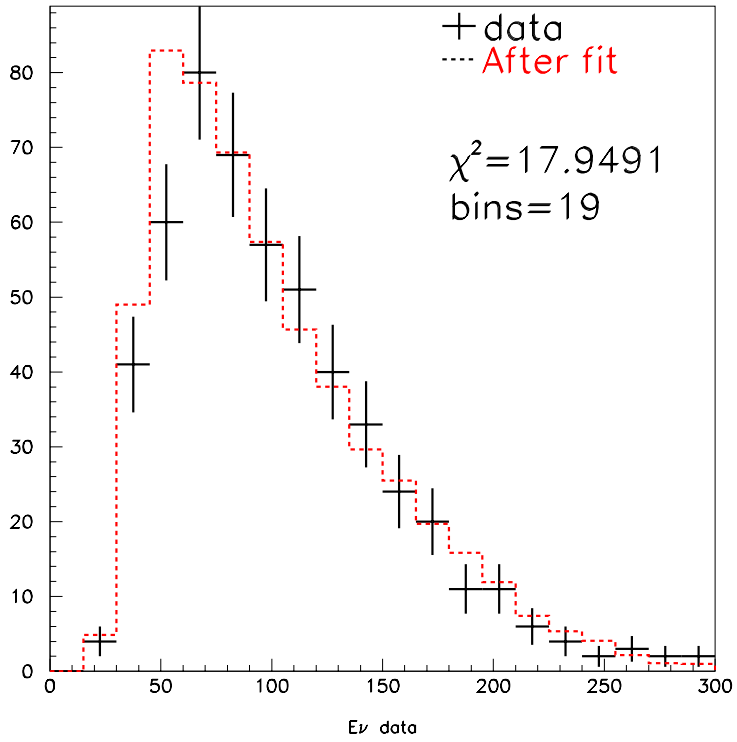
data
After fit
χ^2=17.9491
bins=19
Eν data

a)

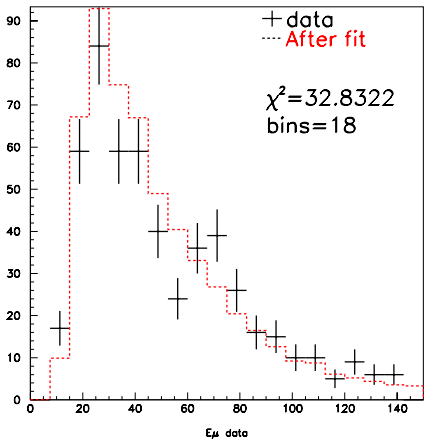
data
After fit
χ^2=32.8322
bins=18
Eμ data

b)

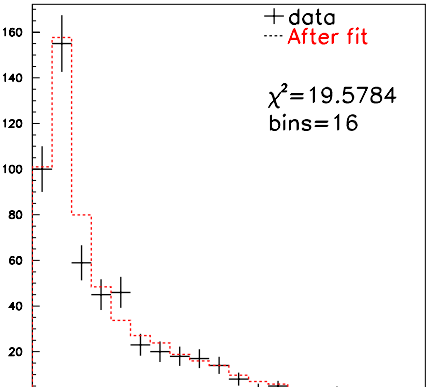
data
After fit
χ^2=19.5784
bins=16

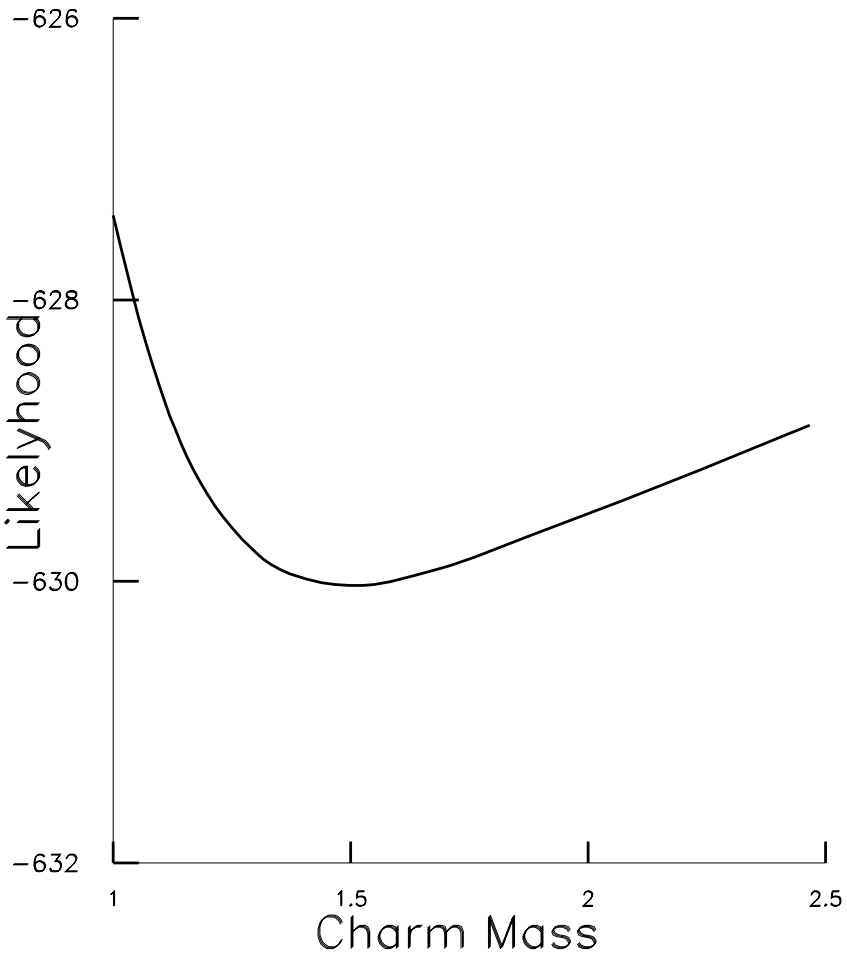

Figure 7.6: The likelihood function for the WSM ν-mode fit with $E_{had} > 50$ GeV.

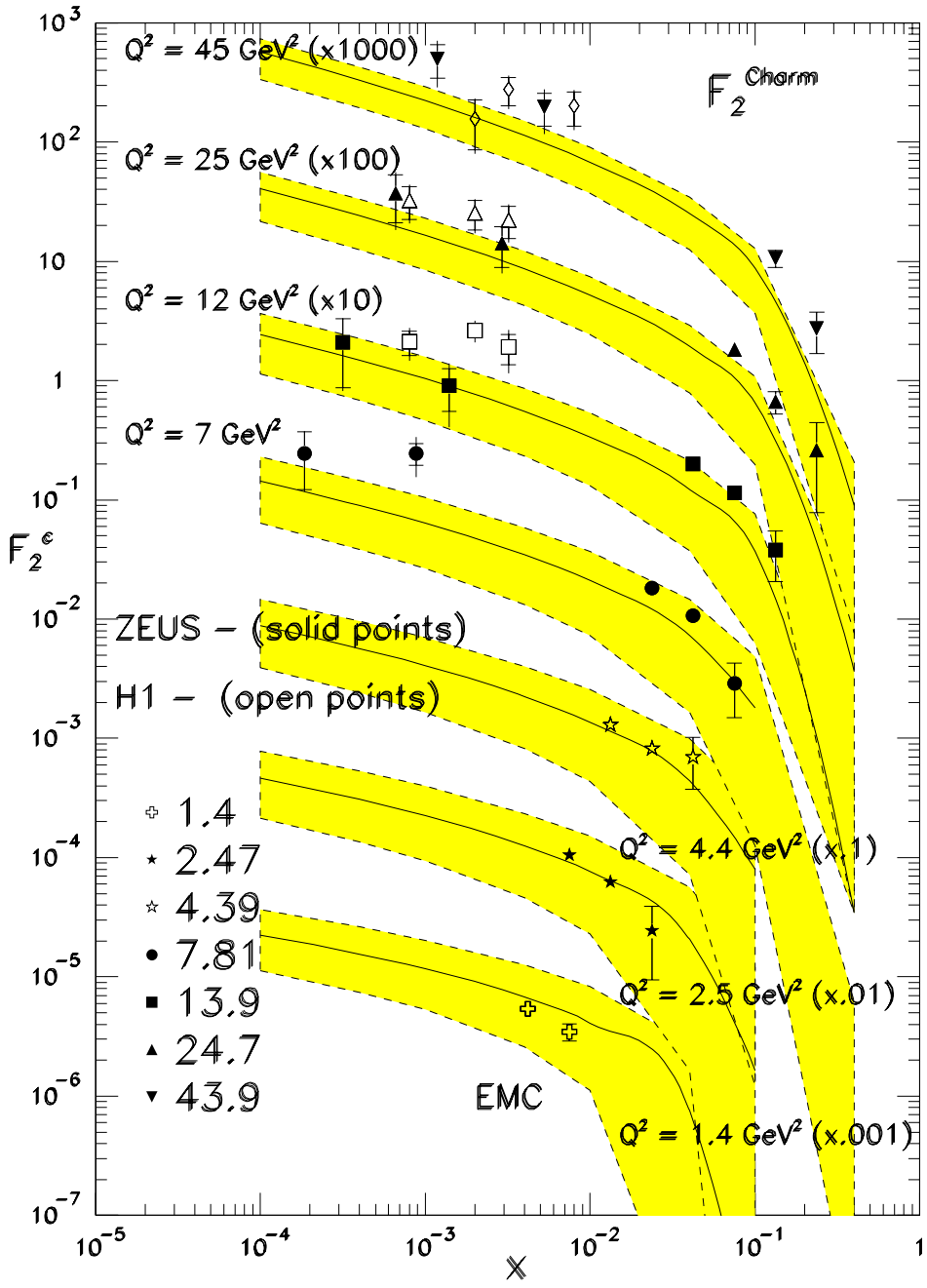

Figure 7.7: F_2^{charm} as a function of x, for various Q^2. The curves are the gluon-boson fusion cross section using an m_c of 1.40 and the GRV94 gluon PDF. Data points are from charged lepton scattering. Our data is sensitive in a region that overlaps EMC but extends to slightly higher Q^2 and slightly lower x.

Chapter 8

Flavor Changing Neutral Current Analysis and Results

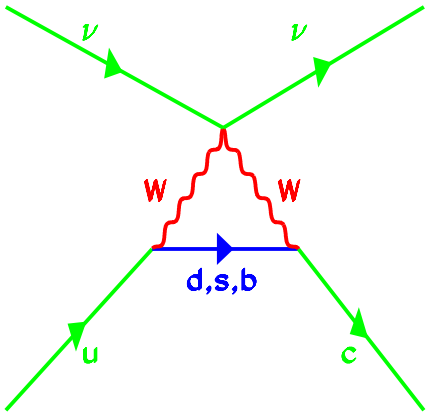

Figure 8.1: Loop diagram of a FCNC-like interaction.

Flavor-changing neutral-currents(FCNC) are suppressed by the GIM mechanism[3] as explained in Chap 2. While FCNC's are forbidden in the

standard model in leading order, higher order loop diagrams, such as shown in Fig 8.1, predict FCNC-like interactions at the roughly the 10^{-8} level. Studies of rare kaons have been able to reach the level of these second order FCNC-like decays [47, 48] in the strange quark sector. Studies in the charm, bottom and top sector have not reached this level of precision.

Extensions to the standard model which include additional particles are particularly apt to change the level at which FCNC-like interactions occur. For this reason FCNC's are a good way to search for and limit new physics. This can happen in two general fashions: 1) The new physics can allow first order FCNC interactions forbidden in the SM, or 2) the new physics can enhance the rate of FCNC-like events which occur through loop diagrams in the SM. Specific physics models include: extra quark generations [62, 63], technicolor[64, 65, 66, 67, 68], a multiple Higgs sector as in supersymmetry[69, 70, 71, 72], left-right symmetric models[73], and leptoquarks[74, 75].

This analysis will look at FCNC production of heavy flavor using a neutrino beam. Neutrino scattering is particularly sensitive to FCNC processes which may be mediated by a neutral object that couples more strongly to neutral leptons than charged leptons. In addition the inclusive nature of this study allows one to examine FCNC processes at the quark level rather than the hadron level.

This chapter includes a discussion previous searches for FCNC's, the simulations used in this search, a description of the fitter used for this analysis, the results of this fit, and the kinematic properties of the FCNC sample.

8.1 FCNC Search

This analysis uses the WSM data sample described in Chap. 4 and the simulations described in Chap. 5. For this portion of the analysis the gluon-boson fusion is considered a background and the previous measure of m_c=1.70 $\pm$ 0.19 GeV/c^2 from CC charm production is used. Note that this m_c will generate a smaller NC charm signal than the m_c measured in the previous chapter, and so this is a conservative choice for the purpose of searching for an FCNC source. The measurement is made for $Y_{vis} > 0.5$, a region that was not used in the $\bar{\nu}$-mode fit to the beam impurities in Chap. 6.

8.1.1 FCNC simulations

The cross section for $u \to c$ FCNC events from an isoscalar target is taken to be:

$$\sigma_{FCNC} = \frac{G_F^2 ME}{\pi} \left[g_l^2 + g_r^2(1-y)^2\right] \xi(u(\xi) + d(\xi)) \left(1 - \frac{m_c^2}{2ME\xi}\right) \quad (8.1)$$

Which is transformed into:

$$\sigma_{FCNC} \propto (g_l^2 + g_r^2) \left[\frac{g_l^2}{g_l^2 + g_r^2} + \frac{g_r^2}{g_l^2 + g_r^2}(1-y)^2\right] \quad (8.2)$$

with hard cuts of $\xi \geq \frac{m_c^2}{2M_pE}$, $y \geq \frac{m_c^2}{2M_pE\xi}$, and $W^2 \geq (M_D + M_p)^2$. Defining $V_{uc}^2 \equiv g_l^2 + g_r^2$ and using the notation $cos^2\beta \equiv \frac{g_l^2}{g_l^2+g_r^2}$, Eqn. 8.2 becomes:

$$\sigma_{FCNC} \propto |V_{uc}|^2 \left[cos^2\beta + sin^2\beta \times (1-y)^2\right]$$

The fragmentation of the charm quark is handled in exactly the same format as the charm quark produced in charged current charm production.

At NuTeV's energies it is also possible for FCNC production of bottom. Since FCNC bottom can come from either down or the strange sea, the $u(x)$

above must be replaced by $(d(x) + s(x))$. And we end up with:

$$\sigma_{FCNC} \propto |V_{db}|^2 \left[cos^2\beta' + sin^2\beta' \times (1-y)^2\right] d(x) +$$

$$|V_{sb}|^2 \left[cos^2\beta'' + sin^2\beta'' \times (1-y)^2\right] s(x)$$

for the FCNC bottom cross-section. These samples of bottom can be split into the down produced bottom and the strange produced bottom to allow us put limits on both V_{db} and V_{sb}. The GRV 94 PDF set is used in generation of these samples.

Samples of FCNC charm and bottom events are generated. Two charm and two bottom samples are generated: one that only couples to right handed quarks, and one that only couples to left handed quarks. These last two are then mixed to allow any ratio of right to left handed coupling.

8.1.2 FCNC Fitting Technique

The fitter used in this analysis is very similar to the one described in Sec. 7.1. A major difference is that the charm mass is constrained to m_c=1.7 GeV/c^2 by adding

$$\mathcal{L}_{added} = \sum_{j=1}^{6} \frac{(m_c - 1.70)^2}{\sigma^2_{m_c}} \tag{8.3}$$

to the likelihood. This value was chosen to agree with the NLO measurement of CC charm production[32]. Another difference is obviously the inclusion of the FCNC MC sample, which is included as a fixed shape with the size is allowed to float to find the best agreement. The three flavor samples (FCNC charm, FCNC bottom from d, and FCNC bottom from s) are treated separately. In the FCNC bottom sample, the bottom can decay to either muon through a cascade, for this reason both the ν and $\overline{\nu}$-mode WSM samples are used in the fit.

8.2 FCNC Results

8.2.1 Fit Results

The fit results are found in Table 8.2; in all cases V^2 is consistent with zero. Results are given for each of the three transitions with a range of values of $\sin^2\beta$. The results in Table 8.2 include the NC charm contribution with m_c constrained within errors to 1.7 GeV/c^2. An example of a typical fit is given in Fig. 8.2.

8.2.2 Systematic Errors

Estimates of the systematic uncertainty can be obtained by varying parameters and cuts by reasonable amounts. The systematic errors are determined in the same fashion as described in Sec. 7.3. These systematic errors are due to: *stop* cut, dimuon WSM events normalization, energy scale, and beam impurities. The systematics are listed in Table 8.1. These systematic errors are assumed to be independent and thus can be added in quadrature.

The systematic errors are determined in the same fashion as described in Sec. 7.3. These systematic errors are due to: *stop* cut, dimuon WSM events normalization, energy scale, and beam impurities.

8.2.3 Limits

In no case is there a significant signal for FCNC, and limits are accordingly set. Since Gaussian statistics apply, the 90% confidence level upper limit is set by adding 1.64σ to the best-fit value, if the best-fit value is positive, or 1.64σ to 0 if the best fit is negative. Here, σ consists of the statistical error from the fit added in quadrature to the estimated systematic error.

Transition	Coupling	Stop	Relative	Energy	Beam	Total
$u \to c$	L	0.30×10^{-3}	$0.32\ \times10^{-3}$	0.23×10^{-3}	$0.01\ \times10^{-3}$	$0.50\ \times10^{-3}$
$u \to c$	R	8.08×10^{-3}	$3.22\ \times10^{-3}$	0.24×10^{-3}	$0.02\ \times10^{-3}$	$8.70\ \times10^{-3}$
$d \to b$	L	0.36×10^{-3}	$0.22\ \times10^{-3}$	0.51×10^{-3}	$0.14\ \times10^{-3}$	$0.68\ \times10^{-3}$
$d \to b$	R	0.25×10^{-3}	$0.10\ \times10^{-3}$	0.04×10^{-3}	$0.55\ \times10^{-3}$	$0.61\ \times10^{-3}$
$s \to b$	L	2.37×10^{-3}	$0.21\ \times10^{-3}$	0.91×10^{-3}	$2.42\ \times10^{-2}$	$3.51\ \times10^{-2}$
$s \to b$	R	1.08×10^{-3}	$0.06\ \times10^{-3}$	0.20×10^{-3}	$0.54\ \times10^{-2}$	$1.22\ \times10^{-2}$

Table 8.1: Table of systematic errors on FCNC results.

The Table 8.2 summarizes the fit results, and includes the limits set. The region of $|V_{uc}|^2 - \sin^2\beta$, $|V_{db}|^2 - \sin^2\beta$‘, and $|V_{sb}|^2 - \sin^2\beta$“ space excluded by these fits is shown in Fig. 8.3,8.4, and 8.5 respectively.

8.3 Previous Searches for FCNC

All previous experimental searches for FCNC events involving c and b have looked for FCNC decays of particles. For this reason FCNC limits are given as upper limits on a specific branching ratio. Fermilab E791 collected tens of thousands of charm events, and placed some of the best limits available in the charm sector [49]. CDF[51], Mark II[55] and CLEO[53] have set limits on FCNC's in B meson decays. A summary of these limits are given in Table 8.3. The column for this limit with BR error is determined by shifting the BR on the allowed decay by one error bar.

This analysis looks at the FCNC's in the generation of heavy flavors. For comparison purposes, the following expressions are used to relate the branching ratio results to the parameters V_{uc},V_{db} and V_{sb}; named for their similarity to the CKM Matrix elements.

$$B(D^0 \to l^+ l^-) = 2 \left|\frac{V_{uc}}{V_{cs}}\right|^2 \frac{m_l^2}{m_\mu^2} B(D_s^\pm \to \mu^\pm \nu_\mu), \tag{8.4}$$

$$B(D^\pm \to \pi^\pm l^\pm l^\mp) = \left|\frac{V_{uc}}{V_{cd}}\right|^2 B(D^\pm \to \pi^0 \mu^\pm \nu_\mu),$$

$$B(D_s^\pm \to K^\pm l^\pm l^\mp) = \left|\frac{V_{uc}}{V_{cs}}\right|^2 B(D_s^\pm \to \eta \mu^\pm \nu_\mu).$$

For B decays it is assumed that

$$B(B^0 \to l^+ l^-) = 2 \left|\frac{V_{bd}}{V_{ub}}\right|^2 \frac{m_l^2}{m_\mu^2} B(B^\pm \to \mu^\pm \nu_\mu), \tag{8.5}$$

$$B(B^\pm \to \pi^\pm l^\pm l^\mp) = \left|\frac{V_{bd}}{V_{ub}}\right|^2 B(B^0 \to \pi^\pm l^\mp \nu_l),$$

$$B(B_s^0 \to l^+ l^-) = 2 \left|\frac{V_{bs}}{V_{ub}}\right|^2 \frac{m_l^2}{m_\mu^2} B(B^\pm \to \mu^\pm \nu_\mu),$$

$$B(D^\pm \to K^\pm l^\pm l^\mp) = \left|\frac{V_{bs}}{V_{bc}}\right|^2 B(B^\pm \to D^0 \mu^\pm \nu_\mu).$$

Measured values for the branching fractions on the right hand side are used. The leptonic decay $B^\pm \to \mu^\pm \nu_\mu$ is an exception, as it has not been measured, and it is assumed that:

$$B(B^\pm \to \mu^\pm \nu_\mu) = \frac{G_F^2 f_B^2 m_B m_\mu^2 \tau_B}{8\pi} \tag{8.6}$$

$$= 2.2 \times 10^{-6}$$

It is interesting to note that some of the strongest limits, such as $D^0 \to e^\pm e^\mp$, are not useful for new physics searches due to helicity-suppression.

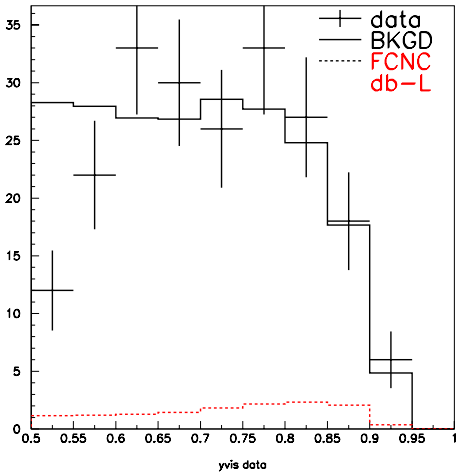

a)

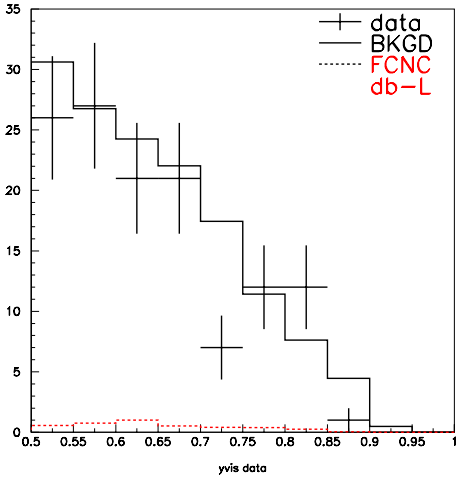

b)

Figure 8.2: The results of a typical FCNC fit. This example is d to b transition with left handed coupling ($\sin^2\beta'$=0). a) ν-mode b) $\bar{\nu}$-mode.

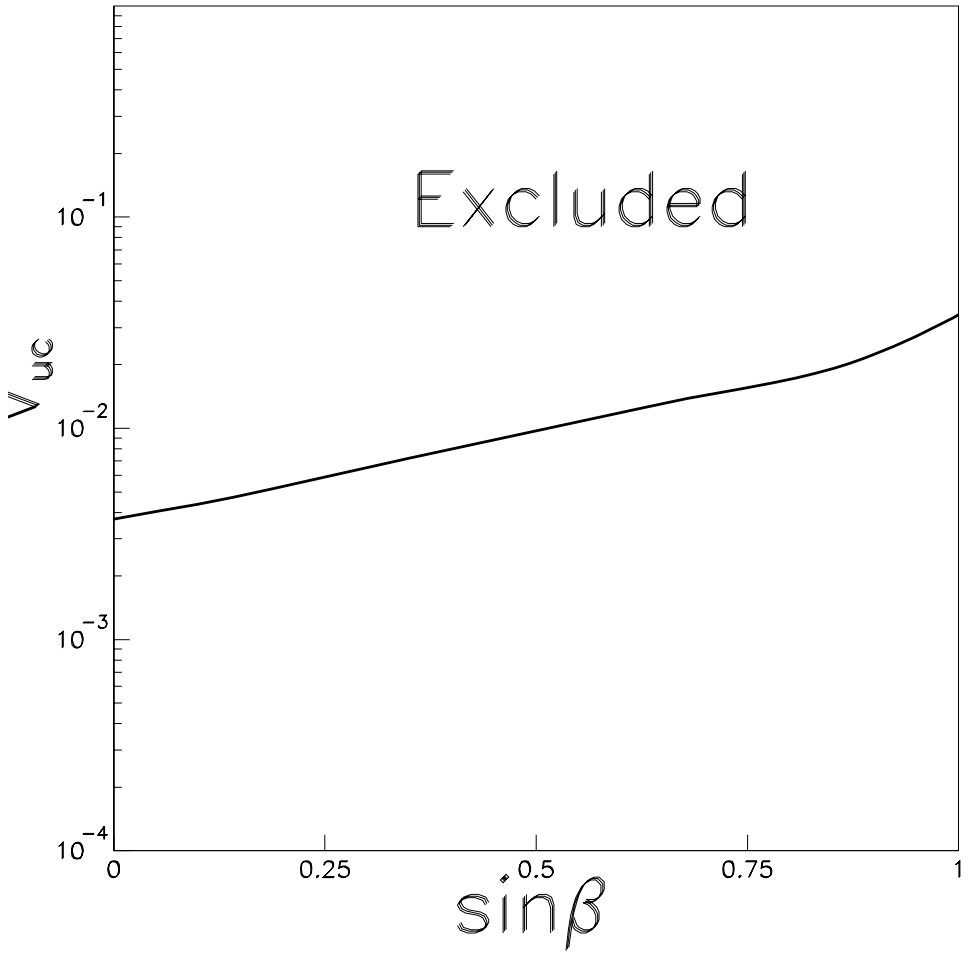

Figure 8.3: The region of $|V_{uc}|^2 - \sin^2\beta$ space excluded by this fit.

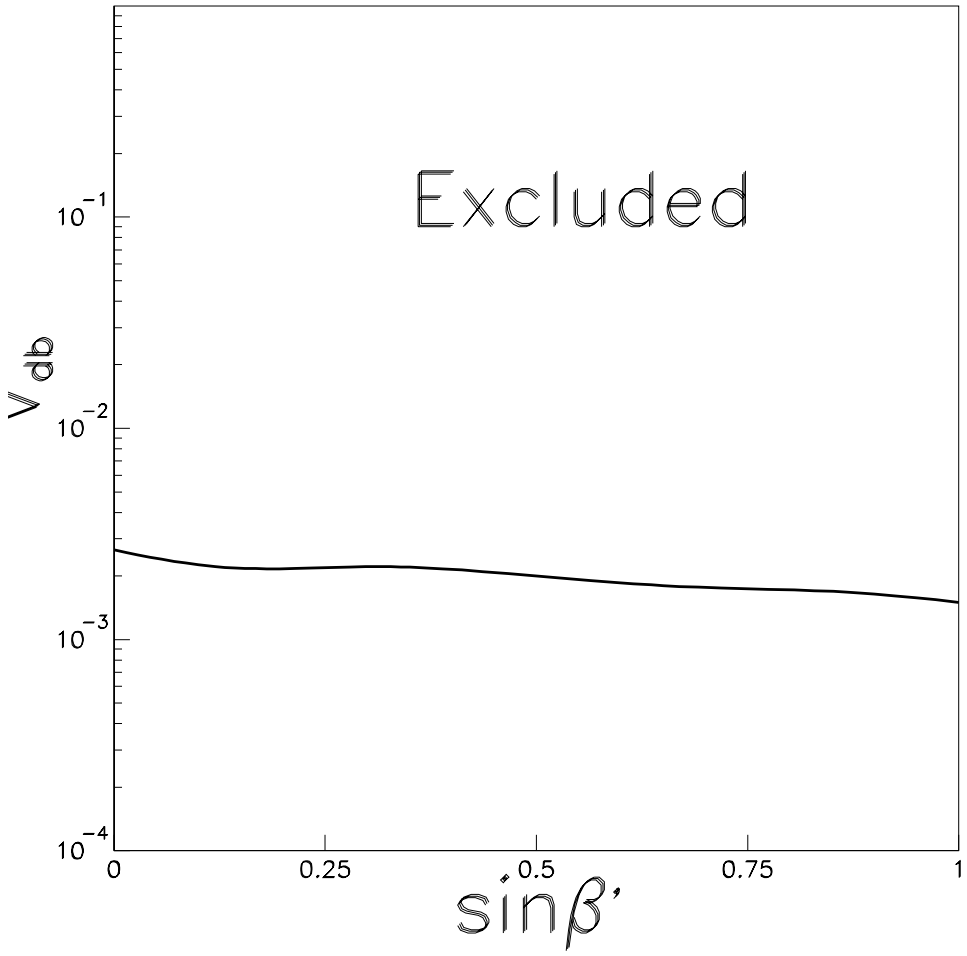

Figure 8.4: The region of $|V_{db}|^2 - \sin^2 \beta'$ space excluded by this fit.

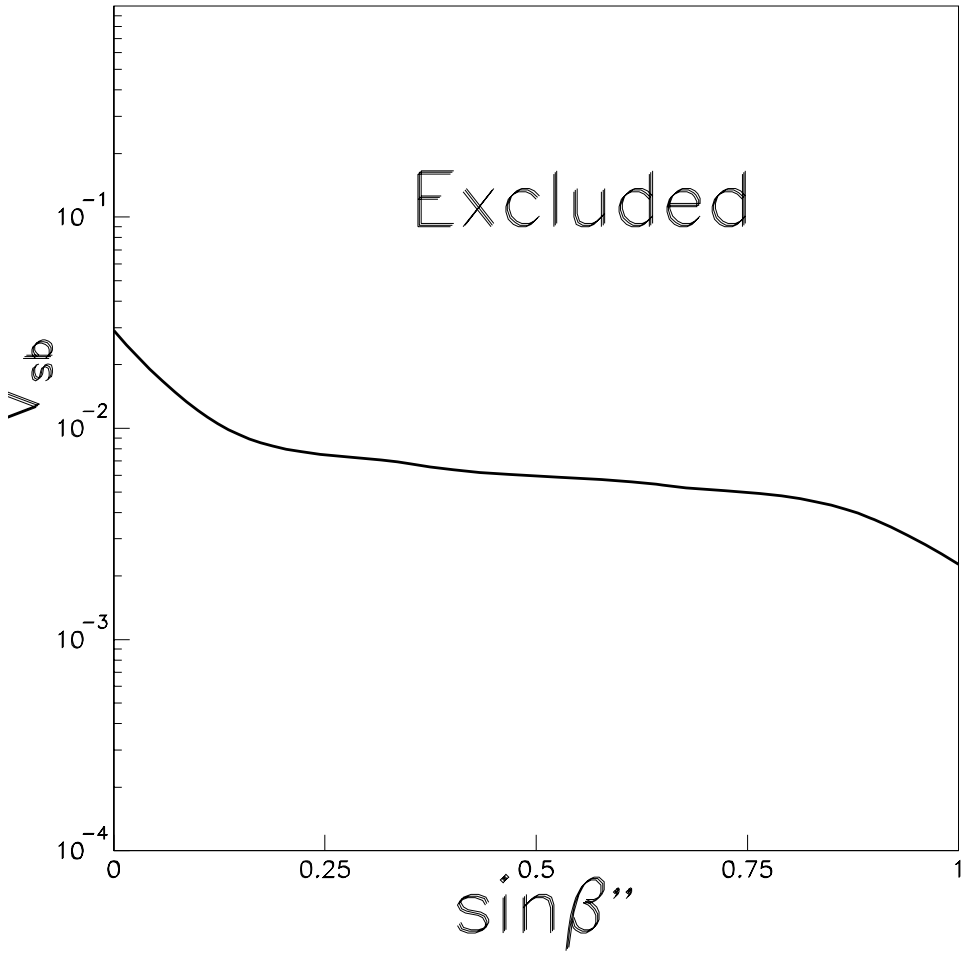

Figure 8.5: The region of $|V_{sb}|^2 - \sin^2\beta''$ space excluded by this fit.

Transition	Coupling	m_c	V^2	Limit
$u \to c$	0.0	1.82 ± 0.41	(1.13±1.50±0.50)×10^{-3}	3.72×10^{-3}
$u \to c$	0.10	1.82 ± 0.37	(1.23±1.69±0.91))×10^{-3}	4.38×10^{-3}
$u \to c$	0.22*	1.81 ± 0.41	(1.38±1.93±1.40)×10^{-3}	5.29×10^{-3}
$u \to c$	0.35	1.81 ± 0.38	(1.58±2.24±2.60)×10^{-3}	7.21×10^{-3}
$u \to c$	0.65	1.72 ± 0.40	(2.46±3.57±5.42)×10^{-3}	13.1×10^{-3}
$u \to c$	0.90	1.72 ± 0.41	(4.14±7.91±7.86)×10^{-3}	22.4×10^{-3}
$u \to c$	1.00	1.75 ± 0.42	(4.38±13.7±8.70)×10^{-3}	34.5×10^{-3}
$d \to b$	0.00	1.77 ± 0.57	(0.31±1.26±0.68)×10^{-3}	2.66×10^{-3}
$d \to b$	0.10	1.67 ± 0.56	(-0.15±1.21±0.67)×10^{-3}	2.26×10^{-3}
$d \to b$	0.22*	1.59 ± 0.42	(-0.72±1.32±0.66)×10^{-3}	2.42×10^{-3}
$d \to b$	0.35	1.51 ± 0.57	(-1.22±1.17±0.66)×10^{-3}	2.20×10^{-3}
$d \to b$	0.65	1.48 ± 0.50	(-1.55±0.90±0.63)×10^{-3}	1.80×10^{-3}
$d \to b$	0.90	1.54 ± 0.41	(-1.37±0.79±0.62)×10^{-3}	1.64×10^{-3}
$d \to b$	1.00	1.55 ± 0.41	(-1.29±0.68±0.61)×10^{-3}	1.50×10^{-3}
$s \to b$	0.0	1.44 ± 0.42	(-17.3±17.3±3.51)×10^{-3}	29.0×10^{-3}
$s \to b$	0.10	1.32 ± 0.41	(-13.6±6.64±3.28)×10^{-3}	12.1×10^{-3}
$s \to b$	0.22*	1.53 ± 0.40	(-5.62±2.85±3.01)×10^{-3}	6.80×10^{-3}
$s \to b$	0.35	1.55 ± 0.41	(-3.63±1.85±2.71)×10^{-3}	5.38×10^{-3}
$s \to b$	0.65	1.57 ± 0.41	(-1.91±1.00±2.02)×10^{-3}	3.70×10^{-3}
$s \to b$	0.90	1.57 ± 0.42	(-1.39±0.72±1.45)×10^{-3}	2.66×10^{-3}
$s \to b$	1.00	1.57 ± 0.40	(-1.25±0.65±1.22)×10^{-3}	2.27×10^{-3}

Table 8.2: Results of the FCNC fits. The transition type is given, and the value of $\sin^2\beta$, the SM value of $\sin^2\beta$ is denoted by *. The systematic error and limits are included.

FCNC decay	BR Limit	Allowed Decay	$\|V\|^2$ limit	Limit with BR error	reference
$D^0 \to e^\pm e^\mp$	9.3×10^{-6}	$D_s^\pm \to \mu^\pm \nu_\mu$	4.5×10^{1}	6.9×10^{1}	[49]
$D^0 \to \mu^\pm \mu^\mp$	2.6×10^{-6}	$D_s^\pm \to \mu^\pm \nu_\mu$	2.9×10^{-4}	4.5×10^{-4}	[49]
$D^\pm \to \pi^\pm e^\pm e^\mp$	6.5×10^{-5}	$D^\pm \to \pi^0 l^\pm \nu_l$	8.8×10^{-4}	1.0×10^{-3}	[49]
$D^\pm \to \pi^\pm \mu^\pm \mu^\mp$	1.7×10^{-5}	$D^\pm \to \pi^0 l^\pm \nu_l$	2.3×10^{-4}	2.7×10^{-4}	[49]
$D_s^\pm \to K^\pm \mu^\pm \mu^\mp$	2.4×10^{-4}	$D_s^\pm \to \eta l^\pm \nu_l$	6.7×10^{-3}	8.9×10^{-3}	[49]
$D_s^\pm \to K^\pm e^\pm e^\mp$	4.7×10^{-4}	$D_s^\pm \to \eta l^\pm \nu_l$	1.3×10^{-2}	1.7×10^{-2}	[49]
$B^0 \to e^\pm e^\mp$	5.9×10^{-6}	$B^0 \to \mu^\pm \nu_\mu$	1.1×10^{5}	N/A	[50]
$B^0 \to \mu^\pm \mu^\mp$	6.8×10^{-7}	$B^\pm \to \mu^\pm \nu_\mu$	1.5×10^{-1}	N/A	[52]
$B^\pm \to \pi^\pm e^\pm e^\mp$	3.9×10^{-3}	$B^0 \to \pi^0 l^\pm \nu_l$	1.6×10^{-3}	2.1×10^{-3}	[55]
$B^\pm \to \pi^\pm \mu^\pm \mu^\mp$	9.1×10^{-3}	$B^0 \to \pi^0 l^\pm \nu_l$	3.7×10^{-3}	4.9×10^{-3}	[55]
$B_s^0 \to e^\pm e^\mp$	5.4×10^{-5}	$B^\pm \to \mu^\pm \nu_\mu$	1.0×10^{6}	N/A	[54]
$B_s^0 \to \mu^\pm \mu^\mp$	2.0×10^{-6}	$B^\pm \to \mu^\pm \nu_\mu$	4.5×10^{-1}	N/A	[52]
$B^\pm \to K^\pm e^\pm e^\mp$	3.9×10^{-5}	$B^0 \to D^0 l^\pm \nu_l$	2.4×10^{-5}	2.1×10^{-5}	[53]
$B^\pm \to K^\pm \mu^\pm \mu^\mp$	1.0×10^{-5}	$B^0 \to D^0 l^\pm \nu_l$	4.0×10^{-6}	5.4×10^{-6}	[55]

Table 8.3: Previous FCNC decay limits. (An allowed decay is used to relate the BR limit to V_{uc},V_{db}, and V_{sb} as summarized in Eqns. 8.4-8.5) $|V|^2$= $|V_{uc}|^2$,$|V_{db}|^2$, or $|V_{sb}|^2$ as appropriate

Chapter 9

Conclusions

NuTeV's use of the SSQT make it possible to look at WSM's. Wrong sign muons are a good window into heavy flavor production. Three basic measurements come out of this analysis, and they are:

- The cross section for charm production in proton scattering
- The cross section for charm production in neutrino scattering
- Limits on FCNC production of charm and bottom.

Using the $\bar{\nu}$-mode WSM sample one extracts the normalizations for all known sources of beam impurities. The corrected charm production at the target measures $\sigma_{p+p\to c\bar{c}} = 49 \pm 11 \pm 5.6\ \mu b$, using linear A dependence. The fit also indicates that the GHEISHA[24] simulation underpredicts the ν contribution due to scraping by about 20%. Other sources (muon decay, K^0 production, and prompt decays of π's and K's) are consistent with their nominal values.

The ν-mode WSM sample provides the first direct observation of Z boson-gluon fusion in lepton scattering. Previous experiments[15][18] have

observed NC charm production using charged leptons, however this is dominated by photon-gluon fusion. Others have observed NC charm production of the J/ψ [76]. Using a boson-gluon fusion model the charm mass is determined to be $m_c = 1.40^{+0.83}_{-0.36} \pm 0.26$ GeV/c^2. The average energy of ν's which produce a pair of c quarks is 154 GeV, and at this energy the cross section is $\sigma_{\nu+N\to c\bar{c}} = (2.14^{+1.76}_{-1.54}) \times 10^{-1} fb$. This m_c is within errors of previous measurements. It provides no evidence for an intrinsic charm, and no evidence that there is a difference between this m_c and the one measured by CC charm production, photoproduction, or charmonium.

Both modes of WSM are valuable for extracting information of FCNCs. Searching for FCNC in the production of heavy flavor means that one must establish a new method for setting limits on this process. We set forth a convention of placing limits on quantities similar to the elements of the CKM matrix. Limits on the V_{uc},V_{db}, and V_{sb} are given using SM couplings and as a function of $\sin^2\beta$. Previous measurements are converted into this convention and compared to our limits. We set a limit on V_{db} which is better then all but one previous measurement [55], and very close to that limit.

Our FCNC search has a couple of qualities that make it of special interest. This is the only time FCNC has been looked at on the production side. The use of a neutrino beam is also particularly sensitive to any FCNC process in which the propagator couples more strongly to neutrinos then to charged leptons (a coupling pattern found, for example, with the Z^0).

Other experiments and other signals in NuTeV can be used to isolate the same physics as we have examined. The measurement of $\sigma_{p+p\to c\bar{c}}$ could be confirmed both by NuTeV and by FNAL-E872(DONUT). NuTeV currently has an analysis underway to search for $\nu_\mu - \nu_e$ oscillations. In this analysis events that appear to be CC ν_e interactions are identified. In $\bar{\nu}$-mode charm is responsible for approximately 10% of the ν_e's and it should

be possible to determine if this data agrees with the measurement made by the WSM's. The experiment FNAL-E872 is searching for direct observation of ν_τ (DONUT). They have intentionally tried to remove all ν_μs, and thus most of their ν_μs are from $p + p \rightarrow c\bar{c}$. So they are in a fine position to confirm this measurement.

There are still searches for heavy flavor production by neutrinos that NuTeV might attempt and many that other experiments could attempt. NuTeV's access to charm is almost exhausted; however, one might be able to use the events which appear to be CC ν_e interactions described above to search for $\nu_\mu + N \rightarrow c\bar{c}$ where one or both of the charmed mesons decay into electrons. NuTeV still has some fertile ground to explore as far as bottom production goes. Because the B's can decay to multiple muons, searches of NuTeV's events with three or more muons may provide evidence for CC b or NC $b\bar{b}$ production. In addition one can examine the same-sign dimuon sample, or the opposite-sign dimuon sample in the regions where $E_\mu^{rs} < E_\mu^{ws}$, or $E_\mu^{rs} \simeq E_\mu^{ws} \simeq 50$ GeV.

Other experiments should also be able to say something about heavy flavor production by neutrinos. DONUT is searching for the kink that a τ makes when it decays to a μ, and this means it is set up to search for heavy flavor decays. Though limited by their flux, their ability to identify displaced vertices is powerful. Another future prospect for this type of work comes from the plans for a Neutrino factory[78]. While these plans are in their rough stages they do provide possibility of a very pure high intensity ν beam.

Appendix A

The Cross Section

A general form for the neutrino-nucleon differential cross section is:

$$\frac{d^2\sigma^{\nu(\overline{\nu})}}{dxdy} = \frac{G_F^2 ME}{\pi}\left[(1-y)F_2^{\nu(\overline{\nu})}(x,Q^2) + \frac{y^2}{2}F_1^{\nu(\overline{\nu})}(x,Q^2) \pm y\left(1-\frac{y}{2}\right)xF_3^{\nu(\overline{\nu})}(x,Q^2)\right]. \tag{A.1}$$

For the process $Z^o g \to c\overline{c}$, xF_3 turns out to be zero. The rest of the cross section is taken from Ref. 11. Beginning with Eqn. 2.2 of that paper:

$$F_1(x,Q^2) = \int_{ax}^{1}\frac{dz}{z}G(z,\hat{s})f_1\left(\frac{x}{z},Q^2\right)$$

$$F_2(x,Q^2) = \int_{ax}^{1}\frac{dz}{z}zG(z,\hat{s})f_2\left(\frac{x}{z},Q^2\right) \tag{A.2}$$

Where $a = 1 + \frac{(m+m')^2}{Q^2}$. We transform $z = \frac{x}{y}$ and $dz = -\frac{x}{y^2}dy$. This transforms Eq. A.2 into:

$$F_1(x,Q^2) = \int_{1/a}^{x} -\frac{dy}{y}G(\frac{x}{y},\hat{s})f_1\left(y,Q^2\right)$$

$$F_2(x,Q^2) = \int_{1/a}^{x} -\frac{dy}{y}\frac{x}{y}G(\frac{x}{y},\hat{s})f_2\left(y,Q^2\right) \tag{A.3}$$

which becomes

$$F_1(x,Q^2) = \int_{x}^{1/a} \frac{dy}{y}G(\frac{x}{y},\hat{s})f_1\left(y,Q^2\right)$$

$$F_2(x,Q^2) = \int_{x}^{1/a} \frac{dy}{y}\frac{x}{y}G(\frac{x}{y},\hat{s})f_2\left(y,Q^2\right) \tag{A.4}$$

In general, f_1 and f_2, have complicated forms; however for pair-production of equal mass quarks,

$$f_1(z,Q^2) = \frac{\alpha_s}{\pi}\frac{q_+}{4}\left\{-v\overline{v}\left[(1-2z)^2 + \frac{q_+}{q_-}\frac{m^2}{Q^2}4z(1-z)\right] + \left[1-2z(1-z)+\frac{q_+}{q_-}\frac{m^2}{Q^2}4z(1-z-z\frac{2m^2}{Q^2})\right]L\right\},$$

and

$$f_2(z,Q^2) = \frac{\alpha_s}{\pi}q_+ z\left\{v\overline{v}\left[-\frac{1}{2}+(4z-\frac{2m^2}{Q^2})z(1-z)\right] + \frac{1}{2}\left[1-2z(1-z)+\frac{2m^2}{Q^2}(1+2z-6z^2)-\frac{q_+}{q_-}\frac{2m^2}{Q^2}-\frac{8m^4}{q^4}z^2\right]L\right\}. \tag{A.5}$$

Where $v\overline{v} = \sqrt{1-\frac{4m^2}{Q^2}\frac{z}{1-z}}$, $L = \log\frac{1+v\overline{v}}{1-v\overline{v}}$, and the vector(V) and axial vector(A) couplings enter via $q_\pm = V^2 \pm A^2 = (\frac{1}{2}-\frac{4}{3}\sin\theta_w)^2 \pm (\frac{1}{2})^2$. Separating these in terms of factors of q_+ and q_- yields.

$$f_1(z,Q^2) = \frac{\alpha_s}{4\pi}\left\{q_+\left[-v\overline{v}(1-2z)^2 + [1-2z(1-z)]L\right] + q_-\left[-v\overline{v}(\frac{m^2}{Q^2})4z(1-z)+\frac{m^2}{Q^2}4z(1-z-z\frac{2m^2}{Q^2})L\right]\right\}$$

$$f_2(z,Q^2) = \frac{\alpha_s}{\pi}\left\{ q_+ \left[v\overline{v}[-\frac{z}{2} + (4z - \frac{2m^2}{Q^2})z^2(1-z) \right] \right.$$
$$\left. + L[\frac{z}{2} - z^2(1-z) + \frac{m^2}{Q^2}z(1+2z-6z^2) - \frac{4m^4}{q^4}z^3] - q_- z\frac{m^2}{Q^2}L \right\} \quad \text{(A.6)}$$

Appendix B

The Beam Simulation

B.1 Introduction

The GEANT based flux simulates processes that are not in the TURTLE based flux. For the wrong sign muon(WSM) analysis it is necessary to account for all beam impurities. About a quarter of the $\overline{\nu}_\mu(\nu_\mu)$ in $\nu(\overline{\nu})$-mode is due to scraping. Scraping refers to hadrons produced by interaction between beam hadrons and elements of the beamline. Another 18% of these are due to cascade decays, of the type,

$$K^+ \rightarrow \pi^+\pi^+\pi^- \tag{B.1}$$

$$\hookrightarrow \mu^-\nu_\mu$$

Neutrinos from these sources are an important source of wrong sign neutrinos, and, at a few energies, reach the level of 1% of the right sign flux.

B.2 Production

This flux was generated with the π/K production parameterization [20] used by TURTLE. GEANT propagated these particles through the geometry of the SSQT allowing them to decay or interact anywhere along the way.

GEANT was modified to treat wrong sign hadrons(π^-,K^-, and K_L in ν-mode and π^+, K^+ and K_L in $\overline{\nu}$-mode) differently from right sign hadrons. These particles were treated as if they had infinite lifetimes but at each step were forced to decay into a ν_μ or $\overline{\nu}_\mu$ with an appropriate weight. The weight is determined by the probability of decaying in that step and the branching ratio for decay into that neutrino type. This effectively generated a more statistically significant sample of wrong sign ν's without needing to generate unnecessary right sign statistics.

The GEANT flux propagates π^+,π^-,K^+,K^-,K_S, K_L, and protons through the SSQT beamline. This flux also includes contributions from $D^{\pm}$, D^0, and Λ_c decays, however these charm sources decay promptly and so TURTLE was used for their propagation. Protons and K_L were treated differently from the other particles. The protons were run in such a way that scraping products of either charge had an infinite lifetime and were forced to decay at every step, similar to how wrong sign hadrons are treated above. This was done because right sign ν's from scraping of protons was a significant fraction of the right sign flux. A difference was found between K_L's generated at the target and propagated as described above, and K_L's generated at the target and propagated with the real lifetime and decay probabilities. It is believed this difference is because a large fraction of the ν's produced by K_L's come from the decay products. For example:

$$K_L \rightarrow \pi^+ \pi^o \pi^- \tag{B.2}$$
$$\hookrightarrow \mu^- \nu_\mu$$

For this reason the K_L created in the target were propagated with the real lifetime and decay probabilities.

B.3 Beam Elements

This section gives descriptions of the beam elements, and their locations in the GEANT simulation. TURTLE uses a straight line for a given energy particle, and bends around this straight line. GEANT however uses normal (un-bent) coordinate systems, so there are offsets in y (the bend direction) compared to TURTLE. The bend due to the dipoles were calculated by putting neutral particles through TURTLE, and measuring the change in theta. The GEANT beamline had 5 straight regions: the region before the first dipole, the length of the first dipole, the region between the two dipoles, the length of the second dipole, and the region after the second dipole. GEANT uses cm for length and describes geometric objects in terms of their half-lengths so all dimensions and positions are given in cm, and all dimensions are half-lengths.

The first beam element is the target, a one interaction length BeO rod. It is at (0.,-7.297,17.78) in the GEANT coordinate system. It has a radius of 1.27 and, a half-length of 17.78. Note that the GEANT z=0 point is the front of the target. The target has a 7.968 mr bend in y with respect to the z dimension. It should be noted that the target isn't used in this simulation, as particle production uses Malensek (which is a thick target model) and particles are produced right after the target.

The large angle pile(LAP or dipole shield) is the next element. This removes a majority of the particles which are unable to make it down the beam line. It is modeled as a $40.\times40.\times17.78$ (half lengths) aluminum block, with a 1.95×1.95 hole in the center. This is located at 0.,-6.973,58.42. The

LAP has a 7.968 mr bend in y with respect to the z dimension.

The first dipole follows the LAP. The dipoles are both 17.15×31.12×152.4 blocks of iron with a 1.79×6.35 hole down the center. The first magnet has a field of 17. kG. This dipole has a 4.861 mr bend in y with respect to the z dimension.

The first dump (NC1DMP1 in TM or CF1 in SSQT_GEANT) is a block of Iron 71.12×96.52×182.9 with a hole 7.94 in x, but changing in y from 7.11 at the upstream end to 7.46 at the downstream end. This is located at (0.,-4.3304,853.4) While this element is suppose to be along the 1.754 mr line, the TURTLE documentation shows that it is offset so there is an additional .694 mr offset.

Just after the first dump is the neutral dump, or Photon-Be-Gone(PBG). The PBG is located at (0.,-3.9517,1069.3) and is a 15.0×15.0×17.78 block of iron with a 4.98×4.98 hole. The PBG is along the 1.754 mr line.

The next element is the first quadrapole. The quadrapoles start as a 29.21×43.8×152.4 block of iron with an aluminum pipe with inner radius of 6.5. However the quadrupole coils occupy part of this pipe, the material of these is simulated as 4 aluminum rods with radii of 7.0 and positioned at ±8.5 in x and ±8.5 in y with respect to the center of the pipe. This is approximately the same as the hyperbolic and circular slit that are used in TURTLE. The first quad has a magnetic field of 5.50 (focus in the bend angle) kG/inch, is located at (0.0762,-3.795,1249.7) and has an angle of 1.754 mr with respect to z.

The second dump (NC1DMP2 or CF2) is a block of iron 71.12×96.52×182.9 with a hole 7.94×5.76 located at (0.,-4.79,1767.8) with an angle of 1.754 mr.

The second quad has the same structure as the first, it is located at

(-0.0762,-2.152,2164.1), has a magnetic field of 5.50 (defocus in the bend angle) kG/inch, and an angle of 1.754 mr.

The third quad has the same structure as the first, it is located at (-0.0127,-.6304,3017.5), has a magnetic field of 4.97 (focus in the bend angle)kG/inch, and an angle of 1.754 mr.

The second dipole has the same structure as the first. It is located at (0.,-0.1337,3376.88), has a magnetic field of 4.8 kG, and has an angle of .877 mr.

The fourth, fifth and sixth quad come next. They are 30.48×52.07×45.26 blocks of iron, with a 9.843 radius pipe through them. Each of them has a field of 2.49 (defocus in the bend angle)kG/inch. They are located at (0.,0.0254,4190.85) (-0.254,0.0762,4322.83),and (-0.356,-0.0127,4455.11) respectively.

After these quads are the trim magnets. The trim magnets look just like the two dipoles. They were placed here in case the hadron beam needed to be directed towards the Lab E detector, however this was not necessary so they have no field.

Details can be found in the source code or extracted from the list of elements below.

```
************************************************
*              OBJECT POSITIONS                *
************************************************
 DEFINING DIPOLES, DUMPS
                XYZ CENTERS                  XYZ 1/2 LENGTHS
VAC DIP 1:   .000       .000       .000       1.790     6.350   152.400
VAC DIP 1: -.021     -5.873    243.800      17.150    31.120   152.400
```

```
VAC DMP 1:  .000    -2.540      .000     7.940     7.940     7.110
 FE DMP 1:  .000    -4.330   853.400    71.120    96.520   182.900
VAC DMP 2:  .000    -4.790      .000     7.940     5.760   182.900
 FE DMP 2:  .000      .000  1767.800    71.120    96.520   182.900
VAC DIP 2:  .000      .000      .000     7.630     7.630   152.400
 FE DIP 2:  .000     -.134  3376.880    17.150    31.120   152.400
PHOTON BG:  .000    -3.952  1069.300    15.000    15.000    17.780
 DEFINING QUADS, TRIM, PLUG
No copper insert in 4Q120s
              XYZ CENTERS                 XYZ 1/2 LENGTHS
 VAC QD 4:  .000      .000      .000       .000     9.843    45.260
  FE QD 4:  .000      .025  4190.850     30.480    52.070    45.260
 VAC QD 5:  .000      .000      .000       .000     9.843    45.260
  FE QD 5: -.254      .076  4322.830     30.480    52.070    45.260
 VAC QD 6:  .000      .000      .000       .000     9.843    45.260
  FE QD 6: -.356     -.013  4455.110     30.480    52.070    45.260
 VAC TRIM:  .000      .000      .000     10.160    10.160    76.200
  FE TRIM:  .000      .000  4615.280     17.150    31.120    76.200
 DEFINING THE SHIELDING, WINDOWS W/ FLANGES AND DECAY PIPE
              XYZ CENTERS                 XYZ 1/2 LENGTHS
 SHIELD 1:  .000   -45.720 10972.800    155.000   800.000  3048.000
 WINDOW 0:  .000      .000  -152.375      7.630     7.630      .028
 WINDOW 1:  .000      .000  3045.130       .000    19.368      .060
 WINDOW 2:  .000      .000 -8138.160       .000    45.720      .028
 FLANGE 0:  .000      .000      .000       .000      .000      .000
 FLANGE 1:  .000      .000 14016.990     19.368    21.907     1.270
 FLANGE 2:  .000      .000 -8138.160     46.030    46.360     1.270
 DKPIPE 0:  .000      .000  6512.660     14.287    15.240  1546.860
 DK CHANG:  .000      .000  8059.500     14.287    20.320     1.270
```

```
DKPIPE 1:   .000      .000    -1.270     19.368    20.320  2956.560
DK TRANS:   .000      .000-17326.711       .000    44.767     1.270
DKPIPE 2:   .000      .000 -3885.150       .000    45.720 17327.881
DKPIPE 3:   .000      .000      .000       .000      .000      .000
VACUUM 1:   .000      .000      .000       .000    19.368  3048.000
VACUUM 2:   .000      .000   274.320       .000    44.767 17327.881
VACUUM 3:   .000      .000      .000       .000      .000      .000

DEFINING THE SWIC(s)
              XYZ CENTERS                  XYZ 1/2 LENGTHS
  SWIC 1:   .000      .000 -7985.760       .000    45.720    15.240
SWIC VW1:   .000      .000   -15.215       .000    45.720      .025
SWIC VW2:   .000      .000    15.215       .000    45.720      .025
SWIC MW1:   .000      .000   -10.106       .000    45.720      .004
SWIC MW2:   .000      .000    -9.697       .000    45.720      .004
SWIC SG1:   .000      .000   -10.002       .000    45.720      .000
SWIC SG2:   .000      .000    -9.801       .000    45.720      .000
```

B.4 Running GEANT and Producing a Flux

One runs GEANT using the script *dogeant*. Dogeant expects one argument which is the name of a card file ending in .dat, but without the .dat. For example if one wants to use the card file test1a.dat, one should type *dogeant test1a* . In order to have good statistics I have generated 50 million pions, 30 million kaons, and 20 million K_L. I generated 5 million of each D^o, $D^{\pm}$, and Λ_c. Finally I generated 1 million each of protons which did not interact, protons which did interact, pions of the wrong sign, and kaons of the wrong sign, all of which have forced wrong sign decays at every step.

When GEANT runs it saves all the neutrinos which come near the detector. These neutrinos can then be projected into a numonte style flux. A numonte style flux gives the energy weighted number of events in a certain energy range, and a two dimensional x-y plot for that energy bin. In producing these one must choose a normalization. I choose to stick to TURTLE's 10^6 protons on target. To do this one must know the production weight of individual hadrons:

Table B.1: Production weight of various particles

Type	Positive	Neutral	Negative
Pion	.5366		.4383
Kaon	.09221	.06448	.05523
Proton	.3679		
Proton	.2682		
D	9.628×10^{-4}	7.194×10^{-4}	9.628×10^{-4}
Λ_c	2.312×10^{-3}		2.312×10^{-3}

The first proton entry refers to protons which have interacted in the target, while the second refers to protons which passed through the target without interacting.

The Lab E detector is 4000 feet downstream of the decay pipe. Because of this if the final leg of the simulation is off by a tenth of a miliradian that would result in a shift in y of 5 inches. Because of this the Lab E detectors location was assigned by running the flux through numonte and shifting the detector to make the vertx and verty distributions match between data and monte carlo.

B.5 TURTLE-GEANT comparison

After a lot of work GEANT has been adjusted so that beam elements agree between TURTLE and GEANT. The following figures and similar ones which are not included here, indicated that the two simulations agree.

B.6 Data-MC comparison

The true test of the simulation is to see how it agrees with data. Note that the fudges produced with this flux are approximately the same as the fudges on the TURTLE flux.

In addition to agreement in the energy spectrum the vertx and verty agree well. Recall that the mean positions were forced to agree, however the shape is also in very good agreement.

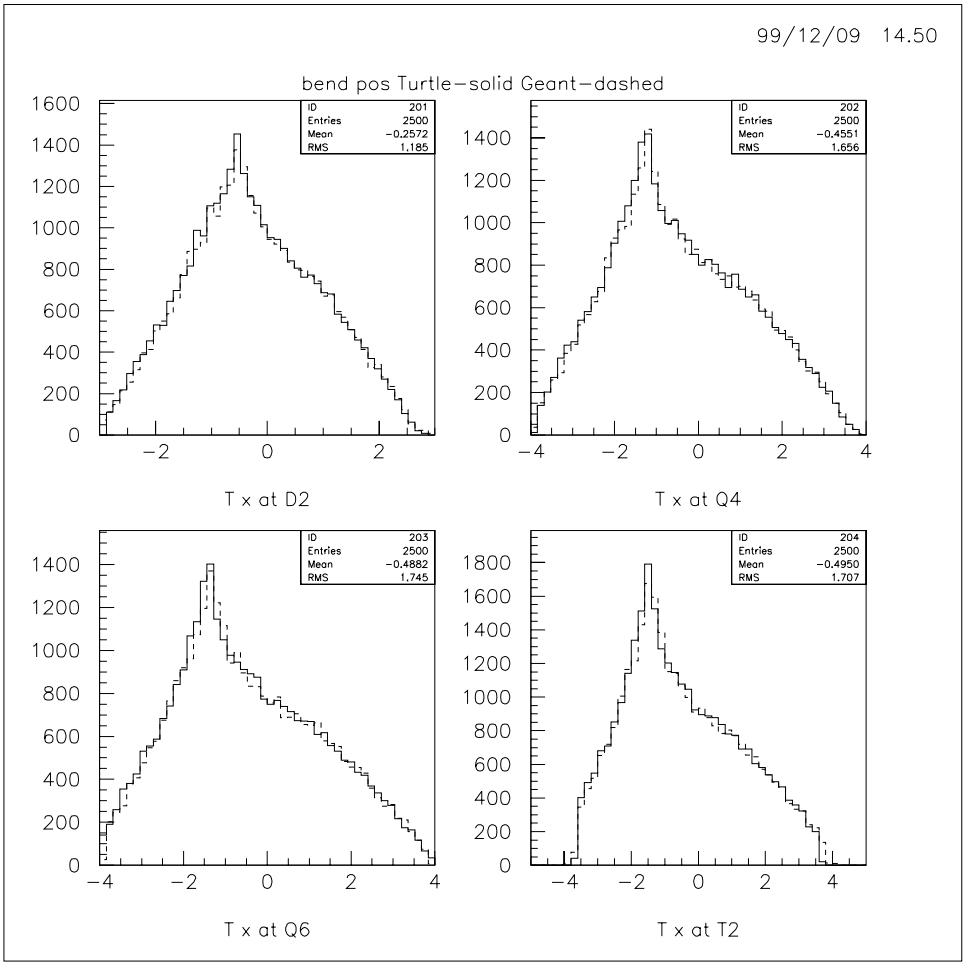

Figure B.1: This plot shows the position with respect to the beam centerline in the bend dimension for TURTLE and GEANT. TURTLE is shown in solid, and GEANT is shown as dashed. The z location for these plots are a) after the second dipole, b) after the 4th quad, c) after the 6th quad, and d) after the second trim magnet.

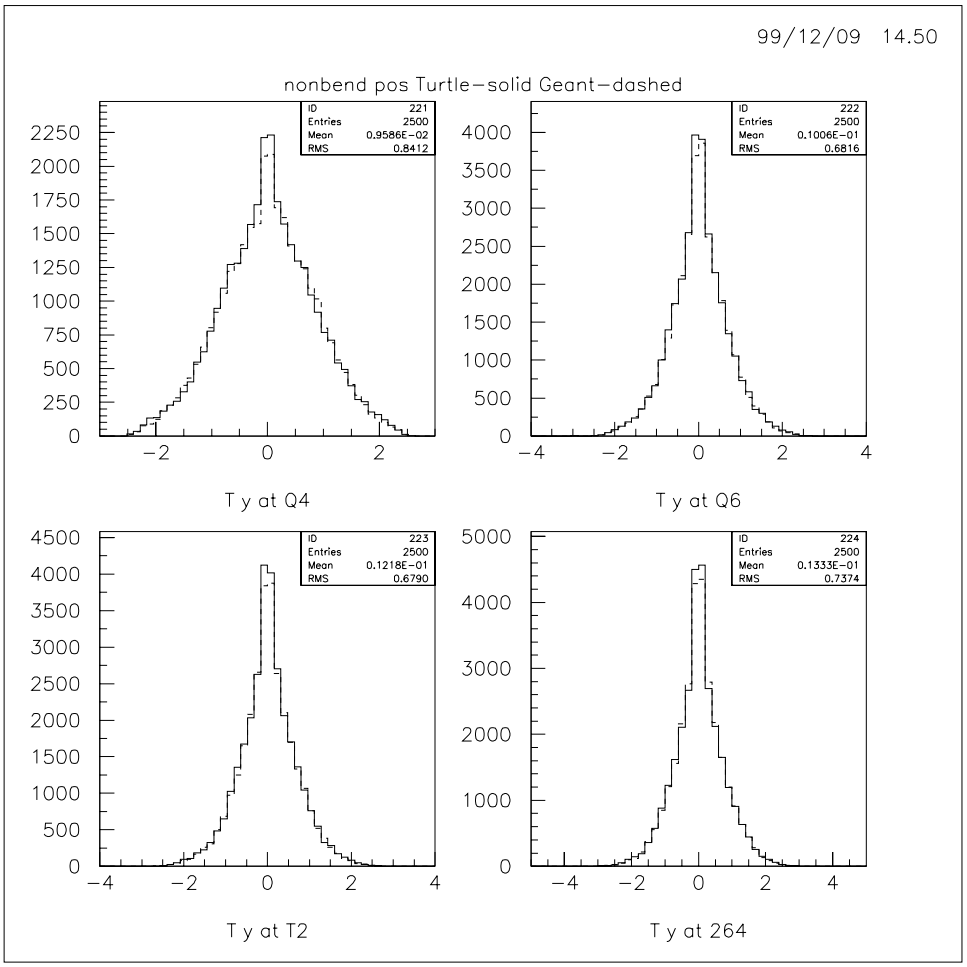

Figure B.2: This plot shows the position with respect to the beam centerline in the non-bend dimension for TURTLE and GEANT. TURTLE is shown in solid, and GEANT is shown as dashed. The z location for these plots are a) after the second dipole, b) after the 4th quad, c) after the 6th quad, and d) after the second trim magnet.

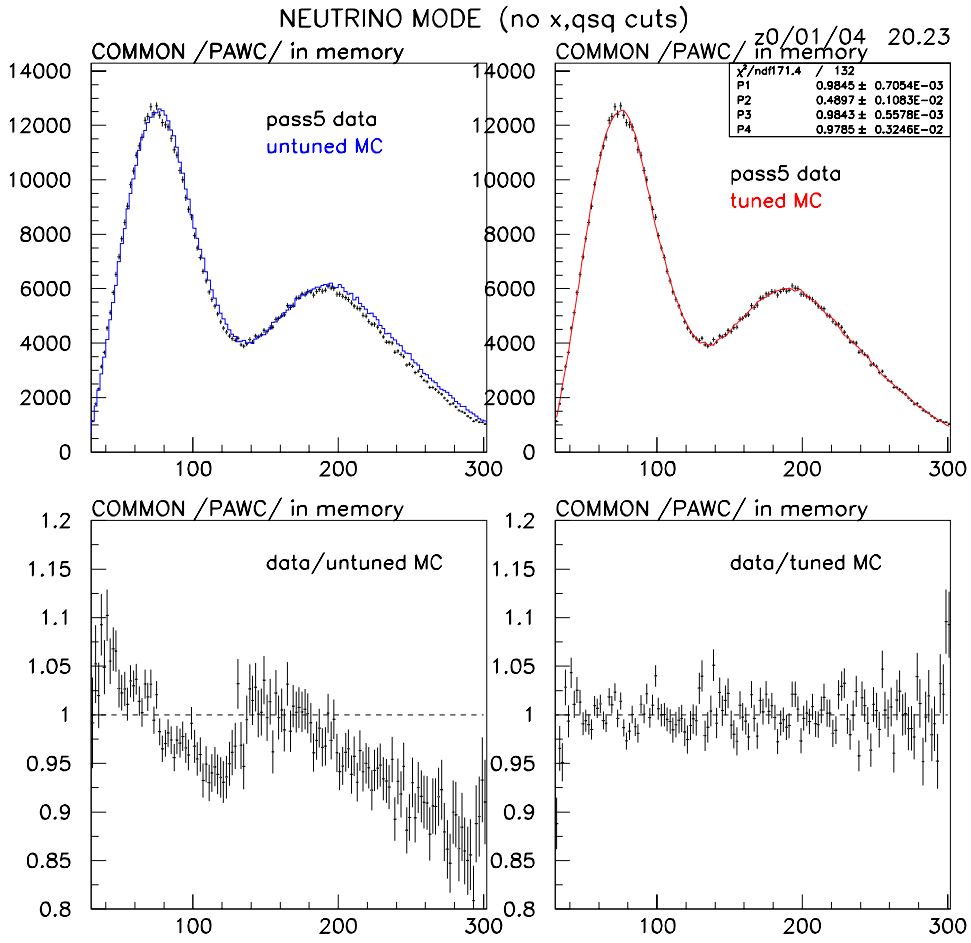

Figure B.3: This plot shows the energy distribution of charged current events in ν mode: a) Before fudging the flux, b) ratio before fudges c) after fudging the flux, and d) ratio after fudges.

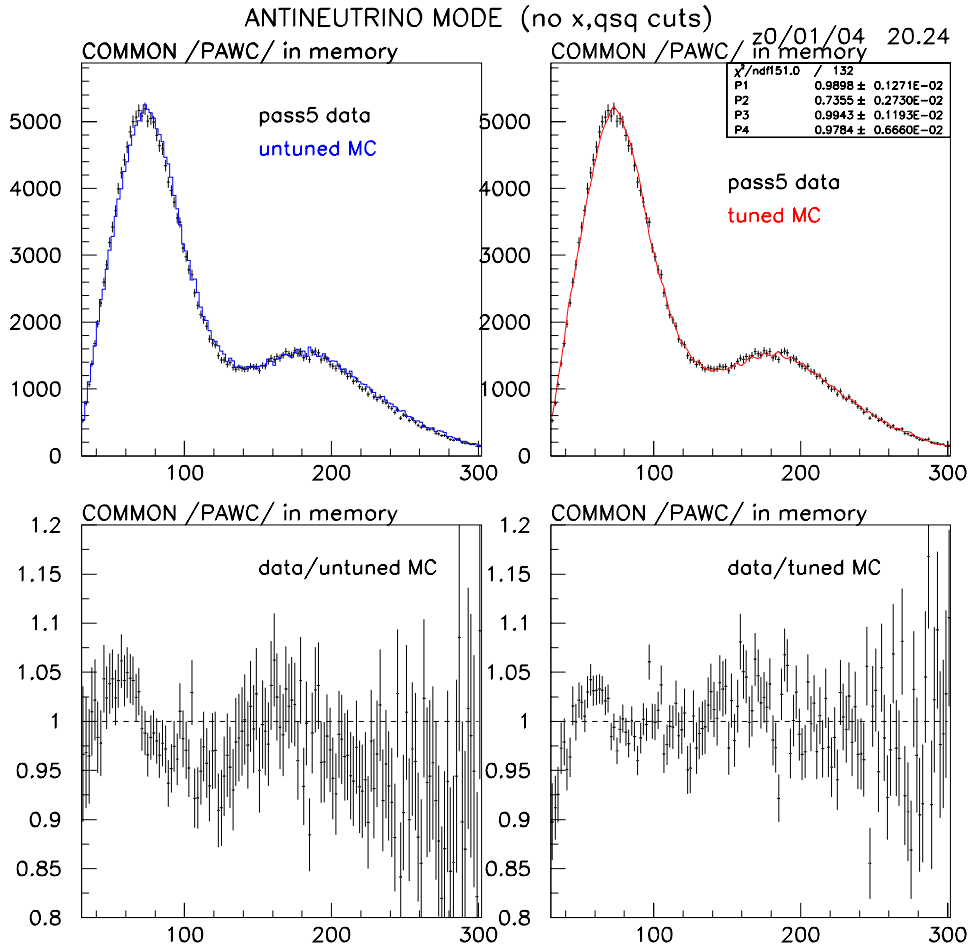

Figure B.4: This plot shows the energy distribution of charged current events in $\overline{\nu}$ mode: a) Before fudging the flux, b) ratio before fudges c) after fudging the flux, and d) ratio after fudges.

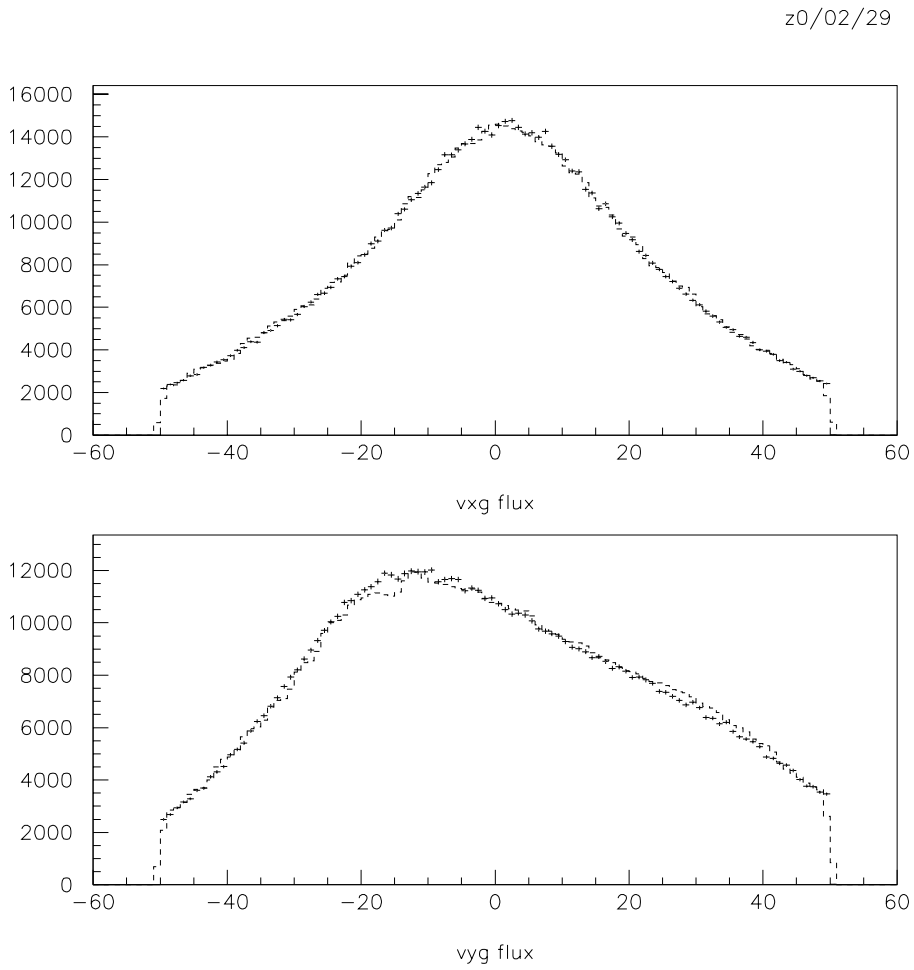

Figure B.5: This plot shows the agreement between data and GEANT in a)vertx and b) verty

Bibliography

[1] D. Halzen and Martin, *Quarks & leptons: An Introductory Course in Modern Particle Physics*(New York: Wiley, 1984).

[2] S.L. Glashow, Nucl. Phys. **22**, 579 (1961).

[3] S.L. Glashow, J. Iliopoulos, L. Maiani, Phys. Rev. D**2**, 1285 (1970).

[4] S. Weinberg, Phys. Rev. Lett. **19**, 1264 (1967).

[5] R. Brock *et al.* [CTEQ Collaboration], Rev. Mod. Phys. **67**, 157 (1995).

[6] D. Griffiths, *Introduciton to Elementary Particles*(New York: Wiley, 1987).

[7] J.D. Bjorken, Phys. Rev. **179**, 1547 (1969).

[8] F.S. Navarra, M. Nielsen, C. A. A. Nunes, and M. Teixeira, "On the Intrinsic Charm Content of the Nucleon," hep-ph/9504388.

[9] G. Ingelman and M. Thunman, "Signals for Intrinsic Charm in High Energy Interactions," hep-ph/9604289.

[10] R. Bernstein *et al.*, "Technical Memorandum Sign-Selected Quadrupole Train," FERMILAB-FN-0341.

[11] M. Gluck, R. M. Godbole and E. Reya, Z. Phys. **C38**, 441 (1988).

[12] C. Adloff *et al.*, Zeit. Phys. C**72** 593 (1996).

[13] J. Breitweg *et al.*, Phys. Lett. **B407** 402 (1997).

[14] A. Vaitaitis *et al.* [E815 Collaboration], Phys. Rev. Lett. **83**, 4943 (1999) [hep-ex/9908011].

[15] J.J. Aubert *et al.*, Nucl. Phys. **B213** 31 (1983).

[16] J. Huston, S. Kuhlmann, H. L. Lai, F. Olness, J. F. Owens, D. E. Soper and W. K. Tung, FERMILAB-CONF-98-180-T *To be published in the proceedings of 6th International Workshop on Deep Inelastic Scattering and QCD (DIS 98), Brussels, Belgium, 4-8 Apr 1998.*

[17] J.J. Aubert *et al.*, Phys. Lett **B123** (1983).

[18] T. Handler [E687 and E831/FOCUS Collaborations], *In *Frascati 1999, Hadron spectroscopy* 507-514.*

[19] D. H. Perkins, *Introduciton to High-Energy Physics,*2d Ed.(Reading, MA:Addison-Wesley, 1982)

[20] A.J. Malensek, "Empirical Formula For Thick Target Particle Production," FERMILAB-FN-0341.

[21] H. W. Atherton *et al.*, CERN-80-07.

[22] D. A. Harris *et al.* [NuTeV Collaboration], hep-ex/9908056.

[23] G. Ambrosini *et al.* [NA56/SPY Collaboration], Eur. Phys. J. **C10**, 605 (1999).

[24] H. Fesefeldt, PITHA-85-02.

[25] G. Collazuol, A. Guglielmi, A. Ferrari and P. R. Sala, CERN-OPEN-98-032

[26] Aplication Software Group, "GEANT Detector Description and Simulation Tool",(1993).

[27] D. C. Carey, K. L. Brown and F. C. Iselin, Including Decay Calculations," SLAC-0246.

[28] M. Goncharov *et al.*, to be published in *Proceedings of the 34th Rencontres de Moriond, QCD and Hadronic Interactions* (2000).

[29] S.A. Rabinowitz *et al.*, Phys. Rev. Lett. **70**, 134 (1993).

[30] P. Vilain *et al.* [CHARM II Collaboration], Eur. Phys. J. **C11**, 19 (1999).

[31] R. Barbieri, J. Ellis, M. K. Gaillard and G. G. Ross, Nucl. Phys. **B117**, 50 (1976).

[32] A.O. Bazarko *et al.* [CCFR Collaboration], Z. Phys. **C65**, 189 (1995)

[33] A. Pineda and F.J. Yndurain, Phys. Rev. **D58**, 094022 (1998) [hep-ph/9711287].

[34] C.A. Dominguez, G.R. Gluckman and N. Paver, Phys. Lett. **B333**, 184 (1994)

[35] A.S. Kronfeld, Nucl. Phys. Proc. Suppl. **63**, 311 (1998)

[36] J.C. Anjos *et al.* [Tagged Photon Spectrometer Collaboration], Phys. Rev. Lett. **65**, 2503 (1990).

[37] P.D. Collins and T.P. Spiller, J. Phys. **G11**, 1289 (1985).

[38] C. Peterson, D. Schlatter, I. Schmitt and P. Zerwas, Phys. Rev. **D27**, 105 (1983).

[39] P. Sandler, PhD Thesis, Univ. of Wisconsin, 1992.

[40] F. Olness, Private communication.

[41] T. Bolton, "Determining the CKM parameter V(cd) from nu N charm production," HEP-EX 970814(1997).

[42] J. G. Korner and G. A. Schuler, Z. Phys. **C46**, 93 (1990).

[43] F. J. Gilman and R. L. Singleton, Phys. Rev. **D41**, 142 (1990).

[44] E. M. Aitala *et al.* [Fermilab E791 Collaboration], Phys. Lett. **B450**, 294 (1999) [hep-ex/9812013].

[45] E. M. Aitala *et al.* [E791 Collaboration], Phys. Lett. **B440**, 435 (1998) [hep-ex/9809026].

[46] E. M. Aitala *et al.* [Fermilab E791 Collaboration], Phys. Rev. Lett. **80**, 1393 (1998) [hep-ph/9710216].

[47] T. Yamanaka, XXXIVth Rencontres de Moriond, March 13-20, 1999

[48] A. Alavi-Harati, *et al.* "Search for the Decay $K_l \rightarrow \pi^0\mu^+\mu^-$" hep-ex/0001006.

[49] N. Witchey, PhD Thesis, Ohio State University, 1996.

[50] R. Ammar *et al.* [CLEO Collaboration], Phys. Rev. **D49**, 5701 (1994).

[51] T. Affolder, "Search for the Flavor-Changing Neutral Current Decays $B^+ \rightarrow \mu^+\mu^-K^+$ and $B^0 \rightarrow \mu^+\mu^-K^{*0}$ ", hep-ex/9905004.

[52] F. Abe *et al.* [CDF Collaboration], Phys. Rev. **D57**, 3811 (1998).

[53] P. Avery *et al.* [CLEO Collaboration], Phys. Lett. **B183**, 429 (1987).

[54] M. Acciarri *et al.* [L3 Collaboration], Phys. Lett. **B391**, 474 (1997).

[55] A. Weir, Phys. Rev. D**41**, 1384 (1990)

[56] See for example: T.K.Gaisser, "Cosmic Rays and Particle Physics", Cambridge University Press 1990.

[57] B. King, PhD Thesis, Columbia University, 1994.

[58] R. Ammar *et al.*, Phys. Rev. Lett. **61**, 2185 (1988).

[59] K. Kodama *et al.* [Fermilab E653 Collaboration], Phys. Lett. **B263**, 573 (1991).

[60] F. James and M. Roos, Comput. Phys. Commun. **10**, 343 (1975).

[61] B. Anderson *et al.*, Phys. Rep. **97**,1983.

[62] V. Barger, M.S. Berger, and R.J.N. Phillips, Phys. Rev. **D53** (1995)1663.

[63] K. S. Babu, *et al.*, Phys. Lett. **B205** (1988) 540.

[64] S. Dimopolous, H. Georgi, and S. Raby, Phys. Lett. **B127** (1983) 101.

[65] V.A. Miransky, S. Peris, and S. Raby, Phys. Rev. **D47** (1993) 2058.

[66] C.D. Carone and R.T. Hamilton, Phys. Lett. **B301** (1993) 162.

[67] E. Eichten and K. Lane, Phys. Lett. **B90** (1980) 125.

[68] R.S. Chikula, H. Georgi, and L. Randall, Nucl. Phys. **B292** (1987) 93.

[69] M. Luke and M.J. Savage, Phys. Lett. **B307** (1993) 387.

[70] J. L. Diaz-Cruz and G.L. Castro, Phys. Lett. **B301** (1993) 405.

[71] K. Koike, Prog. Theor. Phys. **91** (1994) 161.

[72] J. G. Koner, A. Pilaftsis, K. Schilcher, Phys. Rev. **D47** (1994) 1080.

[73] F. J. Gilman, K. Kleinknecht, and B. Renk, Phys. Rev. **D50** (1994) 1315.

[74] W. Buchmuller, D. Wyler, Phys. Lett. **B177** (1986) 377.

[75] S. Davidson, D. Bailey, and B.A. Campbell, Z. Phys. **C61** (1994) 313.

[76] H. Abramowicz *et al.* [CDHS COLLABORATION Collaboration], Phys. Lett. **B109**, 115 (1982).

[77] C. Caso *et al.*, Eur. Phys. J. **C3**, 1 (1998).

[78] S. Geer, Phys. Rev. **D57**, 6989 (1998) [hep-ph/9712290].